UNIVERSITY OF HELSINKI
DIVISION OF GEOPHYSICS

REPORT SERIES IN GEOPHYSICS

No 47

SEASONAL SNOW IN ANTARCTICA DATA REPORT

K. Rasmus, H. Granberg, K. Kanto, E. Kärkäs, C. Lavoie and M. Leppäranta

HELSINKI 2003

UNIVERSITY OF HELSINKI
DIVISION OF GEOPHYSICS

REPORT SERIES IN GEOPHYSICS

No 47

Cover: Eija Kärkäs making snowpit measurements on the Högisen ice dome 6.1.2001. Photograph by H. Granberg.

SEASONAL SNOW IN ANTARCTICA DATA REPORT

K. Rasmus[1], H. Granberg[2], K. Kanto[1], E. Kärkäs[1],
C. Lavoie[2] and M. Leppäranta[1]

[1]University of Helsinki, Division of Geophysics, Helsinki, Finland
[2]Université de Sherbrooke, Centre d'applications et de recherches en teledetection, Sherbrooke, Canada

HELSINKI 2003

ISBN 952-10-0953-5
ISSN 0355-8630

Helsinki 2003
Yliopistopaino

PREFACE

The project 'Seasonal Snow in Antarctica' was set up to measure the physical properties of Antarctic snow cover in 1999-2001. The partners in the project are the Department of Geophysics (from 1 August 2001 the Division of Geophysics at the Department of Physical Sciences) at the University of Helsinki and Centre d'Applications et de Recherches en TÉLédétection (CARTEL) at Université de Sherbrooke in Québec, Canada.

The objectives of this Antarctic research project were: to examine the structure and properties of the snow cover; to collect a one year data series of snow cover evolution; to examine the albedo and the internal radiation climate in snow and ice; to examine snow by satellite remote sensing; and to study the snow on Antarctic sea ice cover.

Fieldwork was done at the Finnish Antarctic research station Aboa in Dronning Maud Land during FINNARP 1999 and 2000 and at the South African research station SANAE 4 during FINNARP 2000. Measurements were made using classical snow pit method, ground-penetrating radar for the spatial variability of snow properties, and automatic snow stations for the snow accumulation and temperature over the Antarctic winter. Also measurements were made of reflected radiation and the attenuation of radiation inside the snow cover. Some sea ice measurements were made during the FINNARP 1999 expedition.

The present document is the project data report. An introduction is given of the project, descriptions of the experiments are made, and the data obtained by the scientists in the different working groups during the two expeditions to Antarctica are described. A CD containing the data is available at the Division of Geophysics on request.

FINNARP (FINNish Antarctic Research Programme) coordinated by the Finnish Institute for Marine Research is acknowledged for making these expeditions possible. The expedition chiefs at Aboa (Henrik Sandler and Jaakko Mäkinen) and SANAE 4 (Adriaan Dreyer) together with the personnel are thanked for their help and advice. This project is financed by the Academy of Finland (Academy project number 43925).

Helsinki, 13 January 2003

Kai Rasmus
Division of Geophysics, University of Helsinki

Contents

1. Introduction

The Antarctic continent is an important component of our global thermostatic control system. Its surface beams thermal radiation directly to space through a very large, clear window of dry, descending air known as the Antarctic anticyclone. The height of the ground surface in most of this window exceeds 3 km; so much of the CO_2 and other greenhouse gases are below this level. The descending air is mainly of upper tropospheric and stratospheric origin. It is therefore dry, and its potential temperature is relatively high. During the descent its potential temperature is lowered by emission of thermal radiation directly to space and via the surface, which radiates this heat to space. The process generates vast quantities of air with the lowest potential temperature found anywhere in the terrestrial atmosphere. Such air is capable of displacing upward all other air, and as such controls the atmospheric circulation. The katabatic outflow of cold, dry air that results from this cooling is a function of ice cap topography and therefore lacks an Arctic counterpart. Descending from the high Antarctic icecap this cold wind is a powerful controller of both sea ice and bottom water formation in the oceans surrounding Antarctica. As such, the Antarctic continent is an important controller also of the oceanic thermohaline circulation. At the present wintertime temperatures of -30 to -90 °C and summertime temperatures of +10 to -50 °C, the heat sink capacity of the Antarctic continent is enormous and very important to our global climate.

Snow is draped over nearly everything in Antarctica including the ice cover on the surrounding seas. Therefore, it is a considerable extent of the properties of the snow cover that give the continent its important climatic role and determine its energy and mass balance. The snow cover generates signals detectable by remote sensing. To better understand these signals in terms of the snow properties they represent and to better understand the climatic role of the snow cover, it is essential to know not only the annual accumulation and its spatial variations but also the properties of the snow cover.

The 'Seasonal Snow in Antarctica' project has been set up to examine the seasonal snow conditions in the Dronning Maud Land region of Antarctica. The project is a collaboration between the University of Helsinki (UH), Division of Geophysics, and the University of Sherbrooke (US), Center d'applications et de recherches en télédétection.

The objectives of the project were:
- To examine the structure and properties of the snow cover;
- To collect a one-year data series of snow cover evolution;
- To examine the albedo and the internal radiation climate in snow and ice;
- To examine satellite remote sensing for snow properties; and
- To map and model the snow-ice portion in the Antarctic sea ice cover.

This data report details the measurements made during the FINNARP 19999 and 2000 expeditions to Antarctica (Fig. 1), and describes data sets. Firstly a theoretical background is given to the experiments and the factors taken into account in their design are overviewed. Then the basic strategy is outlined. After this, the two expeditions are described together with the conditions experienced in Antarctica.

2. Snow in Antarctica

2.1 Snow and accumulation

According to Bromwich (1988) precipitation over Antarctica is an important climatic variable whose study has been limited by the frequent inability to discriminate between actual snow precipitation and drifting snow. Strong surface winds can pick up recently deposited snow and transport it nearly horizontally. The topographic features control the amount of precipitation and dynamics of ice sheets. Most precipitation falls in the winter. Precipitation characteristics at the coast and in the high interior are very different. In the interior precipitation is always solid and snowfall amounts are very small and it is very difficult to make direct precipitation measurements.

Strong winds and sudden changes in the weather are more typical for coastal areas. Coastal snowfall is episodic in association with synoptic scale features such as cyclones and fronts (Bromwich, 1988). Direct orographic lifting with accompanying adiabatic cooling is the dominant precipitation formation mechanism inland of the 1000 m elevation contour and above 3000 m elevation where terrain slopes are gentle, radiative cooling is the primary mechanism by which precipitation is formed (Bromwich, 1988). In the interior the proportion of precipitation associated with clouds decreases and the semi continuous fall of ice crystals from cloud-free skies becomes progressively more important as elevation increases (Bromwich, 1988).

Accumulation has been considered a more sensitive climatic parameter than mass balance because accumulation has a correlation with air temperature. Accumulation values are subject to significant uncertainty due to the wind transport and previously deposited snow. Accumulation has generally high values near the coast. In the some places of the western side of the Antarctic Peninsula annual accumulation is reaching 800 mm or more (Bromwich, 1988). Desert like accumulation values (< 50 mm) are found for elevations above 3000 m (Bromwich, 1988). An accumulation value near 150 mm ±13 % has been found for the continental average (Bromwich et al., 1998). The iceberg calving and basal melting of ice shelves are the main ablation mechanisms of the Antarctica.

The net accumulation can be observed in the field by stake measurements and firn cores. Ice layers indicate summer melting but cannot be used alone to measure accumulation and seasonal layering. Annual layers can be detected in laboratory from snow and firn samples by oxygen isotope ($\delta^{18}O$) ratio or β-activity (Isaksson and Karlén, 1994). If using oxygen isotopes there has to be enough precipitation during the summer and winter seasons to see seasonal variations. According to previous studies accumulation in our research area (Fig. 2) in Riiser-Larsen Ice Shelf is 400 mm a^{-1} and above the grounding line in Ritscherflya it is about 300 mm a^{-1} (Isaksson and Karlén, 1994). Longwave dunes and sastrugi topography cause variability greater than one year's snow accumulation (Goodwin et al., 1994).

Snow surface in Antarctica is heavily eroded by katabatic winds. There is a lot of a blowing and drifting snow in the air mixed with the precipitation. The amount of drift snow deposited or eroded by wind redistribution is controlled by the local surface roughness and its effect on wind turbulence and speed (Goodwin, 1991). Previous studies have classified surface micro relief into three types that reflect their unique mode of formation. (i) Stationary depositional features formed during precipitation, (ii) mobile depositional or redistribution features formed from wind transported friable snow and (iii) erosion features formed from the long-term exposure to the katabatic winds during the hiatus in precipitation (Goodwin, 1991). Strong winds and summer time radiation cause seasonal surface glaze (Goodwin, 1991).

2.2 Snow properties in Antarctica

On the ground snow quickly looses the shape it had in the atmosphere and it goes through many metamorphoses. The weight of overlying snow, temperature, wind and snow accumulation have an effect to density profile of the first 10-20 meters (Van den Broeke et al., 1999). In winter a high-density layer with fine grains forms while the summer layer has a lower density and bigger grains (Mosley-Thompson et al., 1985). Depth hoar layers with a low density are an annual phenomenon in Antarctica usually found near the surface under the wind crust. Typically the surface density is about 300-400 kgm^{-3} and the density at 10 m depth is about 500-600 kgm^{-3} (Kojima, 1964).

Snow in Antarctica is almost always dry being a mixture of ice and air. The electromagnetic properties of dry snow, such as dielectric constant, are dependent on snow density and crystal shape (Hallikainen and Winebrenner, 1992). The mean annual air temperature in a dry-snow zone is approximately equal to the temperature at a depth of 10 m in the firn (Paterson, 1994). Daily temperature changes do not penetrate deeper than 0.5 m.

Snow depth, density, crystal size, liquid water content and impurities affect the optical properties of snow. Snow is formed of small ice crystals (submillimeter scale in radius), and so there exist a large number of crystal boundaries in the snow pack. There is a difference in index on refraction between air and ice and so light rays change direction at these boundaries; as a result the light is scattered. High scattering of light by these crystal boundaries is the main reason for the high albedo. The optical properties of snow are well outlined in a review article by Warren (1982); developments there after can be found at: http://wwwflag.wr.usgs.gov/USGSFlag/Space/RSIce/abstracts/swarren.html.

Incident solar radiation is given by the downwelling irradiance $E_d(0,\lambda)$, where 0 designates the surface and λ is the wavelength. The spectral albedo, by definition, is the ratio of the upwelling irradiance, which is composed of the radiation that is reflected from the surface and scattered back from inside the snow, $E_u(0, \lambda)$, to the downwelling irradiance and can be expressed as:

$$\alpha(\lambda) = \frac{E_u(0,\lambda)}{E_d(0,\lambda)} \qquad (1)$$

The broadband albedo over interval $[\lambda_1,\lambda_2]$ is then obtained by integrating the irradiances over the specified wavelength interval, and the total albedo is obtained by integrating over the whole spectrum. Changes in the spectral distribution of the incident radiation (e.g. caused by changes in cloud cover, water vapour pressure etc.) also cause changes in the total albedo.

Extinction of light can be computed using the Bouger-Lambert's law. This states that deep in a homogeneous snowpack (uniform density and grain size distribution and far from any boundaries) the spectral flux is attenuated exponentially (Warren, 1982):

$$\frac{\partial L(\lambda)}{\partial z} - bL(\lambda) = 0 \qquad (2)$$

where L is the downwelling flux intensity (radiance) and b is the extinction coefficient. Even though the definition specifies that Eq. (2) is applicable deep in a homogeneous medium, it is used to estimate the attenuation coefficient also near the snow surface, in a shallow snowpack, and in blue ice.

Ice absorbs light weakly in the visible wavelengths (between 400 and 750 nm), a minimum at 460 nm, but has strong absorption in the near infrared. The result is that snow has lower albedo in the near infrared. In the visible band the albedo is dominated by the snowpack thickness and impurities. Because of low absorption, light is able to penetrate the snowcover, reflect back from below, and to propagate back through the snow. Impurities absorb visible radiation. In the Antarctica the snow is basically a semi-infinite slab. When snow ages, its grain size increases producing a reduction in the albedo. Liquid water in snow lowers the albedo.

An increase in solar zenith angle causes an increase in the albedo at all wavelengths. The albedo is most sensitive to changes in the zenith angle at 1000 nm. The bi-directional reflectance of solar radiation (reflectance of solar radiation into a specific direction) is most sensitive to grain size, surface roughness and impurities. Cloudcover changes the effective solar angle and the spectral distribution.

2.3 Snow on sea ice

Sea ice around Antarctica is mostly first year ice. Flooding and snow-ice formation are common phenomena. In the Weddell Sea average ice thicknesses of 0.91±0.64 m have been measured (Massom et al., 1997). Up to 60% of snow accumulation on sea ice can change to snow-ice (Jeffries et al., 1998) and it has been estimated that snow ice make up 16 % of the ice mass in the Weddell Sea (Wadhams, 1998).

The average thickness of snow cover on the first-year ice is 16-23 cm and 63-79 cm on the second-year ice in the NW Weddell Sea (Wadhams, 1998). The reasons for the much greater thickness in the second year are that the snow does not necessarily melt during the first summer, and during its second year it enters the inner part of the Weddell Sea where precipitation is greater (Wadhams, 1998).

2.4 Snow on nunataks and blue ice areas

Of the surface area of the continent 98% is covered by snow and ice. The last 2% is bare rock. Nunataks can be seen as islands of rock and/or mineral soil in the glacier; strong absorption of solar radiation due to a low albedo takes place in them. Solar radiation heats the surface beneath the thin snow layer providing the necessary energy for the snow to evaporate, leading to a very special microclimate during the summer time. The deeper snow does not evaporate fast and thence some very old snow can be found at the bottom of snow patches on the nunataks.

Near nunataks airflow is accelerated by their geometry and therefore its erosive power of the wind increases, resulting in snow erosion prevailing over deposition upwind. The drifting snow is trapped by the micro roughness of the nunatak surface, so that for a considerable distance downwind erosion again prevails over deposition of the wind-blown snow. However, for the nunatak to trap new snow, it is necessary that the snow trapped earlier is removed between snow storms. The mechanism for this removal is mainly snow evaporation. The very dry air that descends into the Antarctic anticyclone creates conditions favouring evaporation over melt. Although there was some melt on the nunatak during the 1999/2000 and 2000/2001 summers, there was never enough to generate significant filtration or surface runoff. There are little or no patterned ground indications of any significant subsurface ice accumulation in the permafrost.

An additional aspect of the Antarctic katabatic outflow that is important to the generation of the blue-ice areas and the snow-free nunataks is the persistent wind direction. Omni-directional winds would allow a much more extensive build up of the snow cover on and around nunataks and would reduce downwind where erosion prevails over deposition the size of the areas. More

importantly, their location would shift from one storm to another, thus allowing the accumulation of finely fragmented, rapidly hardening snow onto potential blue ice areas, preventing blue ice from forming. The unidirectional snow-driving wind also reduces snow accumulation around structures erected on the nunatak.

Blue ice areas are another minor exception in the Antarctic snow cover. These areas exist only in Antarctica and they cover about 1% of the surface area (Bintanja, 1999). They have net ablation mainly by sublimation and any snow accumulation is easily swept off of their aerodynamically smooth surface by gusty winds (Bintanja, 1999). Blue ice areas exist mainly in the vicinity of mountain ranges and nunataks. They form either by wind erosion or by a nunatak blocking the snowdrift.

In high altitude blue ice areas (more than 1500 m a.s.l.) no melting occurs. In low altitude blue ice areas some subsurface melting occurs during the summertime. Strong absorption of solar radiation creates a meltwater layer beneath the ice surface. This kind of water layer is found during summer e.g. next to Basen nunatak where the Finnish station Aboa and the Swedish station Wasa take water for their needs.

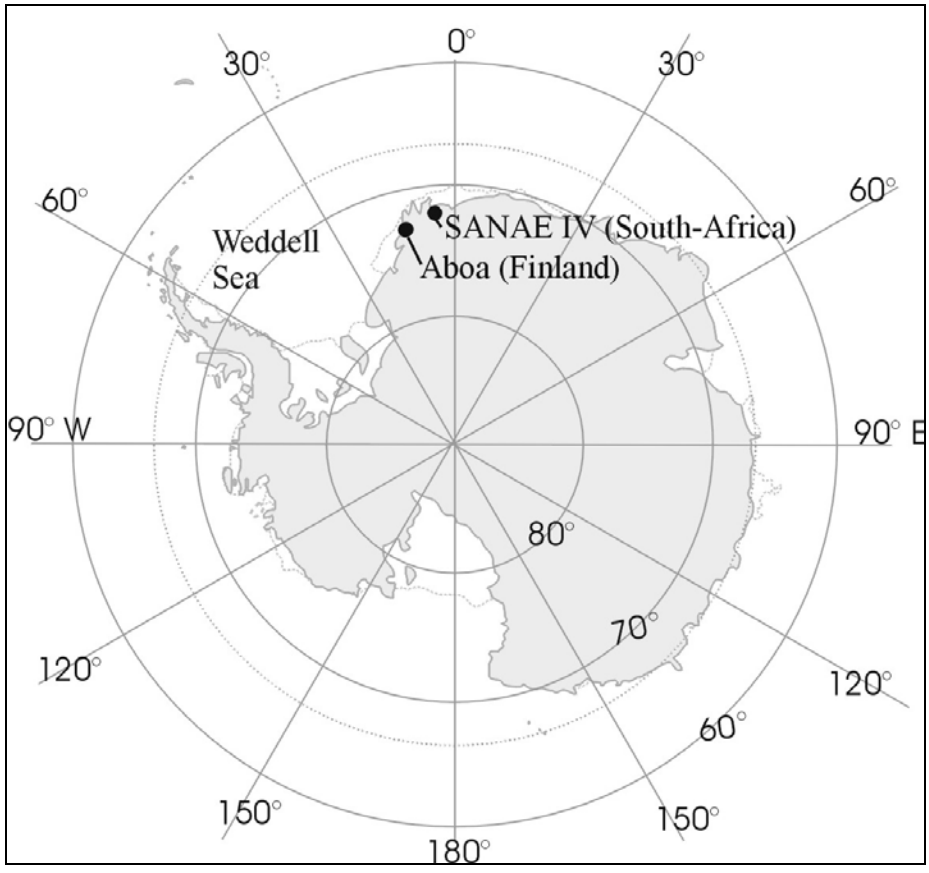

Figure 1. Map of Antarctica showing the locations of the Finnish Antarctic research station Aboa, and the South African research station SANAE 4.

3. Expeditions

3.1 Description of the research area and research stations

The research area was western Maudheimvidda in Dronning Maud Land (Fig. 2). Two mountain ranges are situated in the area. Vestfjella is about 130 km long range near the grounding line of the ice sheet and Heimefrontfjella is situated about 150 km further inland. It blocks partly the ice flow from Amundsenisen. Riiser-Larsen is a small ice shelf, and Ritscherflya is an ice sheet between those two mountain ranges. In Vestfjella area the altitude is about 400 m a.s.l. and low altitude blue ice areas are very common. Ice thickness on the grounding line is about 500 m and on the ice shelf 200 m (Holmlund and Näslund, 1994). Kvitkuven ice rise and Högisen ice dome are located in the area.

The locations of Aboa, the available land routes and variations in radar backscatter observed in the RADARSAT synthetic aperture radar (SAR) mosaic of Antarctica determined the measurement sites (Fig. 2). The backscatter intensity is shown in grey scale in the image. Compared to other measurement sites lower backscatter coefficient was seen in Högisen and Kvitkuven in the RADARSAT mosaic.

Research station Aboa (Fig. 3) is located in north Vestfjella on Basen nunatak (73° 03' S, 13° 25' W) about 120 km from the coast near the grounding line. Aboa is built for 10 people and only for a summer use. In the Basen nunatak there is also Swedish research station Wasa, and together Aboa and Wasa are called Nordenskiöld base. Sweden has also a small field station Svea (74° 35'S, 11° 13'W) in Heimefrontfjella.

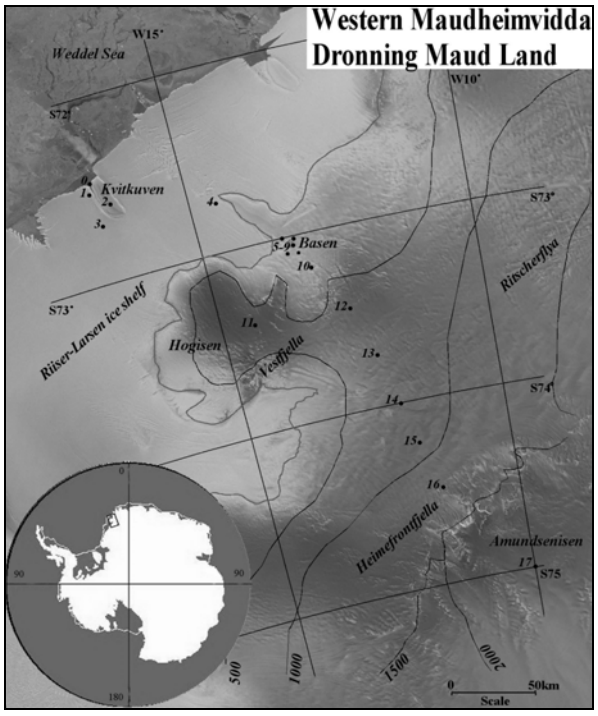

Figure 2. Map over the measurement area in western Maudheimvidda showing measurement sites and the altitude contours (in m a.s.l.). Site 0 was on the sea ice. Finnish research station Aboa is located in Basen nunatak. Part of a RADARSAT synthetic aperture radar mosaic has been used as a background of the map (RADARSAT data © Canadian Space Agency 1997).

Figure 3. Research station Aboa is located on Basen nunatak (73° 03′ S, 13° 25′ W). (Photograph by E. Kärkäs)

During the season 2000/2001 measurements were also made in the vicinity of South African base SANAE 4 (Fig. 4) located 170 km from the coast on the Vesleskarvet nunatak. South Africa is one of the original signatories of the Antarctic Treaty, and has occupied bases, all year round, on the Fimbul Coastal Ice Shelf of Western Queen Maud Land since 1960. The new South African base, "SANAE 4", was completed in the summer of 1997/8 and is the newest base on the continent.

Figure 4. Aerial photograph showing SANAE 4 nestled atop the Vesleskarvet nunatak. (Photograph courtesy of Dr. Armin Deffur of the SANAE 40 overwintering team)

3.2 FINNARP 1999

FINNARP 1999 was the biggest Finnish expedition this far and probably had the stormiest season in FINNARP history. Finnish Institute of Marine research (http://www.fimr.fi/) was responsible for the logistics of Finnish, Swedish and Norwegian expeditions. FINNARP 1999 consisted of four different scientific projects: aerosol, geology, paleo-climatology and seasonal snow.

The voyage from Cape Town to Antarctica started aboard the Russian research vessel R/V Akademik Fedorov on December 1. In the ship there were scientific laboratories and two MI-8 helicopters for transportation. In December 8 the vessel got the first time sight to the ice shelf near Norwegian unloading place. The first sea ice measurement site was made there (Fig. 5) and after that the vessel started her way to the unloading place 220 km from Norwegian research station Troll (72° 01'S, 2° 32'E). On December 10 MI-8 helicopter flew the snow team to the sea ice to have the second sea ice site. The vessel arrived to the Finnish and Swedish unloading place Ramppi (72° 32'S, 16° 34'W) near Kvitkuven ice rise (Fig. 2) on December 15. The snow team made the third sea ice measurement site there but had problems with coring. The route from Ramppi to Aboa is 162 km.

First snow measurements on the continent were made on December 24 near Aboa. December 25-28 a tracked vehicle caravan was accomplished back to Ramppi and two from the snow project was measuring snow along the route. January 2-5 the snow group made measurements near Aboa by snowmobiles and radiometry flights from Aboa to Ramppi and Svea by South African Jet Ranger helicopter transportation. January 6 the half of the snow group spent on Högisen ice dome doing snow pit measurements and installing the snow sensor.

On January 8 the snow group worked near Aboa and late night of January 9 started the tracked vehicle caravan towards Svea with logistics (Fig. 6). Snow is a bit harder for driving heavy vehicles during the night. Snow measurements were made along about a 200 km route from Aboa to Svea. On January 14 part of the snow group flew to Amundsenisen by helicopter from Svea to install snow sensor and accomplish snow pit measurements. Back to Aboa the caravan arrived January 17. January 18 one snow sensor was installed to Kvitkuven by helicopter. The late season measurements were made around Basen. January 23 half of the snow team did radiation measurements on Högisen by helicopter transportation.

Scientific season ended January 24 when cargo transportation commenced back to the coast to be ready for the vessel. Akademik Fedorov arrived to Ramppi January 30, and February 8 the ship was back in Cape Town.

The summary of the snow project's activities in 1999/2000:

December 1	R/V Akademik Fedorov departs from Cape Town
December 8	First sighting of Antarctic
December 9	First sea ice measurement site
December 9	Arrival to Norwegian unloading place
December 10	Second sea ice measurement site near Norwegian unloading place
December 15	Arrival to Finnish and Swedish unloading place Ramppi
December 15	Third sea ice measurement site near Ramppi
December 16	Tracked vehicle caravan from Ramppi towards Finnish station Aboa
December 20	Rest of the expedition to Aboa from Akademik Fedorov
December 24	First snow measurements near Basen nunatak by snowmobiles from Aboa
December 25-28	Nasu caravan from Aboa to Ramppi and three snow measurement sites along the route

January 2	Snow measurements by snowmobiles from Aboa
January 2	Radiometry flight from Aboa to Ramppi by helicopter
January 3	Radiometry flight from Aboa to Svea by helicopter
January 4	Installing a snow sensor near Aboa by snowmobiles
January 5	Snow measurements and a snow sensor installation by snowmobiles from Aboa
January 6	Snow measurements and snow sensor installation in Högisen by helicopter
January 8	Snow measurements and a snow sensor installation by snowmobiles from Aboa
January 9-17	Nasu caravan from Aboa to Svea and five snow measurement sites and three snow sensor installations along the route
January 14	Snow measurements and snow sensor installation in Amundsenisen by helicopter from Svea
January 18	Snow measurements and snow sensor installation in Kvitkuven by helicopter
January 21	Radar and radiation measurements near Basen by snowmobiles
January 22	Blue ice measurements near Basen by snowmobiles
January 23	Optical measurements in Högisen by helicopter
January 23	Snow measurements and snow sensor installation close to Basen by snowmobiles
January 26	Flight attempt to Ramppi by helicopter to install a snow sensor, had to turn around because of bad weather
January 26	Blue ice measurements near Basen by snowmobiles
January 27	Blue ice measurements near Basen by snowmobiles
January 28	Flight attempt to Ramppi by helicopter to install a snow sensor, had to turn around because of bad weather
January 28	Last snow sensor installation near Basen by snowmobiles
January 30-31	MI-8 and Court helicopter flights from Aboa back to Ramppi and Akademik Fedorov
February 8	Arrival in Cape Town

Figure 5. Sea ice measurements being made. Chantale Lavoie is making radiation measurements in the foreground. Kai Rasmus and Eija Kärkäs in the centre extracting a sea ice core. (Photograph by H. Granberg)

Figure 6. A heavy portable fieldcamp consisting of two survival modules on sledges pulled by articulated tracked vehicles. The red Scott-tent was used as a toilet. (Photograph by H. Granberg)

3.3 FINNARP 2000

Norway was responsible for logistics of Norwegian and Finnish expeditions in the season 2000/2001 and the expedition members flew to the continent instead of sailing with a vessel. The expedition consisted of two legs and five different scientific projects; four as a year earlier and one new concerning geodetic investigations.

One scientist (Kai Rasmus) from our project sailed down to the continent by R/V Agulhas together with the paleo-climatology project, and he stayed the season at the South African station SANAE 4 (71° 40'S, 02° 51'W) for optical measurements around the station.

R/V Agulhas started her voyage on December 6. Iljushin plane flew the main expedition group to the Blue One airfield area (71° 19'S, 08° 28'E) on December 10 (Fig. 7). Distance to Aboa is about 800 km. From Blue One the Finnish expedition flew at the first to South African station SANAE 4 and from there to Aboa by Canadian Twin Otter.

All cargo, also scientific equipment, was transported with R/V Agulhas to the South African unloading place E-base (70° 18'S, 02° 24'W) and German Dornier planes flew cargo from E-base to Aboa. First Dornier flight came in the Christmas Eve.

Geological and snow projects were in field in turns. The snow team made within the snowmobile range from Aboa during December 27-31. Between January 6-8 part of the snow team and one logistics made measurements towards the coast from Aboa. During January 12-20 the snow team flew to Amundsenisen, Högisen and Kvitkuven to do snow pit measurements and to retrieve the snow sensors and made also one radiometry flight by helicopter. During the flights routes were

Figure 7. The Iljushin IL-76TD at Blue One (71°19'S, 08°28'E). (Photograph by E. Kärkäs)

reconnoitred. Some snow measurements were made near Aboa by snowmobiles. January 20-24 two snow scientists and two logistic persons made a longer field trip to Svea. At the end of the season all equipment and samples were driven to Ramppi (72° 32'S, 16° 34'W) from where the Norwegian research vessel R/V Lance picked up equipment early February. The snow team made the last measurements at Ramppi. A Bazzler (modified DC-3) plane came to Aboa on February 6 to pick up the expedition members back to Blue One, and on February 10 Iljushin took off from Blue One to Cape Town.

Summary of the snow project's activities in 2000/2001 at Aboa:

December 3	Gathering of Norwegian and Finnish expeditions in Cape Town
December 6	Departure of R/V Agulhas from Cape Town
December 10	Iljushin flight from Cape Town to Antarctica, Blue One airfield
December 11	Twin Otter flight from Blue One to South African base SANAE 4
December 14	Twin Otter flight from SANAE 4 to Finnish station Aboa
December 24	First Dornier cargo flight from E-base to Aboa
December 28	Radiometry flight towards Ramppi by helicopter, some clouds in the coast and had to turn back to Aboa before Ramppi
December 29	Snow measurements near Basen by snowmobiles
December 31	Removing the first snow sensor near Basen by snowmobiles
January 1	Snow measurements between Basen and Plogen nunataks by snowmobiles
January 3	Snow measurements near Basen by snowmobiles
January 4	Last Dornier cargo flight from E-base to Aboa
January 6-8	Snowmobile trip towards coast and snow measurements along the route
January 10	Snow measurements between Basen and Plogen nunataks by snowmobiles
January 12	Snow measurements and a snow sensor removing in Amundsenisen by helicopter and removing two snow sensors on the way back to Aboa
January 13	Snow measurements and a snow sensor removing in Högisen by helicopter and removing one snow sensor on the way back to Aboa
January 15	Radiometry flight from Aboa to Svea by Helicopter

January 16	Installing a portable weather station to blue ice area near Basen by snowmobiles
January 19	Attempt flight by Court helicopter towards Kvitkuven but clouds made to turn back to Aboa
January 20	Snow measurements and a snow sensor removing in Kvitkuven by helicopter
January 20-24	Snowmobile trip from Aboa to Svea and snow measurements along the route
January 27	Digging a long snow blower trench near Basen by snowmobiles
January 28	Removing of the weather station from blue ice area near Basen by snowmobiles
January 30	All equipment from Aboa to Ramppi by snowmobiles and tracked vehicles, snow pit measurements at Ramppi
February 7-8	DC-3 flights from Aboa to Blue One
February 10	Iljushin flight from Blue One to Cape Town

3.3.1 Fieldwork at SANAE 4

Measurements of spectral and total albedo together with some other physical properties of the snow were made on the glacier at several locations SANAE 4. The measurement area and the sampling points are marked on the map shown in Figure 8. The measurements included:

(i) Spectral and total albedo at one location east of SANAE 4.
(ii) Weekly snowpit measurements at the same site as (i).
(iii) Snow stake measurements (stake height and surface density) at the same site as (i).
(iv) Snowpit measurements at several locations within a 30 km radius of SANAE 4.
(v) Blue ice measurements (radiation and physical properties) in the wind scoop downwind of SANAE 4.
(vi) Observations of snow and ice formations recorded using photographic methods.

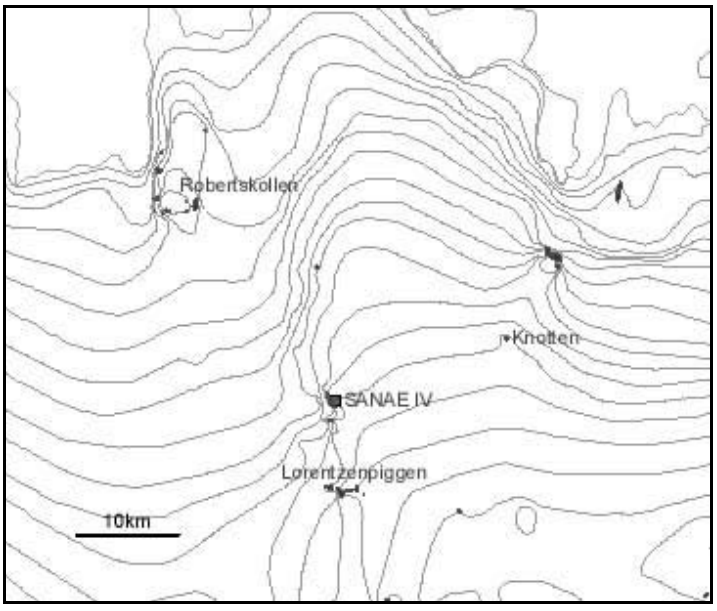

Figure 8. Map of the environment of SANAE 4.

3.4 Strategy

The structure of the work (1999-2001) was determined by the two expeditions to Antarctica during austral summers 1999/2000 and 2000/2001. These gave total of the two months of time in the field, and the deployment and recovery of automatic snow-temperature sensors was possible.

In Antarctica, the available logistical support, and the ever-present crevasse danger dictate the possible sampling locations. When moving by a motor vehicle along the surface of the glacier, it is necessary to stay on known 'safe' routes. Remote locations had to be visited by helicopter. These restrictions allowed a sampling to inland. The route almost 350 km long contains the ice shelf, the grounding line and the uphill towards the polar plateau. The line was extended onto the plateau behind the Heimefrontfjella mountain range by using helicopters. Areas of high ground, such as Kvitkuven (an ice rise on the ice shelf) and Högisen (an ice dome) showed a different backscattering signature from the surrounding glacier. It was then decided that these two locations would be sampled in addition to the sampling made along the line. In the 2000/2001 season the possibility of using the South African base SANAE 4 opened up the possibility for increasing the spatial dimensions of the sampling area.

4. Snow measurements

4.1 Methods

4.1.1 Snow pit measurements

Snow pits were dug and sampled using classical methods. Eija Kärkäs was responsible for the snow pit work. During FINNARP 2000 Kimmo Kanto made a number of shallow snowpits for remote sensing ground truth purposes.

Snow pit measurements were made in shallow snow pits covering at least 1 year's accumulation. They were dug using shovels to 1-2 meter depth with clean wall (Fig. 9). The vertical wall was cleaned with a snow knife and saw, and snow properties were measured at 2-10 cm intervals. The clean wall was in shadow side. In 2000/2001 a tent was used as a cover over the snow pit in some measurement sites. One snow pit took 4-8 hours of work. In 2000/2001 also a snow blower was used to excavate longer snow trenches. The measured quantities were temperature, density, stratification, grain size and shape, dielectric constant, wetness, snow hardness, pH, conductivity and oxygen isotope ratio.

Snow density measured with 0.5 litre cylinder (diameter 0.06 m and height 0.18 m) in 1999/2000 and with 0.25 litre (diameter 0.05 m) cylinder in 2000/2001 (Fig. 10). Snow samples were taken with a small cylinder or with 1 litre snow density box (0.135 * 0.155 * 0.05 m^3). They were weighted with Pesola spring balance (Fig. 11). Temperature profiles were measured with an Ebro TLC1598 thermometer fitted with 0.106 m temperature probe (diameter of 0.003 m) in 1999/2000 and with Ebro TFX 392 thermometer with a Pt 1000 temperature probe in 2000/2001. The real part of dielectric constant and wetness measured with a French LEAS TEL 051-device in 1999/2000 and with the Finnish snow fork designed by Toikka Oy in 2000/2001 (Sihvola and Tiuri, 1986). The snow fork also measures density from electrical parameters (Fig. 12).

The hardness was measured only in 2000/2001 with the Rammsonde using 0.5 kg and 1 kg weights. Conductivity and pH were measured from melted samples. SCHOTT handylab BlueLine 24 was used to measure pH and SCHOTT handylab LF 1 to measure conductivity. Snow grains were photographed using the Olympus OM Ti-4 camera with a special camera stand (Pihkala and Spring, 1985) and a slide with a millimetre scale (Fig. 13). The analysis of $\delta^{18}O$ concentration

Figure 9. Snow properties were measured from the wall of the snow pit. (Photograph by K. Kanto)

values was performed from snow samples at the Laboratory of Isotope-Palaeoclimatology from snow samples, Tallinn Technical University. Surface snow samples were collected with the snow box for the Finnish Meteorological Institute (Fig. 14).

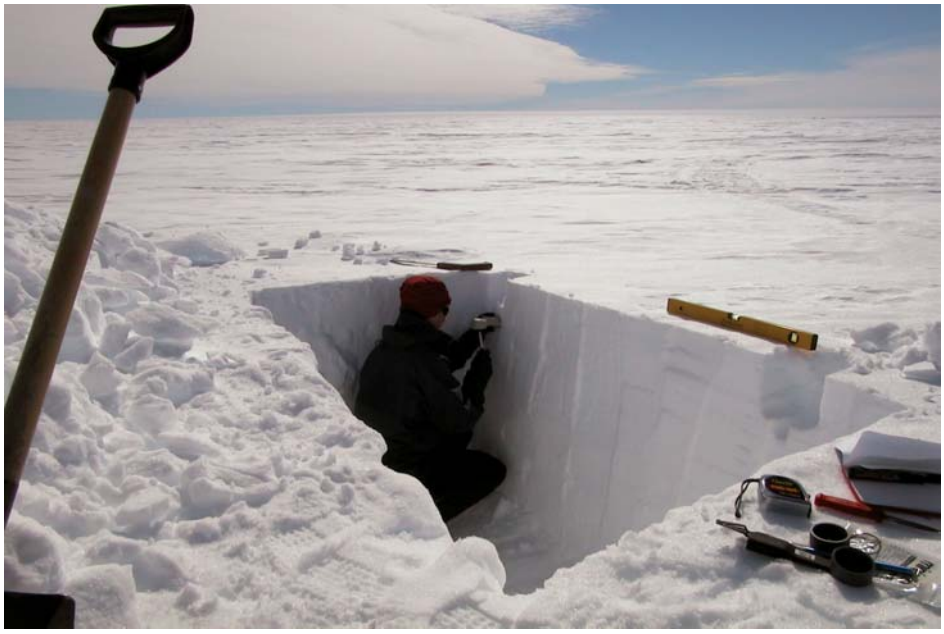

Figure 10. Snow samples were taken with a cylinder. (Photograph by K. Kanto)

Figure 11. Snow samples were weighed with a spring balance. (Photograph by K. Kanto)

Figure 12. The snow fork measures the dielectric constant of snow. (Photograph by K. Kanto)

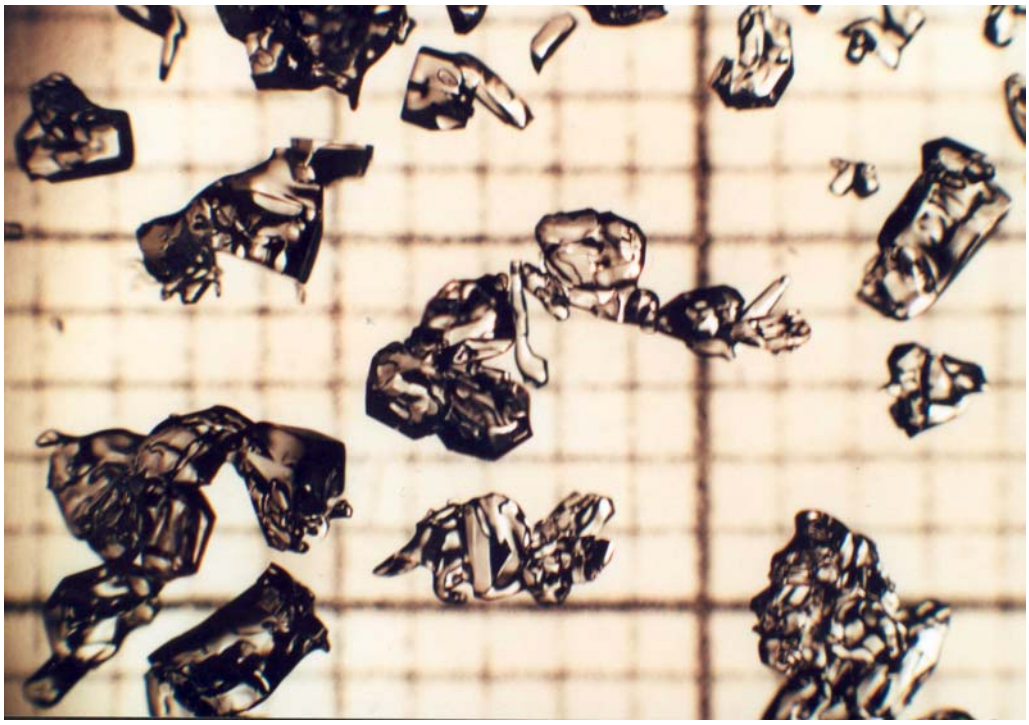

Figure 13. A millimetre scale was used to determine the size of snow grains. These grains are from 2000/2001 (site 1) in loose depth hoar at 23 cm depth. (Photograph by E. Kärkäs)

Figure 14. Sterile overalls were used when collecting snow samples from the surface. (Photograph by K. Kanto)

During the 2000/2001 season, the conductivity of the melt water of the snow samples was measured in the wet laboratory at SANAE 4 using a Cyberscan CON 10 conductivity meter. The pH was measured using an Orion 420A pH meter that was calibrated using solutions of 4, 7 and 10 respectively.

4.1.2 Ground penetrating radar

An EKKO 1000 ground probing radar system by Sensors and Software Inc.of Missisagua, Canada was employed to determine the potential usefulness of such a system in determining the internal stratigraphy of the annual layers of the snow cover, and also in determining the annual layering in the near-surface layers of the glacier. Three antennae (110, 900 and 1200 MHz) were used.

The radar system was mounted onto two Komatik sleds available at Aboa. Such sleds are constructed by tying the runners to the load platform, and, as such, do not generate significant electromagnetic interference with the radar system. For the high-frequency antennas, a small plastic sled was towed behind the aft Komatik sled. The computer and control unit was protected against the elements by a Coleman thermally insulated box that was attached to the forward sled. On the aft sled, which carried the 110 MHz antennas, an odometer was mounted. This odometer is programmable to trigger the radar system at specific user selectable distance intervals.

4.1.3 Surface ground truth measurements

Surface roughness in centimetre and meter scale was evaluated at the snow pit sites by using Sokkisha optical level and scale in 2000/2001. In some sites pictures of surface roughness in millimeter-scale was taken. Most surface roughness measurement lines were with 1 m intervals. Line was measured against prevailing sastrugi to get maximum deviations. Directions were estimated together with vertical variations. Between snow pit sites surface roughness and variations snow cover was estimated visually while driving snowmobiles (Fig. 15).

Figure 15. The compass is showing the orientation of snow erosion. (Photograph by K. Kanto)

4.2 Field measurements 1999/2000 at Aboa

Snow pit measurements covered about 350 kilometre line from the sea ice to the plateau. A map over the research area and the measurement sites are shown in Figure 2 and in Table 1. The location of the Finnish research station Aboa, the land routes used, and the RADARSAT image determined our measurement sites. In the 1997 RADARSAT mosaic from Antarctic Mapping Mission (200 m resolution) a significantly lower backscatter coefficient is observed for Högisen and Kvitkuven, which are topographic highs.

The measurements were made from 17 shallow snow pits (1-2 m), the average depth was 1.5 m. Nine automatic snow stations were deployed to measure the vertical temperature distribution over the winter, marked by * in Table 1. The used time is UTC. Tracked vehicles (two Nasu Sisus) were in the field for long distance transportation. Helicopters were used for measurement sites without known routes (Kvitkuven, Högisen and Amundsenisen), snowmobiles were used in short distances near Aboa.

The snow sensors were installed in flat, unobstructed snowfields, so as to represent conditions of steady-state snowdrift transport. They were installed at the coordinates shown in Table 2, measured by hand-held GPS.

*Table 1. Location of snow measurement sites in 1999/2000 as in Figure 2. The mark * is for the sites of the automatic snow stations.*

Site	Chronology of sites	Date	Starting time (UTC)	Latitude	Longitude	Approx. altitude (m a.s.l.)	Approx. distance from coast (km)	Snow pit depth (cm)	Air temp. (°C)	Cloud cover
1	#4	26 Dec 1999	17:00	72° 32.0'S	16° 34.0'W	40	3	100	5.0	8/8
2*	#16	18 Jan 2000	12:20	72° 36.6'S	16° 18.6'W	250	15	150	-1.6	1/8
3	#3	26 Dec 1999	9:30	72° 40.0'S	16° 41.9'W	55	20	100	-1.6	7/8
4	#2	25 Dec 1999	20:00	72° 45.2'S	14° 18.3'W	70	75	200	-2.3	7/8
5*	#5	2 Jan 2000	15:20	72° 57.9'S	13° 34.7'W	270	110	150	-1.1	1/8
6	#1	24 Dec 1999	14:20	73° 02.0'S	13° 19.5'W	250	120	200	-4.2	7/8
7	#6	3 Jan 2000	18:45	73° 03.6'S	13° 21.8'W	250	120	100	-4.3	1/8
8	#7	5 Jan 2000	17:40	73° 05.3'S	13° 20.2'W	240	120	120	1.6	6/8
9*	#17	23 Jan 2000	17:00	73° 04.1'S	13° 28.2'W	235	125	150	-1.0	-
10*	#9	8 Jan 2000	15:00	73° 12.5'S	13° 13.0'W	375	140	150	-3.4	2/8
11*	#8	6 Jan 2000	12:40	73° 26.3'S	14° 26.7'W	990	130	200	-3.3	0/8
12*	#10	10 Jan 2000	11:15	73° 27.4'S	12° 33.3'W	905	170	150	-5.5	7/8
13	#11	10 Jan 2000	22:35	73° 43.0'S	12° 18.6'W	930	195	110	-10.2	7/8
14*	#12	12 Jan 2000	15:00	74° 00.8'S	12° 01.1'W	980	230	150	-5.2	8/8
15	#13	12 Jan 2000	21:15	74° 13.9'S	11° 48.0'W	1000	250	130	-7.9	7/8
16*	#14	13 Jan 2000	22:00	74° 28.7'S	11° 33.1'W	1100	275	220	-9.1	8/8
17*	#15	14 Jan 2000	15:00	74° 59.9'S	10° 00.5'W	2550	355	160	-15.5	2/8

Table 2. Locations of the snow stations

Date	Snow site (Table 1)	Latitude	Longitude	Snow sensor #
18 Jan 2000	2	2° 36.6'S	16° 18.6'W	8
2 Jan 2000	5	72° 58.0'S	13° 34.7'W	1
23 Jan 2000	9	73° 04.1'S	13° 28.2'W	9
8 Jan 2000	10	73° 12.5'S	13° 13.0'W	3
6 Jan 2000	11	73° 26.3'S	14° 26.7'W	2
10 Jan 2000	12	73° 27.4'S	12° 33.3'W	4
12 Jan 2000	14	74° 01.1'S	12° 01.1'W	5
13 Jan 2000	16	74° 29.0'S	11° 33.1'W	6
14 Jan 2000	17	75° 00.0'S	10° 00.5'W	7

The RADARSAT SAR mosaic showed a significantly lower backscatter coefficient for Högisen (Sensor #2) and Kvitkuven (Sensor #8) (Fig. 2). Sensor #9, originally intended for installation on the ice shelf near Ramppi was relocated to our radar test site subsequent to two unsuccessful attempts to reach the ice shelf location by helicopter.

Most of the radar work was carried out at the Radar Site (where we installed Snow sensor #9), where SWEDARP members had already extracted a 20 m deep core for stratigraphic analysis and where studies had also been made using another type of ground probing radar. The main tuning of the radar was made at this site and test profiles were made using different antenna frequencies. The profiles were oriented parallel to and perpendicular to the prevailing direction of snow transporting winds.

4.2.1 Preliminary snow pit results 1999/2000

In Appendix A are seen measured snow pit profiles from the season 1999/2000. Table 3 shows a summary of the snow pit measurements. Most are in situ data, but conductivity, pH and $\delta^{18}O$ have been analysed from melted samples. $\delta^{18}O$ profiles are only from five sites and they were taken with too coarse resolution, providing only rough estimates for the accumulation. According to $\delta^{18}O$ analyses the first summer peak was found in 80 cm depth on the ice shelf, in 60 cm depth near the grounding line and in 40 cm depth behind Vestfjella mountain range. The lowest temperature –34.5°C measured in Amundsenisen (site 17) from 440 cm depth while installing a snow sensor. Only in two places (sites 13 and 16) temperature maximum was under the surface. Those places were measured close to midnight. Daily temperature variations had an effect down to 0-30 cm depth. That was seen in temperature profiles made late at evening. An average temperature gradient of 30-150 cm was –0.05 °C cm^{-1} and in depth of 150-400 cm it was –0.02 °C cm^{-1}. Temperature values have a strong correlation with surface height (r = -0.91) and a good correlation with the distance of sea (r = -0.87).

Table 3. Summary of snow pit measurements in 1999/2000: mean values, standard deviations (S.D.) and standard errors (S.E.).

Site	Temp. gradient 30-100 cm ($°C\ cm^{-1}$)	Density 0-100 cm ($kg\ m^{-3}$)	Grain diameter 0-100 cm (mm)	Surface Dielectric constant	Conductivity 0-100 cm ($\mu S\ cm^{-1}$)	Number of ice layers (m^{-1})	$\delta^{18}O$ 0-100 cm (‰)	Albedo	Approx. accum. ($mm\ w.e.\ a^{-1}$)
1	-0.05	420	5	2.07	99.4	6	-	0.85	340
2	-0.05	390	-	1.44	13.2	3	-16.46	-	260
3	-0.07	445	2	1.89	16.9	2	-	0.86	360
4	-0.07	415	1	1.65	5.7	0	-	0.86	340
5	-0.06	425	1	1.83	4.7	2	-20.55	0.82	335
6	-0.07	395	1.5	-	-	-	-	0.88	
7	-0.03	400	1.25	1.75	15.8	5	-	-	
8	-0.04	465	0.75	1.81	9.9	2	-26.14	-	230
9	-0.03	390	-	1.71	-	5	-	-	240
10	-0.02	435	1.5	1.85	4.8	7	-	0.81	220
11	-0.04	320	1.5	1.34	4.3	0	-19.25	-	
12	-0.04	410	1	1.71	6.5	8	-	0.81	205
13	-0.05	425	1	-	4.9	7	-	-	
14	-0.05	430	-	1.65	7.6	9	-29.91	0.86	160
15	-0.05	425	-	1.71	-	10	-	-	
16	-0.07	390	1.25	1.69	3.4	8	-	0.85	190
17	-0.07	380	-	-	2.3	8	-	-	100
Mean	-0.05	409	1.6	1.72	7.7*	5	-22.46	0.84	250
S.D.	0.02	32	1.1	0.2	4.8	3	5.45	0.03	
S.E.	0.005	8	0.3	0.05	1.3	1	2.44	0.01	

*Site 1 has been left out from the mean value.

In Figure 16 are seen how the temperature of one-meter depth and the upper meter average density, grain size, conductivity, number of ice layers and surface dielectric constant varied from the coast to inland. Near the coast there were thick (1-5 cm) ice layers, but above the grounding line there were many thin (0.5-2 mm) ice layers in the top meter. In Högisen (site 11) there were no ice layers in the top meter. In the density and dielectric constant graph lower values are from local topographic highs (Högisen and Kvitkuven). The first value of conductivity is from the edge of the ice shelf. On the sea ice conductivity of snow was 2.7 mS cm^{-1}. The first value of dielectric constant is from snow cover above the sea ice. The grounding line is located about 80 km from the coast.

The snow cover was strongly layered because of sastrugi topography. Snow was wind packed but still hard with alternating softer layers. In the summer time strong radiation forms ice layers on the surface. On average the first meter of snow pack contained five ice layers. Near the coast ice layers were few centimetres thick and farther inland only few millimetres thick. Ice layers had a good correlation with surface height (r=0.70). An average density of top meter was 409±8 kg m^{-3} in the whole area. On the ice shelf snow density was higher than behind the grounding line. Local

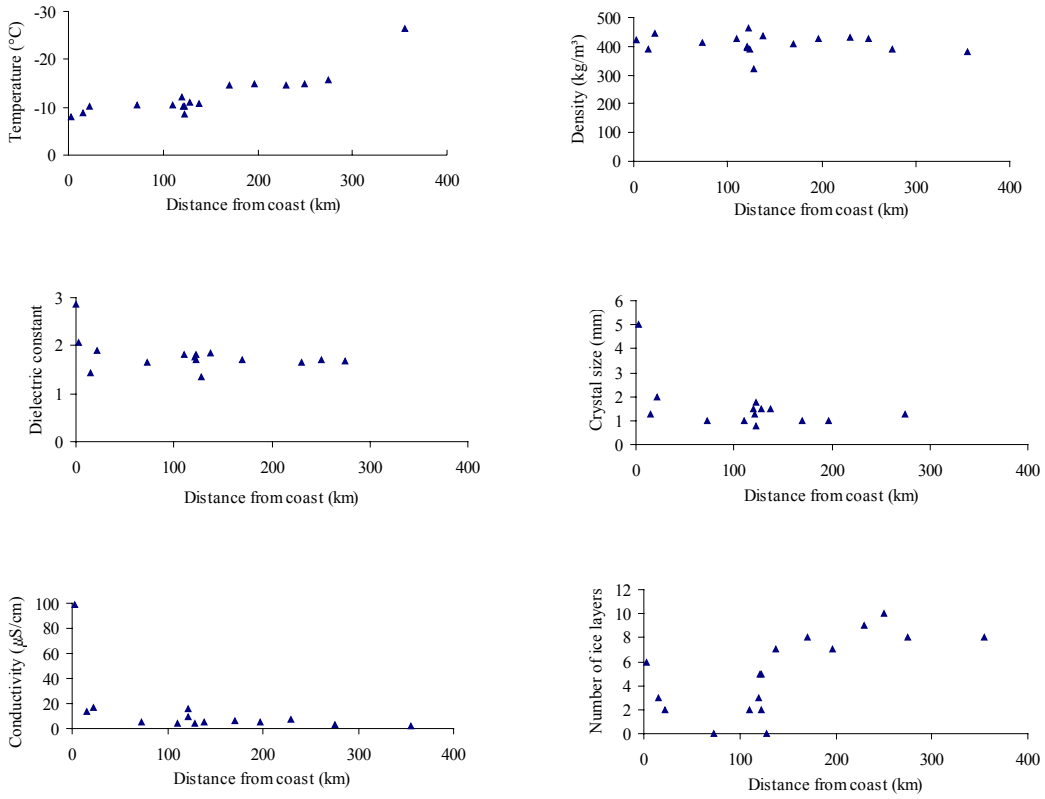

Figure 16. Plot showing variations of the measured quantities with distance from coast. Mean values over first meter for density (kg m^{-3}), crystal size (mm), conductivity (μS cm^{-1}) and number of ice layers. Temperature (°C) has been measured from one-meter depth and dielectric constant from the surface.

topographic highs (Kvitkuven and Högisen) had lower density snow than the surroundings and they also had the clearest increase of density with depth. Approximate accumulation values have been calculated from oxygen isotope data and snow pit stratigraphy.

An average grain diameter was 1.5-2 mm in the whole area. On the surface the average was 1 mm. According to The International Commission on Snow and Ice of the International Association of Scientific Hydrology (ICSI) classification (Colbeck et al., 1990) most grains had a shape of 3lr i.e. big (>0.5 mm) well rounded particles (Fig. 17). Hard winds and strong solar radiation make grains round at a very early state. In some profiles there was a clear increase of grain size with depth. The biggest grains were near the edge of the ice shelf. Near the ice edge melting occurred and the grains stack together (class 6mf, rounded polycrystals). Högisen was exception. In the 0-60 cm layer grains of 2dc and 2 bk classes were found. Grains still had shapes of precipitation particles. Surface grain size have a correlation with a distance from sea (r = -0.55) also grain sizes of the first 0-100 cm had some correlation with distance (r = -0.37).

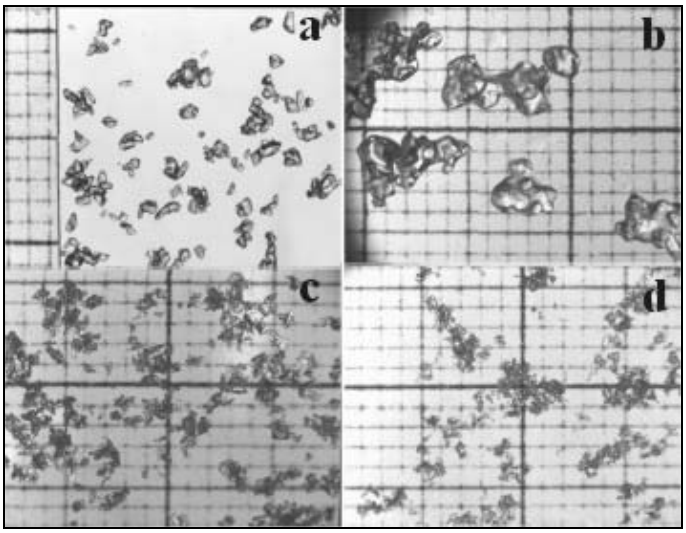

Figure 17. Snow grains from three different sites in 1999/2000: a) well-rounded particles at 20 cm depth near Aboa station, they look like average grains found in the area; b) big polycrystals at 20 cm depth found near the coast; c) surface grains from Högisen ice dome, fragments of the precipitation particles can be seen; and d) grain from 60 cm depth in Högisen, some forms of the precipitation particles can still be seen. The background is a millimetre scale. (Photographs by E. Kärkäs)

Figure 18 shows the dielectric constant (ε_r) measurements as a function of density. The linear trendline $\varepsilon_r = 0.9+2.2\rho$(g cm^{-3}) is near the empirical formula $1.0+2.1\rho$ of Ulaby (1986). The average dielectric constant of surface was 1.72±0.05 and the average of all measurements was 1.81±0.02. Topographic highs had the lowest values. Surface dielectric constant had some correlation with the distance of sea (r = -0.38). According to dielectric constant values the average volume snow wetness was 0.9±0.1 %. The measured snow can be considered to be dry.

Conductivity and pH were measured from melted samples. Snow salinity was less than 10^{-4} in every measurement site on the continent but on the sea ice it was 2 ppt. The site near the ice edge (site1) had the highest conductivity (99.4 µS cm^{-1}). When we leave that out of measurements, the

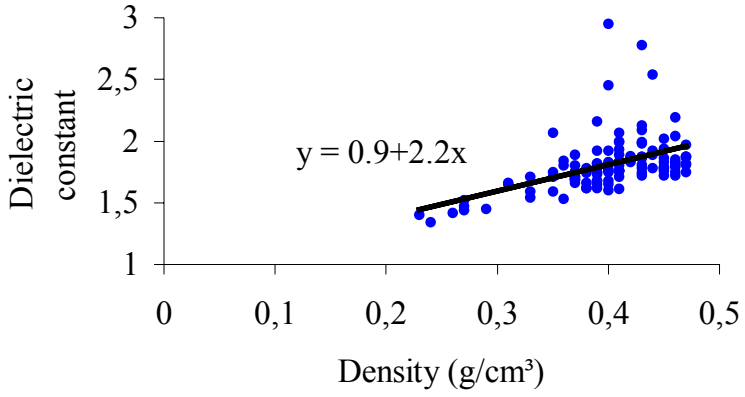

Figure 18. Dielectric constant vs. density (g cm^{-3}).

average is 7.7±1.3 μS cm^{-1}. Snow on the sea ice had an average value of 2.9 $mScm^{-1}$. On the continent the average value of pH was 6.7±0.1. Conductivity of the top 0-100 cm layer had a correlation with distance from sea (r = -0.52) and pH of surface had a correlation with distance from the coast (r = -0.50). In Table 4 correlation values for snow properties with the distance from sea and the surface elevation are seen. Temperature values had the best correlation.

The snow cover of the study area can be divided to five zones; 1) sea ice, 2) the seaward edge of the ice shelf, 3) the inner parts of ice shelf, 4) the glaciers above the grounding line and 5) the local topographic highs. Topographic features near the grounding line block partly the moist air masses coming from the Southern Ocean (Bromwich, 1988). Ice domes and ice rises are locally high points rising from the ice sheet. They are not so much exposed to katabatic winds.

Compared to snow on the ice sheet the sea ice has an annual snow cover that is shallow because of strong winds and formation of snow-ice. Snow on sea ice was saline and had a high conductivity. Near the edge of the ice shelf there occurred big snow grains and thick ice layers because of summer melting. Measured moisture values decreased with increasing distance from the sea. Temperature values had the highest correlation. Dielectric constant, wetness, conductivity and pH of the surface decreased inland from the coast. The effect of the grounding line was seen in the number of ice layers and in grain sizes.

Interesting phenomena were the local topographic highs. They had different snow conditions compared to their surroundings. Blue ice areas and nunataks can be seen as exceptional snow accumulation areas. In the future those will be very interesting to investigate.

4.2.2 Preliminary snow radar results 1999/2000

A preliminary analysis indicates that using 110MHz antennas, the EKKO1000 can probe the snow layering structure to depths well beyond 100 m. At this frequency, it appears that the radar is capable of resolving the main annual layering and some intermediate stratigraphic features. At

Table 4. Correlation between snow properties and both the distance from the coast and the surface elevation.

Quantity	Distance	Elevation
Temperature (surface)	-0.87	-0.91
Temperature (1 m)	-0.88	-0.92
Density (surface)	0.09	0.06
Density (0-100 cm)	-0.16	-0.12
Grain size (surface)	-0.55	-0.28
Grain size (0-100 cm)	-0.37	-0.17
Dielectric constant (surface)	-0.38	-0.20
Wetness (surface)	-0.32	-0.13
Wetness (0-80 cm)	-0.04	0.04
Conductivity (surface)	0.07	-0.23
Conductivity (0-100 cm)	-0.52	-0.36
pH (surface)	-0.50	-0.42
pH (0-100 cm)	-0.36	-0.56
Number of ice layers	0.66	0.70

the radar calibration site (snow site 9), the annual snow depth increment is approximately one meter. A more precise determination would require a set up for velocity determination, which, unfortunately, we did not have time to do during this field season. Our primary aim for this first season was merely to determine the potential usefulness of the radar system in determining snow stratigraphy.

The 900 MHz antennas gave good signal to well beyond 20 meters depth. At this frequency, the radar is able to resolve intermediate layering in the snow cover. It appears that the summer layers can be distinguished from other stratigraphic features by their greater horizontal continuity. The difference may be produced by the tendency for ice layers to form on the snow surface and internal ice layers to form by the freezing of infiltrating water from near surface melt. It may also indicate that the wintertime snow accumulation regime is different from that of the summer, perhaps with more accentuated sastrugi forms during the wintertime. There were visual differences between profiles obtained along with and perpendicular to the main snow transport direction.

The 1200 MHz antennas also gave excellent penetration in the cold snow at the test site. However, a preliminary visual analysis suggests that there may be noise problems at depths greater than about six meters. The resolution is somewhat better than for the 900 MHz antennas.

The preliminary conclusions from the radar surveys are that the EKKO1000 is capable of giving useful information on annual accumulation rates to depths well beyond 100 m. At Aboa this covers snow layers deposited over the past approximately 100 years. Greater stratigraphic detail is obtainable to depths in excess of 20 m using the 900 MHz antennas. Useable data were obtained to a depth of about six meters using the 1200 MHz antennas, but the signal appears noisy beyond this depth. The results suggest that the radar can be used to examine spatial variations in snow accumulation rates and also to examine spatial and temporal variations in snow layering characteristics.

4.3 Field measurements 2000/2001 at Aboa

Measurements were made in western Dronning Maud Land in Maudheimvidda area (Fig. 2) during the FINNARP 2000 expedition. The location of the Finnish research station, known routes, previous measurements and the installed snow sensors determined the measurement sites. The first priority was to remove all snow sensors and then to repeat the same measurements as was made a year before. Time and logistic support were more limited. Snowmobiles were used for the most of the transportation, helicopter for sites without known routes (Kvitkuven, Högisen and Amundsenisen).

The snow pit measurements covered about a 350 kilometer line from the edge of the ice shelf to the plateau. There was no possibility to make snow measurements on sea ice this year. The measurement sites are listed in Table 5 using the same numbering than in Figure 2. Totally 11 main snow pits were accomplished. In addition, there were two snow lines (snow line 1 and snow line 2) between Basen and Plogen nunataks and five minor snow pits (a-f); measurements were made at surface only. The used time is UTC.

Measurements of the surface roughness were made with a grid of 10 x 10 m with 1 m spacing. Other more intensive surface topography lines were measured close to Aboa, associated with GPR measurements.

Table 5. Location of snow measurement sites in 2000/2001 in the vicinity of Aboa. Site 3 was not exactly in the same location than in 1999/2000.

Site	Chronology of sites	Date	Starting time (UTC)	Latitude	Longitude	Approx. altitude (m a.s.l.)	Approx. distance from coast (km)	Snow pit depth (cm)	Air temp. (°C)	Cloud cover
Snow pits:										
1	#11	30 Jan 2001	21:45	72° 31.960'S	16° 33.983'W	45	0.2	120	-10.4	8/8
2	#7	20. Jan 2001	10:05	72° 36.570'S	16° 18.535'W	240	10	115		0/8
3*	#4	7. Jan 2001	13:45	72° 44.940'S	16° 00.083'W	60	30	130	-1.3	2/8
5	#3	3. Jan 2001	12:30	72° 57.852'S	13° 34.592'W	270	110	110	1.3	4/8
9	#1	29. Dec 2000	12:00	73° 04.080'S	13° 28.250'W	235	120	110	-0.1	7/8
10	#2	2. Jan 2001	13:00	73° 12.498'S	13° 13.037'W	375	130	110	2.9	1/8
11	#6	13. Jan 2001	10:00	73° 26.219'S	14° 26.730'W	990	120	150	-7.9	1/8
12	#10	24. Jan 2001	11:00	73° 27.363'S	12° 33.323'W	905	165	100	-7.8	2/8
14	#9	23. Jan 2001	10:45	74° 00.801'S	12° 01.066'W	980	215	110	-5.1	7/8
16	#8	22. Jan 2001	12:00	74° 28.668'S	11° 33.131'W	1100	260	110	-7.5	3/8
17	#5	12. Jan 2001	13:00	74° 59.854'S	10° 00.448'W	2540	350	100	-11.8	0/8
Snow line 1:										
1		1. Jan 2001	16:30	73° 07.003'S	13° 33.286'W	37	120	48	1.6	8/8
2		1. Jan 2001	16:55	73° 06.519'S	13° 32.166'W	246	120	44		
3		1. Jan 2001	17:35	73° 06.023'S	13° 31.367'W	239	120	60		
4		1. Jan 2001	18:00	73° 05.561'S	13° 30.538'W	218	120	40		
Snow line 2:										
1		10. Jan 2001		73° 02.542'S	13° 48.899'W	250	120	25		0/8
2		10. Jan 2001		73° 11.821'S	13° 47.827'W	233	120	49		0/8
3		10. Jan 2001		73° 10.617'S	13° 44.789'W	233	120	50		0/8
4		10. Jan 2001		73° 09.302'S	13° 41.484'W	230	120	45		0/8
5		10. Jan 2001		73° 07.980'S	13° 38.079'W	218	120	45		0/8
Minor snow pits:										
a		6. Jan 2001	16:15	72° 49.159'S	14° 00.059'W	210	85	45	-1.0	1/8
b		6. Jan 2001		72° 45.112'S	14° 11.667'W	141	75	55		
c		6. Jan 2001	19:30	72° 45.262'S	14° 30.203'W	68	70	55		
d		6. Jan 2001	20:40	72° 45.278'S	15° 00.180'W	65	55	70		
e		6. Jan 2001	22:30	72° 45.152'S	15° 30.010'W	68	40	70		
f		21. Jan 2001	17:50	74° 34.563'S	11° 13.254'W	1254	280	36	-6.5	

4.3.1 Preliminary snow pit results from Aboa area 2000/2001

In Appendix A are seen measured snow pit profiles from the season 1999/2000 from Maudheimvidda area (Fig. 2). Table 6 shows the summary of snow pit measurements. Only 11 main snow pits have been listed. Approximate accumulations have been calculated from oxygen isotope ratios, conductivity values and snow pit stratigraphy.

In Figure 19 can be seen how the snow characteristics varied with the distance from the coast. There are shown the variations of air temperature, surface temperature, temperature of one meter, average density over the first meter, grain size of surface, average grain size over the first meter, conductivity of surface, average conductivity over the first meter, pH of surface, average pH over the first meter and number of ice layers in the first meter of snow pack.

Table 6. Summary of snow pit measurements from Aboa area 2000/2001.

Site	Temp. gradient 30-100 cm (°C cm^{-1})	Density 0-100 cm (cylinder) (kg m^{-3})	Density 0-100 cm (snow fork) (kg m^{-3})	Grain diameter 0-100 cm (mm)	Dielectric constant 0-100 cm	Conductivity 0-100 cm (µS cm^{-1})	pH 0-100 cm	Number of ice layers 0-100 cm	$\delta^{18}O$ 0-100 cm (‰)
1	-0.04	349	301	1.6	1.66	18.3	5.9	4	-15.43
2	-0.04	383	332	1.6	1.69	9.8	5.5	6	-18,07
3	-0.08	383	360	1.5	1.73	5.3	5.8	3	-21.01
5	-0.07	387	368	2.6	1.75	3.3	5.9	5	-20.85
9	-0.04	388	379	1.5	1.77	3.7	6.1	4	-21.49
10	-0.06	393	397	2.5	1.80	3.7	7.2	3	-24.40
11	-0.04	387	363	1.3	1.71	3.8	5.4	2	-26.27
12	-0.05	345	355	1.5	1.75	2.5	5.6	6	-24.16
14	-0.04	390	352	1.6	1.75	3.3	5.3	5	-32.26
16	-0.05	374	328	1.4	1.68	2.7	5.3	3	-31.19
17	-0.06	350	322	1.5	1.65	2.5	6.3	12	-36.53*

* 0-30 cm average

Site	Surface temp. (°C)	Surface density (cylinder) (kg m^{-3})	Surface density (snow fork) (kg m^{-3})	Surface grain diameter (mm)	Surface dielectric constant	Surface conductivity (µS cm^{-1})	Surface pH	Approx. accum. (mm w.e. a^{-1})
11	-8.8	120	77	0.5	1.17	5.5	6.0	300
7	-4.8	180	121	1.5	1.26	7.7	-	290
4	-0.7	340	319	2	1.62	4.3	6.0	310
3	0.2	-	255	2.5	1.49	3.3	6.6	220
1	0.1	320	400	2.5	1.79	6.1	7.9	200
2	0.2	320	332	2	1.75	-	8.0	165
6	-5.7	320	76	1.5	1.21	5.6	5.4	-
10	-6.2	180	181	1	1.33	3.7	-	180
9	-6.1	240	191	0.5	1.38	3.2	5.3	220
8	-7.8	260	212	0.5	1.45	3.6	5.5	200
5	-14.7	328	294	1	1.59	3.2	7.4	70

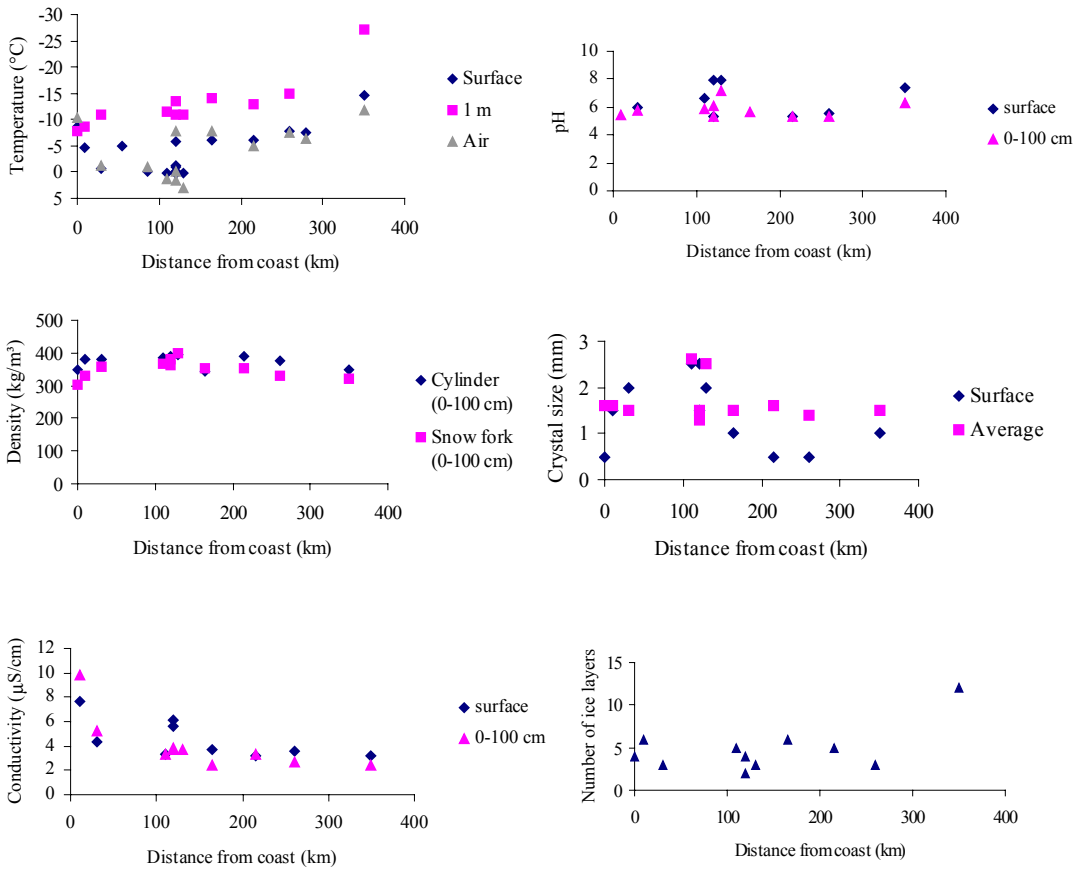

Figure 19. The variations of the snow characteristics with the distance from the coast. Air temperature (°C), surface temperature and temperatures of one meter are seen on the top as well as pH values for surface and the average over the first meter. Density values (kg m^{-3}) show an average over the first meter measured both with the cylinder kit and with the snow fork. Grain size (mm) and conductivity values (µS cm^{-1}) are from surface and an average over the first meter. Number of ice layers tells an average over the first meter.

Temperature values measured every 2 to 5 cm and the average temperature gradient of 30-100 cm was –0.05 °C cm^{-1}. Temperature values had a good correlation with the distance from the coast and with the surface elevation. The correlation of the surface temperature with the distance from the sea was –0.55 and with the elevation was –0.78. For the 1m temperature, these values were –0.87 and -0.96. Near the surface strong solar radiation might have had an effect to temperature values. Temperatures were attempted to be measured always from the shadow wall of snow pit.

Density measurements were done both with the cylinder density kit (volume 0.25 dm^3) and with the snow fork. Snow fork measures the density and the liquid water content of snow from dielectric constant. Density kit measurements give average over five centimetres. Samples were weighted with precision scale with accuracy of ±10 g. With the density kit densities measured every five to 10 centimetres and with the snow fork every two to five centimetres depth. The surface density measured with the density kit refers thus to the average over 0-5 cm. Density kit results gave an average density of 385±2 kg m^{-3} of first meter to the whole area while snow fork data give 351±7 kgm^{-3}.

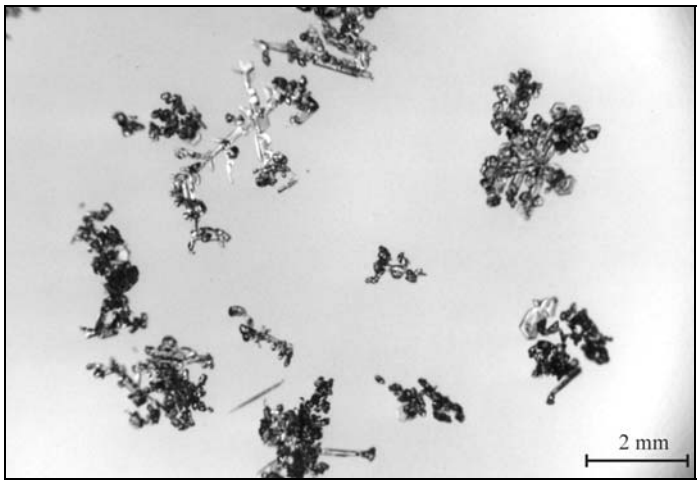

Figure 20. Surface grains from the site 1 in 2000/2001. Forms of stellar shape crystals are still visible. (Photograph by E. Kärkäs)

The year before, in the season 1999/2000, the average of top meter was 409±8 kgm^{-3}. This season was quite stormy and that might have had influence to higher densities. Snow fork measures density of one-point but cylinder measures average over five centimetres. That partly explains the variations. The correlation between cylinder values and snow fork varied from very poor 0.14 to good 0.87.

Snow grains were photographed for their size and shape. Here as the size refers to the diameter of the grain. Most of the grains were either large rounded particles, classified 3lr according to The International Commission on Snow and Ice of the International Association of Scientific Hydrology (ICSI) classification (Colbeck et al., 1990) or solid faceted particles and can be classified 4fa (ICSI). Solid faceted particles were found in loose depth hoar layers in the snow pack. The grains got their rounded shape quite early due to rough winds and strong radiation. Surface layers of new snow consisted often many forms of grains. Partly decomposed precipitation particles (2dc and 2bk) are seen in Figure 20 and surface hoar grains in Figure 21. Usually under the ice layer, even very thin one (1 mm), there was a loose grained layer of big cup-shaped depth hoar grains (Fig. 22). The average size over the top meter layer was 1.7±0.06 mm in the whole area.

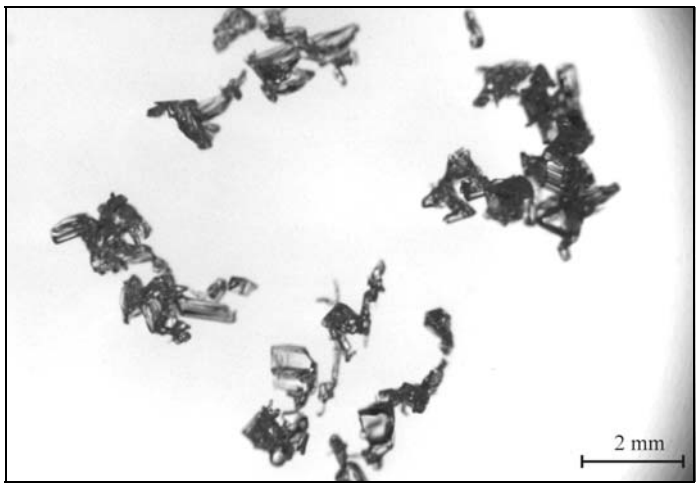

Figure 21. Faceted surface hoar grains near Plogen nunatak from the snow line 2 in 2000/2001. (Photograph by E. Kärkäs)

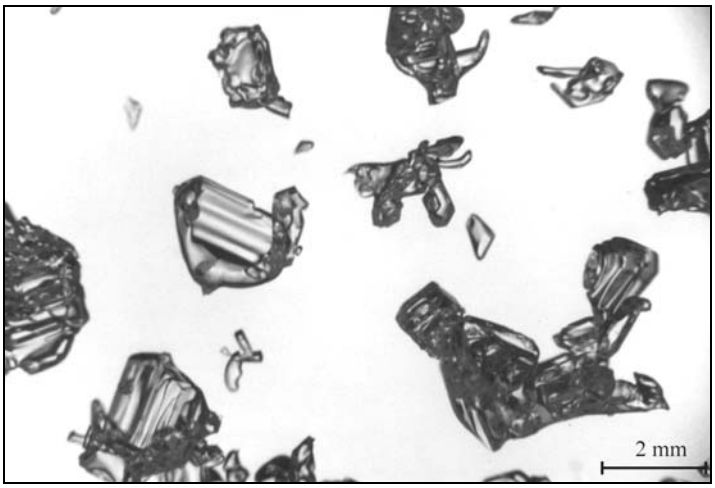

Figure 22. Depth hoar grains with some cup-shaped forms from very loose layer found in site 14 at 12 cm depth. (Photograph by E. Kärkäs)

Dielectric constant and snow wetness were measured with the snow fork. The snow fork measures both the real and imaginary part of dielectric constant. In dry snow the imaginary part can be left out (Hallikainen and Winebrenner, 1992). Measurement profiles with the snow fork have been started from 2 cm depth. Profiles have been measured every 2 to 5 cm intervals. The average dielectric constant of the surface in the measurement area was 1.5 and the average over top one meter was 1.7. Lowest values were from the local topographic highs; Kvitkuven and Högisen. Also during the season 1999-2000 the ice dome and the ice rise had the lowest values. Those have also lower backscatter coefficients in the RADARSAT mosaic compared to the other measurement sites. Average dielectric constant was decreasing inland. Near the coast the top first meter consisted mainly of accumulation of one year but inland on the polar plateau the first meter included accumulation from up to 4 - 5 years. The average surface wetness expressed by volume was 0.5 % and by weight 2.5 %. The average wetness over the first meter was 0.4 % as volume per cents and 1.3 % as weight percents.

PH and conductivity κ were measured from the melted samples. The average surface values were pH = 6.5 and $\kappa = 4.6$ $\mu S\ cm^{-1}$. The average values of the first meter were pH = 5.8 and $\kappa = 5.4$ $\mu S\ cm^{-1}$. Near Vestfjella mountain range (120 km from the coast) there were high pH values. The pH values are very difficult to determine even in laboratory and these values can only give a rough estimate. There was correlation between conductivity and the distance from the coast. For surface values it was –0.69 and for the first meter it was –0.72. Distance from the coast and moisture sources effected to conductivity level, which decreased inland.

Ice layers were found in the snow cover at all sites. Most of the layers are thin (0.5-1 mm) and formed due to solar radiation and winds. Wind-glazed ice crust forms during autumn when there are hiatus in snow supply. Radiation glaze forms during summer and during spring wind-glazed ice crust can also form, but it is not as hard as the one forming in autumn (Goodwin, 1991). Near the coast thicker ice layers (0.5-5 cm) were found. Summer melting occurs in the coastal areas. It is stronger in lower elevation than in the ice rise (Kvitkuven). In Amundsenisen there where a lot of thin ice layers (0.5-1 mm) in the first meter of snow pack and the first meter consisted several years accumulation and the thin ice layers tell about seasonal variations. In some cases there were loose big-grained layers under the ice layer formed by sublimation. At the end of the season thicker ice layers were found near Basen situated 120 km from the coast. There were percolation

pillars from the surface down to 30-50 cm and thick ice layers (1-2 cm). Strong summer melting

occurs also that far from the coast. On average there were 5 ice layers in the first meter of the snow pack. Near the coast there were both thin and thick layers. Further inland there were thin ice layers.

Conductivity and temperature had the best correlation with the distance from the coast. With the distance the surface elevation is increasing moving inland from the coast. This increase in elevation affects the temperatures. Conductivity depends on moisture and snow coming from the north and values decrease with the distance from the coast. Melting occurred quite far inland (120 km) and percolation zones seem to be behind the grounding line. Most of the ice layers seemed to be formed due to radiation and wind and were only 0.5-1 mm thick. Especially surface pH had high values near Vestfjella nunatak range. Material coming from the nunataks can have an influence on pH. Local topographic highs had lowest dielectric constant values and less ice layers in the first meter of snow pack. Winds are mainly blowing along the valleys and ice domes and ice rises are not so much influenced by them.

4.4 2000/2001 season at SANAE 4

An overview of the main measurements made and the field locations is given in Table 7. The campaign was started on 26 Dec 2000 on the southern buttress of the Vesleskarvet nunatak. Radiation measurements were made using the LI1800UW and EP16. The Gantner datalogger did not switch on even though the battery voltage was over 12V, and therefore the pyranometer millivolt values were measured using a digital voltmeter. Measurement site 2 km east of SANAE 4 was set up on 27 Dec 2000. Stakes for accumulation measurements were put into the snow. A snow pit was dug at this time at this site. There was 1/8 cloud with the solar disc visible.

Site 1 was revisited for the first time on 28 Dec 2000. The albedometer was started at 10.44 UTC Z with the head of the instrument 71cm above the snow. It was set to scan at 10 s intervals and record the average of 5 min. The problems with the Gantner datalogger did not recur. The spectral albedo was measured adjacent to (10 m away from) the stake line. There was 6/8 cloud on this day, and the solar disk was visible behind cloud. A digital maximum / minimum thermometer (biltema) was left on the albedometer tripod with one sensor buried under the snow and one sensor in the thermometer unit itself. This instrument was only used to get an idea of the daily variation in temperature.

The Gantner datalogger had stopped logging data at some time before site 1 was visited on 31 Dec 2000 due to the battery voltage becoming too low. During this visit, the maximum / minimum temperature was checked and the height of the stakes was measured. On 2 Jan 2001 two stakes were put into the snowdrifts on the southern side of the base. Stake 1 was 10 m away to the west and stake 2 was 50 m to the west. On the next day observations were made at Site 1 including spectral albedo. The stake array was measured and surface samples for density analysis were taken adjacent to the stakes. The cloud cover was 1/8 in the morning going to 4/8 and then to 6/8 by 14:30. The solar disc was visible initially and then it went behind cloud but remaining visible. The albedometer was set to scan at 10 s intervals and to average 2 min worth of scans. A wind speed profile above the snow was measured using a handheld anemometer. This measurement was made just to get an estimation of the aerodynamic roughness length of the surface.

Table 7. Overview of the research activity at SANAE 4, season 2000/2001

Date	Activity
26 Dec	Radiation measurements on the Southern butress of Vesleskarvet
27 Dec	Stake array set up and snow pit at site 1
28 Dec	Radiation measurements at site 1
31 Dec	Stake array measured
2 Jan	Snow observations at SANAE 4
3 Jan	Radiation measurements at site 1
5 Jan	Observations at site 1
7 Jan	Observations at site 1
8 Jan	Snow pit at site 1
10 Jan	Snow observations at SANAE 4
11 Jan	Radiation measurements at site 1
12 Jan	Observations at site 1, blue ice observations in windscoop below Vesleskarvet
14 Jan	Snow pit at site 2 9km east of SANAE 4
15 Jan	Snow pit at site 1
17 Jan	Snow pit at site 3 behind Lorentzenpiggen
18 Jan	Observations in windscoop below Vesleskarvet
21 Jan	Observations and radiation measurements at site 1
24 jan	Observations at site 1
25 Jan	Wind speed measurements at SANAE 4
26 Jan	Snow pit and radiation measurements at site 1
28 Jan	Snow pit at site 4 adjacent to Robertskollen
29 Jan	Radiation measurements in windscoop below Vesleskarvet

Coordinates	
Site 1	71°40.30'S 002° 46.79'W
Site 2	Between SANAE 4 and Knotten
Site 3	Southern side of Lorentzenpiggen
Site 4	On GPS-route SANAE-E-base adjacent to Robertskollen

Observations at site 1 were continued on 5 Jan 2001. The albedometer was still working but there was some ice build up on the top dome. Cloudcover was 8/8 at this time (16:00) with the sun visible behind cloud. On 7 Jan 2001 the albedometer was still working at 14:30. It was free from ice and straight. The cloudiness was 4/8 and the solar disc was visible. Some indications of surface melting were observed at this time.

Snow observations were made on 10 Jan. 2001 in the direct vicinity of the SANAE 4 station. There was, at 14:30, 8/8 cloud, with a solar disc visible behind cloud, blowing snow and snow fall. A sample was taken from a snowdrift that was hoped to be mainly blowing snow.

Radiation measurements were made on 11 Jan. 2001 at site 1 starting at 14:05. There was 1/8 cloud with a visible solar disc. After the spectral albedo measurements, the LI1800UW was left to measure upwelling spectral irradiance at 60 min intervals for 24 hours. The measurement head was measured to be 69 cm above the snow. The instrument body had melted into the snow and slanted away from the setup bringing the head out of the vertical. For future work it may be necessary to isolate the main body of the LI1800UW from the snow.

On 11 Jan 2001 at 23:15, observations of the blue ice areas in the northern windscoop below Vesleskarvet were made. These included drilling of the ice in search of water, and the taking of a few samples for chemical analysis. The albedometer at site 1 was checked, and the datalogger

was restarted, on 14 Jan 2001 at 13:00. There was 1/8 cloud with a visible solar disc. A snow pit was dug at site 2, which was 9 km between Vesleskarvet and Knotten. Observations were continued at site 1 on 15 Jan 2001. The albedometer was all right. The cloud was 0/8. A snowpit was dug 200 m of the previous snow pit.

A snowpit was dug at site 3 on the southern side of Lorentzenpiggen on 17 Jan 2001. At 3:15 the cloud was 1/8 with a visible solar disc. During these measurements the air temperature went to below –13 °C.

The blue ice areas in the southern wind scoop were measured 18 Jan 2001. The albedometer was visited at site 1 at 2:30. Then there was 6/8 cloud with a visible solar disc. The second snowpit was dug 200 m south of site 1 on 18 Jan 2001 at 16:00. The cloud cover was 1/8 with the solar disc visible.

A wind profile and the stake array were measured at site 1 at 12:00 on 21 Jan 2001. The cloud was 5/8 with the sun visible behind cloud. There was some blowing snow. Spectral albedo measurements were made at 17:00. The cloud was 3/8 with the sun behind cloud and there was still blowing snow around. Samples of surface snow were taken at the Knotten nunatak on 22 Jan 2001. At 0:30 there was 4/8 cloud and a visible solar disc. Site 1 was revisited on 24 Jan 2001. At 15:10 there was 8/8 cloud and an invisible solar disc.

On 25 Jan 2001 wind speed measurements at 2 m height were made around and under the SANAE 4 base to get an idea of the way in which the structure interacts with the wind. The wind profile was measured above rocks on the southern buttress. A snow pit was dug at site 1 on 26 Jan 2001. At 10:30 the cloudiness was 4/8 and the solar disc was visible behind cloud. A 22° halo ring was seen around the sun. A total albedo survey was made at 10 m intervals going east from the stake line. After this, the total albedo measurements were discontinued. There was 5/8 cloud and a totally visible solar disc at 15:00 when spectral albedo measurements were made.

A snowpit was dug at site 4, which was on the vehicle route from SANAE 4 to the coast adjacent to Robertskollen on 26 Jan 2001. At 2:40 the cloudcover was 3/8 and the sun was visible behind cloud. Spectral albedo measurements were made on the different types of blue ice surfaces on 29 Jan 2001 on the southern windscoop blue ice. For these measurements, the cloud was 3/5 and the solar disc was behind cloud. The densities from all snowpits are shown in Table 8.

4.4.1 Preliminary snow pit results from SANAE 4 2000/2001

The maximum value from a snowpit on the southern side of the Lorentzenpiggen nunatak (site 3) at a depth of 75-80 cm. The minimum value was from a fresh snow drift from in front of the SANAE 4 station. As can be seen from the results in Table 8, the density increases with depth. An exponential fit between all of the density values with depth yielded a correlation coefficient of

Table 8. The maximum, minimum and average densities (kg m^{-3}) for the surface layer, for the whole snowcover and for three different layers from the top down.

	average	max	min	Std
surface	431,7	534,2	346,9	50,0
total	497,6	579,3	346,9	51,5
0-30	478,5	550,2	348,0	40,3
30-50	521,9	562,8	476,9	26,4
50-	545,9	579,3	504,6	23,5

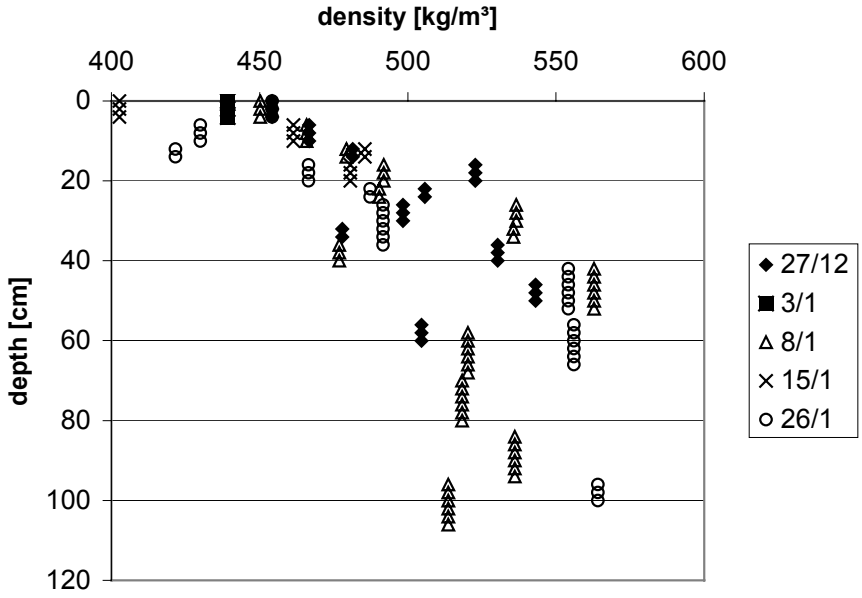

Figure 23. Density profiles from Site 1 for 5 different dates.

0.49 (N=241). A polynomial fit of second order gave a much better correlation coefficient (0.64) but a second order polynomial function for density as a function of depth has no physical basis and cannot be used for mass balance work, which needs a physical model of the density of snow as a function of depth.

The density profiles for 5 different dates at site 1 are shown in Figure 23. The increase with depth is very clearly shown in this figure and it is strongest in the first 40 cm. Some profiles show maxima that are not at the bottom of the profile but somewhere around 50 cm depth. After this depth the decrease in depth becomes smaller for all three profiles that go below 50 cm.

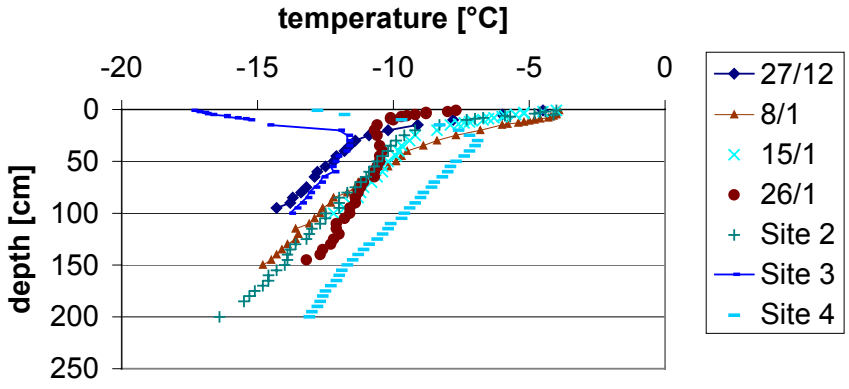

Figure 24. Temperature profiles from the snowpit walls. The lines marked only with dates are all from site 1.

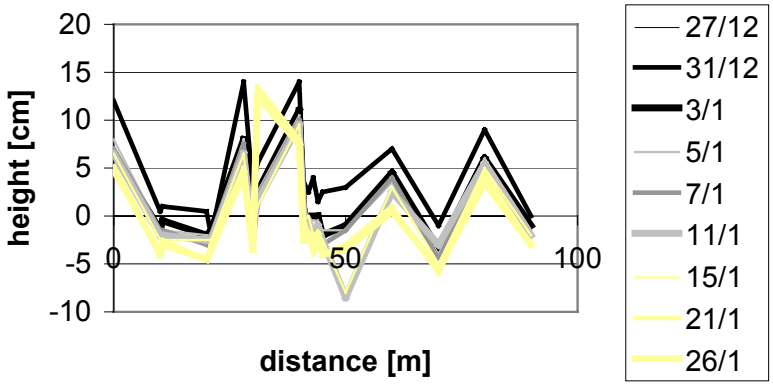

Figure 25. The stake height differences along the stake line. These values have been calculated by subtracting the stake heights at the first measurement from them.

The temperature profiles from the snowpits are shown in Figure 24. They show that the at least in the first 30 cm strong diurnal changes occur. One interesting feature is the change in temperature gradient at site 1. It changes from –7.1 °C m^{-1} to –2.0 °C m^{-1}. The average surface crystal size was 0.34 mm, and the shape of the crystals was round. Icy layers were found in most pits at 30-50 cm depth, at 100 cm depth and then again at 130 cm depth. These icy layers were usually 1 to 2 mm thick. At site 4 there were some unusually thick ice layers at 30 cm depth. These were between 5 and 27 mm thick. They varied in extent being in some places only lenses 26 cm long. The stake height differences are shown in Figure 25. After a period of accumulation, the stake heights start to decrease. This can be either due to sublimation or packing. The latter would manifest itself as an increase in density but that cannot be seen in Figure 25. The two-meter wind speeds under and around SANAE 4 A-block are shown in Figure 26. The values have been normalised to the maximum value. The fastest speeds are underneath the building (SANAE 4 is 4 m above the ground) and just to the leeward side at the end of the building. Snow accumulated in the areas with the lowest wind speeds, and the areas with the largest speeds were totally clear. Either bare rock or polished ice.

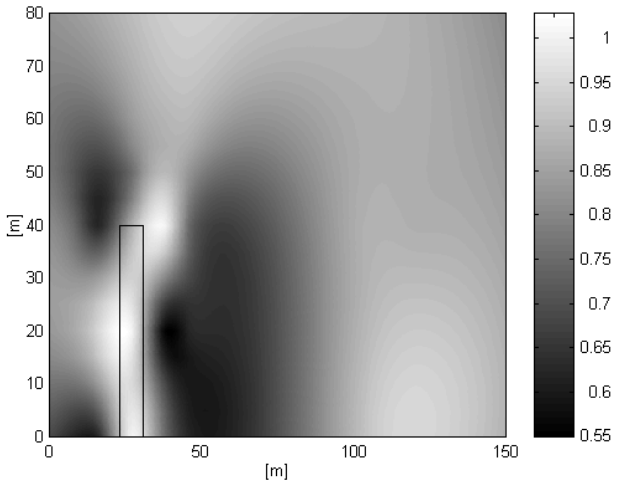

Figure 26. Winds speeds at 2 m height above the surface (the sppeds have been normalized so that the fastest speeds have a speed of 1) under and around one block of SANAE 4. The block is the rectangle in the left of the image. The wind was blowing from left to right.

4.5 Automated snow sensors

The general objective of the snow sensor project is to develop a better understanding of the dynamic properties of the seasonal snow cover and how these properties (i) relate to signals detectable by remote sensing and (ii) play a role in local as well as global climates. The initial stimulus for developing the snow sensor system was the need for a rugged, simple system to acquire spatial snow data useful in the development and validation of a spatial snow cover model. The specific objectives for our program within the 'Seasonal Snow in Antarctica' project were:

(i) to adapt this system for use in Antarctic field conditions,
(ii) to deploy a small number of automated snow sensors in Antarctica for one year,
(iii) to evaluate the logistics of sensor deployment,
(iv) to evaluate the physical performance of the snow sensors under Antarctic winter conditions
(v) to evaluate the usefulness of the data for snow cover process analysis.

To this end, 10 snow sensor systems were manufactured and nine were deployed along a transect from Kvitkuven to Amundsenisen. The overall objective is to assess the feasibility of developing a system that could be used in spatial studies of Antarctic snowcover and climate processes on a year-round basis.

4.5.1 Sensor description

The snow sensor was initially developed in connection with a DND (Department of National Defence, Canada) project dealing with spatial modeling of snowcover properties using both physically based models and statistical models for generation of snow trafficability information. Within this general context there was a need for a sensor system that would be capable of providing snow data for model development and validation. This system forms the basis for the snow sensors we deployed in Antarctica.

The snow sensor detects the presence or absence of snow by its thermal effects. To this end, temperatures are measured with a precision of better than $0.1^{o}C$ along a sensor rod, which can, in principle, be of any length. The interval at which the temperatures are sensed is limited only by data storage considerations. In its Antarctic version, the sensor interval is 2 cm with a total sensor rod length of 120 cm. This allows two daily temperature profiles to be measured over a period of 15 months.

An integral datalogger system of very low power consumption senses the temperature profile and stores the data in non-volatile memory. It can be programmed for essentially any sampling time interval. The electronics for the snow sensors are built to military specifications, i.e. they can tolerate temperatures down to $-50^{o}C$ with no significant calibration drift.

Physically, the sensor consists of a sensor rod of approximately 15 mm diameter and an ABS plastic housing, which protects the electronics.

In earlier applications at Schefferville and Sherbrooke, the power supply has been enclosed with the electronics, forming an extremely compact, easily deployable sensor system. Its field deployment requires only the use of a fence-post auger, or similar tool to dig a hole into which the ABS plastic housing can be installed. The use of non-volatile memory means that the sensors can be returned to the laboratory for data retrieval, although for field testing and reprogramming, they have usually been equipped with external RS-232 access. This option was installed on the Antarctic sensors.

A battery unit consisting of 48 alkaline D cells powers the sensor system. This is well in excess of the battery needs for a full year's operation at more clement temperatures. Because alkaline batteries do not perform well at temperatures below about –40 ^{o}C, a system was developed for protecting the batteries from extreme low winter temperatures. As the average annual air temperature is above –40 ^{o}C throughout the field area, sufficient thermal protection can be achieved by installing the battery pack at or near the depth of zero seasonal temperature variation in the snow cover. The battery protection system consists of a PVC plastic pipe, 4 m long (Shown in Figure 27 being retrieved), which may be inserted into the snow cover, to act as a facility for installing and retrieving the battery packs. The plastic pipe also acts as storage of the sensor during transport and, additionally, provides a firm foundation upon which the snow sensor is installed.

The battery pack is installed at the bottom of the plastic pipe and the rest of the pipe is filled with mineral wool for insulation. During transport, the rather fragile battery pack is held firmly in place by a strap that runs the length of the pipe and is taped to the battery pack and to the outside of the pipe at both ends. This design was made for environmental reasons, to enable battery pack retrieval in case retrieval of the plastic pipe would be unsuccessful. For environmental protection, an absorbent is packed into the pipe below the batteries, to absorb any leakage that may occur. The lower end is sealed with saran wrap, taped to the outside of the pipe. This design is used, rather than a solid PVC end cap, in order to facilitate retrieval of the plastic pipe.

4.5.2 Snow sensor installation and retrieval procedures

During transport, the snow sensor is placed in the top end of the pipe with its sensor rod wrapped in the mineral wool insulation. The top end, with the datalogger casing is saran wrapped to prevent any moisture from entering the pipe. At the installation site, a hole is drilled to about 4.3 m using a CRREL auger. After final preparation, the pipe is installed into the hole and seated at the appropriate depth. Then the saran wrap around the sensor is removed and the sensor inverted into its upright position. A new seal of saran wrap is applied to prevent moisture from entering the pipe. The sensor is then programmed, the RS-232 connector is wrapped in saran wrap, and the cable wound around and taped to the pipe. The hole is then backfilled and markers are placed on the surface. The markers consist of three bamboo poles, two of which are placed equidistantly at opposite sides of the pipe at a distance of 2 m from the pipe. The third is placed at a distance of 1 m from the pipe, in a position described by a line drawn from the sensor to the marker, perpendicular to a line connecting the first two poles.

For retrieval, the sensor is first excavated, and the data dumped to a portable computer. A sensor is shown being excavated in Figure 28. Then the saran wrapping is removed and the snow sensor lifted from the pipe. Should the pipe be irretrievably caught in, for example, an unexpected development of blue ice at the installation site, the batteries and the mineral wool insulation may now be removed by pulling on the strap to which the battery pack is attached, allowing the pipe to be thawed loose by the application of steam. However, normally, the PVC plastic pipe is easily extracted from the hole. The pipe may be frozen to the walls of the hole, but a sharp blow of a sledge hammer to a piece of wood laid across the orifice of the pipe should free it. A jack may in extreme cases be necessary to pull the pipe out of the hole.

Figure 27. The batteries were used as a power supply in snow sensors and they were packed in a 4 meter pipe. (Photograph by E. Kärkäs)

The snow sensors were installed in flat, unobstructed snow fields, so as to represent conditions of steady-state snow drift transport. They were installed at the following coordinates, measured by

Figure 28. The sensor part of the automatic snow sensor was dug out and pipe attached them was then easy to pull out. (Photograph by E. Kärkäs)

hand-held GPS:

Sensor	Day	latitude	longitude	Retrieved	Depth (cm)
1.	03.01.01	72°57.859'S	13°34.560'W	03.01.02	45
2.	06.01.01	73°26.222'S	14°26.723'W	13.01.02	184
3.	08.01.01	73°12.500'S	13°12.996'W	02.01.02	40.5
4.	10.01.01	73°27.362'S	12°33.381'W	13.01.02	47
5.	12.01.01	74°00.794'S	12°01.129'W	12.01.02	38
6.	14.01.01	74°28.688'S	11°33.006'W	12.01.02	35
7.	14.01.01	74°59.866'S	10°00.485'W	12.01.02	19
8.	18.01.01	72°36.546'S	16°18.601'W	20.01.02	48
9.	28.01.01	73°04.085'S	13°28.225'W	31.12.01	48

A RADARSAT mosaic (200 m resolution) was employed in the selection of the sampling points. The mosaic shows a significantly lower backscatter coefficient for Högisen (Sensor #2) and Kvitkuven (Sensor #8), which is why these sites were selected. Sensor #9, originally intended for installation on the ice shelf near Ramppi was relocated to our radar test site (snow site 9) after two unsuccessful attempts to reach the ice shelf location by helicopter.

4.5.3 Problems with the automatic snow stations

Battery packs are typically fragile and therefore difficult to transport. Therefore, they had to be assembled at Aboa. This procedure was rendered more difficult and time consuming than had been anticipated, by the lack of adequate laboratory facilities at the Aboa station. An unforeseen problem was the extensive damage to the data logger units that had occurred during the transport. Cables had been torn, circuit boards loosened, and diodes and internal battery packs shattered, by extremely rough handling during the transport. As a consequence extensive repairs and testing of the sensors had to be made in the cramped living quarters of a survival cabin. Nevertheless, nine out of the ten sensors were rendered operational. The tenth sensor essentially consisted of the remaining broken parts after the workable parts had been pirated and exchanged between the different units.

Upon sensor retrieval in 2000-2001, problems were encountered in the field during the dumping of data from the sensor to the portable computer. In the very dry Antarctic environment static buildup generated random discharges, which interfered with the data transmission. Therefore, repeated attempts were necessary in the field to ensure that as much as possible of the data had been transferred before the sensors were transported back to Aboa. Although the sensors are equipped with non-volatile memory, the rough handling during transport by snowmobile for long distances across hard sastrugi presents considerable risk for fatal damage of the datalogger unit. At Aboa the final data dumps were done for the sensors, which had survived the transport.

The same problem that was affecting the data dumping had affected the sensor operation. Static buildup, presumably in association with snow drifting had caused the onboard computer to reset after a variable time interval. This problem had never been observed during earlier field tests in Sherbrooke and Schefferville and seems to be particular to the Antarctic environment where good grounding is hard to find. The problem has been remedied by modifying the data connection and grounding of the sensor.

One important cause of problems was in design of the datalogger system. More precisely, the internal battery packs for the memory backup batteries were not sufficiently solid. Nor were they sufficiently well attached for the very rough transport conditions in Antarctic operations. This problem has been remedied by affixing more solid battery packs to the base of the datalogger

enclosure. A new method for fixing the sensor rod to the datalogger unit has been employed to prevent snow compaction from pushing the rod into the electronics. This should eliminate problems of the kind encountered at Högisen.

4.5.4 Summary of the performance of individual snow sensors

The following summarises the performance of individual snow sensors during the 2000-2001 Antarctic winter:

Sensor #1 (72°57.859S, 13°34.570W) worked from day 4 until at least 06h on day 85. The field dump was incomplete. The sensor was damaged during transport back to Aboa by snowmobile. The cables to the memory backup battery pack were torn apart and the electronics damaged.

Sensor #2 (73°26.222S, 14°26.723W) at Hogisen did not yield any data. It was severely damaged by the pressures of a very deep accumulation of high density snow. The snow sensing rod had been pushed into the electronics casing, tearing out one memory backup battery cable, severing the power supply cable and tearing out the RS-232 connector cable. Nearly 2 metres of very dense snow had accumulated at this site after the sensor was installed.

Sensor #3 (73°12.500S, 13°12.997W worked from day 8 until at least 18h on day 53. The field dump was incomplete. The sensor was damaged in the snowmobile transport back to Aboa. The cables to the memory backup battery pack were torn apart and the electronics damaged.

Sensor #4 (73°27.362S, 12°33.381W) worked from day 10 until 06h on day 116 when it reset for unknown reasons and began half-hourly observations. The sensor was retrieved by helicopter and survived the transport intact.

Sensor #5 (74°00.794S, 12°01.129W) worked from day 12 until 06h on day 38 when it reset for unknown reasons and began collecting half-hourly data. The sensor was retrieved by helicopter and survived the transport intact.

Sensor #6 (74°28.688S, 11°33.006W) worked from day 14 until 06h on day 75 when it reset and started collecting half-hourly data. The sensor was retrieved by helicopter and survived the transport intact. The data dumping in the field was incomplete. The remainder of the useful data was successfully dumped at Aboa.

Sensor #7 (74°59.866S, 10°00.485W) at Amundsenisen failed to yield any data. The sensor was retrieved by helicopter and survived the transport with no physical damage. No physical damage has been detected on the sensor. However, the memory backup batteries were at only 0.6V when tested. Even after replacing the memory backup batteries, the sensor did not respond. One transistor heated up abnormally, to a very high temperature.

Sensor #8 (72°36.546S, 16°18.601W) at Kvitkuven worked from day 18 until 06h on day 168, when it reset and began collecting half-hourly data. Data dumping in the field was incomplete. The sensor survived helicopter transport and the remainder of the useful data was successfully dumped at Aboa.

Sensor #9 (73°04.085S, 13°28.225W) worked until 06h on day 46, when it reset and began to write half-hourly data with the values of 999.9. The sensor was retrieved using a bandwagon and survived the transport intact. The field data dump was complete.

Apart from the problems with sensors #2 and #7, and the shortened data collection span, seven

of the sensors performed well. All sensors were synchronised and programmed to collect data at 06 and 18h GMT. It is therefore possible to intercompare the data for spatial analysis. Each data record consists of the following information:

Line 1: Julian day.
Line 2: Hour: Minute: Second
Line 3: Reference temperature (datalogger temperature)
Line 4: Temperature offset (used in the calculation of temperature profile)
Line 5: 60 temperatures at 2 cm intervals along the sensing rod. The first value is nearest the datalogger unit.

4.5.5 Data analysis

Snow depth is determined visually from graphs of the vertical temperature profile. The snow surface height can usually be determined even on overcast days. Air temperatures for spatial analysis are best taken from the uppermost part of the snow sensor. Some accuracy improvement can be obtained by averaging, say the five uppermost temperatures. The temperature reference of the dataloggers is accurate to +/- 0.1^{o}C. The accuracy of individual temperature determinations along the sensor rod is estimated to be within about twice that value. Solar radiation generates a variable additional difference between the sensor temperature and that of the air.

5. Solar radiation in the snow cover

5.1 Instrumentation

Radiation measurements were made using three different instruments (Li-Cor LI1800UW (spectral), Middleton EP16 (total) and ASD PS II (spectral)). Kai Rasmus, Chantale Lavoie (FINNARP 99 only) and Hardy Granberg were responsible for these measurements. Radiation measurements were also made from an airborne helicopter along the line from the coast inland.

5.1.1 Description of the LI-1800UW

The LI1800UW essentially measured irradiance. It was used with a fibre-optic cable with a remote cosine collector at the end. This was placed on a pole that was supported 30 cm above the surface of the snow. Both upwelling and downwelling irradiance were measured but unfortunately these could not be measured simultaneously. The LI1800UW uses a bandpass filter wheel and a turning diffraction grating to split the light up. Each waveband of 6nm width is recorded separately. The centre wavelengths were 2 nm apart. Due to the technology used in this instrument, the integrations times were close to 1 minute when scanning from 300 to 1100 nm, which were the normal limits used during this expedition.

Measurements of spectral irradiance were made using a Li-COR LI-1800UW spectroradiometer with a remote cosine collector mounted on the end of a fibre optic cable. The collector was taped onto the end of a pole, which placed the collector 0.3 m above the snow surface, and 0.8 m away from the main body of the LI-1800UW. The instrument is a matt black cylinder with a height of 0.3 m and a diameter of 0.3 m. It is a strong absorber and it may therefore induce errors into the measurements, but it was present in all measurements so its effect was systematic. The cosine collector did not have a spirit level so it had to be levelled by eyeballing. During the measurement the instrument melted its way into the snow tilting the pole holding collector. The instrument had to be straightened several times during one measurement session, which lasted 15 min. Light that is collected by the cosine sensor goes through one of eight filters on a filter wheel, which rotates. The light is then further split up by a diffraction grating, which also rotates, and finally the light passes on to a photodiode sensor. In this way the spectral resolution becomes

6 nm, but it takes 50 seconds to scan the spectrum from 300 nm to 1100 nm. Such a long integration time may become a problem when the weather conditions are variable and there are fast changes in the incoming irradiance, i.e. particularly when the sky is partly cloudy.

5.1.2 Description of EP-16

A Middleton EP-16 pyranoalbedometer system was used to keep track of the incident irradiance during LI-1800UW measurements and to make albedo measurements. This system measured downwelling and upwelling irradiances from 300 to 3000 nm. The instrument is a modified thermopile pyranometer with an additional inverted sensor assembly. The dual sensors have been matched for response and sensitivity and their collector surfaces are parallel. The instrument was mounted on the end of a pole, which was clamped onto a tripod. This set-up placed the sensor head 1 m above the ground. A spirit level, which was built into the sensor assembly, was used to level the instrument.

The EP-16 pyranoalbedometer was connected to a Gantner IDL-100 datalogger, which was set to scan at 10-second intervals, and record an average of 3 scans. This produced a dataset of upwelling and downwelling irradiance and total albedo with a temporal resolution of 30 seconds. The EP-16 gives out microvolts, which need to be converted into energy units using calibration coefficients obtained from the calibration certificate. Each sensor has its own sensor specific calibration constant. Conversion into energy values was performed automatically in the datalogger but the microvolt values were saved in the memory of the datalogger together with the energy values and the value of the total albedo. Calibration of the sensors had been made in March 1999. Initially two EP-16 instruments were available but one of them suffered a dent in the skirt surrounding the instrument body and this unit was used by itself only once and when the other unit was unavailable, and once together with the other unit for intercomparison measurements.

5.1.3 Description of PS 2

In 1999/2000 radiance measurements were made with a Personal Spectrometer II (PS2) from Analytical Spectral Devices. It is designed to collect light from an external source through a bundle of 19 optical fibres. The light that travels through the fibres strikes a grating that diffracts the light into its respective wavelengths. The number of photons is recorded by a silicon photo diode that contains 512 elements. The record count can be stored in a raw format that gives the calculated number of digital numbers (DN) for each element. The instrument covers the ultraviolet, visible, and near infrared parts of the spectrum. It has a starting wavelength of about 350 nm and ends at about 1050 nm, with a spectral sampling interval of 1.40 nm. This range was further constrained to the 400 – 900 nm range, because of noise problems outside this spectral region. Two types of data were acquired with the PS 2. Spectra of digital signals (referred to as radiance in this text) proportional to absolute radiance were made for either a 1° or 15° foreoptic. The 1° foreoptic was used to obtain multi-directional radiance measurements of the snow surface and subsequently integrated in azimuth and zenith to yield an upwelling signal proportional to absolute irradiance. The 1° foreoptic was used to measure upwelling radiance at depth within the snow pack. To measure light attenuation, a fibre optic probe was attached to the instrument and was inserted progressively into the snow or ice. The measurements were performed in three different types of media in order to obtain a variety of optical conditions. All the spectra collected have a starting wavelength of about 350 nm and an ending wavelength of about 1050 nm. This range was further constrained to the 400 – 900 nm range because of noise problems outside of this spectral region. The diode-sampling interval of the PS2 is nominally 1.40 nm.

To measure light attenuation, the ASD was provided with a special fibre optic probe for

sampling within the snow cover. The probe was designed and manufactured by Prof. Granberg and was previously used by Kulkarni (1986). It is essentially a 6.3 mm (¼ inch) quartz fibre bundle installed in a fibreglass tube, which acts as a structural element for insertion in the snow cover. The tube is covered by white heat shrinkable plastic, to minimise its radiant absorption in the visible.

Special weather conditions are required in order to get reliable radiance measurements with the spectroradiometer. It is essential for reflected radiance data collection to have clear sky conditions as cloud cover diffuses the radiation, changing the effective zenith angle. It causes an increase in spectrally integrated albedo, absorbing the same near infrared radiation that snow would absorb, leaving the shorter wavelengths to penetrate to the surface (Warren, 1982). It is also recommendable to get similar conditions for the attenuation measurements, although some had been taken even in partly cloudy or overcast conditions. The effect this had on the data will be evaluated later. Having to take measurements that were highly weather dependant was a great limitation when considering the high frequency of low pressure systems and precipitation events that affected us during the 1999/2000 season. In addition, the instrument was not really cold-weather resistant, and because of this feature several data acquisition events were considerably shortened.

5.2 Albedo measurements

The measurements in 1999/2000 were made mostly on a line going from the coast past the Basen nunatak to Heimefrontfjella. Total albedo measurements were made on sea ice, both snow covered and bare, outside the Norwegian research station Troll, which is several hundred kilometres further east, and on the Basen nunatak itself. Spectral albedo measurements were also made on the Högisen ice dome, which is in the Vestfjella mountain range southwest from Basen. Table 9 list the sites and the measurements made at these sites. The waypoint numbers refer to the waypoints on the Rampen-Basen-Svea route. The measurement locations of albedo shown in Table 9 coincided with the snow sites so that albedo results could be compared to details of snow structure. On Högisen however the snow structure measurements and the radiation measurements were separated by a period of several weeks and so these albedo measurements cannot be studied for effects of snow properties.

Table 9. List of points where the albedo was measured with the LI1800UW and EP16 during the 1999/2000 season.

Name	Snow site number	Date DDMMYY	Latitude	Longitude
Waypoint 044	6	241299	73° 02.0' S	013° 19.5' W
Waypoint 005	4	251299	72° 45.2' S	014° 18.3' W
Waypoint 003	3	261299	72° 40.0' S	016° 42.0' W
Waypoint 007	5	020100	72° 57.9' S	013° 34.9' W
Aboa blue ice		060100	73° 03.1' S	013° 27.7' W
WPT348	10	080100	73° 12.5' S	013° 13.0' W
Waypoint 019	12	100100	73° 27.4' S	012° 33.4' W
Svea blue ice		140100	74° 34.3' S	011° 13.0' W
Waypoint 050	16	150100	74° 28.7' S	011° 33.0' W
Waypoint 022	14	160100	74° 00.8' S	012° 01.0' W
Högisen	11	230100	73° 26.3' S	014° 26.7' W

5.2.1 Data handling

A cloud cover correction algorithm by Virta and Blanco (1995) was used on the LI-1800UW spectra to make them comparable with each other. A coefficient is calculated by normalising the downwelling irradiance values and then the spectrum is multiplied by this coefficient. This algorithm however did not work because the pyranometer (EP-16) used has its sensitivity in the whole of the solar spectrum (300-3000 nm) and the LI-1800 measures only from 300 to 1100 nm.

The spectra have been used as they are. The spectral albedos were then calculated using Eq. (1) and the broadband albedos were calculated using Eq. (2). The EP-16 data was checked and the irradiances were recalculated from the microvolt values, because the IDL-100 datalogger seemed to have calculated them incorrectly. Total albedos were then calculated from these values.

5.3 Preliminary results

A total of 154 irradiance spectra were measured using the LI-1800UW spectroradiometer. Of these, 74 were used in the spectral albedo calculations resulting in 37 spectral albedos from a total of 11 sites. One fourth (24% or 9 out 37) of these albedos were not good and were not used for further analysis. Both albedo measurements form Waypoint 050 had to be discarded. Of the eleven sites, 9 were at locations with a snow cover and two were at blue ice fields.

A total of 63 downwelling irradiance spectra were measured during the radiometry flights made by Professor Granberg. This equates to two hours total over two days with two-minute intervals.

The mean spectral albedo (LI1800UW) from snow-covered areas is shown with the mean spectral albedo for blue ice areas in Figure 29. The snow albedo is an almost constant 0.92 from 300 nm to 600 nm after which it starts to drop rapidly. It reaches a minimum of 0.62 at 1030 nm, but there are some spectral features before this as well.

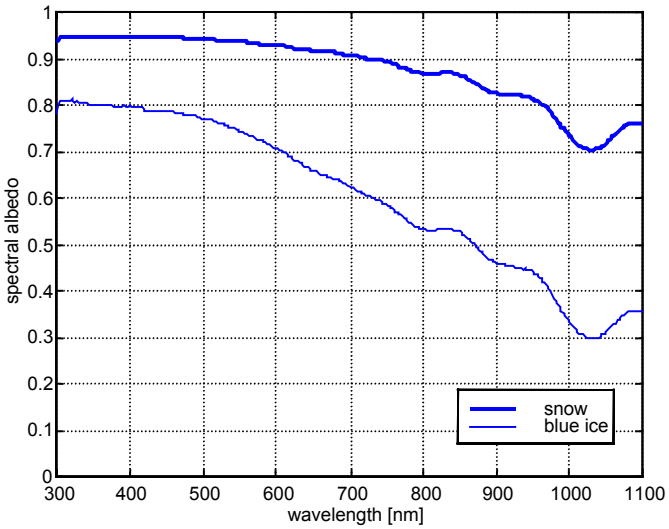

Figure 29. Spectral albedo over snow and blue ice measured with the LI1800.

Table 10. The mean total albedo for different surfaces.

Region	Albedo
Snow	0.844
Blue ice	0.594
Rock	0.133
Sea ice (snow)	0.769
Sea ice (no snow)	0.517

The EP-16 pyranoalbedometer was used at 13 sites. Two of these were on sea ice, two on blue ice, one on rock and the rest (8) on snow. The mean values of total albedo obtained for the different areas are shown in Table 10. All of the total albedo values obtained for all of the areas are shown in Figure 30 and together with broadband albedos calculated from LI-1800UW in Figure 33. These have been obtained as the ratio of the spectrally integrated downwelling and upwelling irradiances. The broadband albedos obtained using the EP-16 are 92 % of those obtained using the LI1800UW.

At SANAE 4 the mean total albedo was 0.79 (averaged over two days of measurements) at the beginning of the period and it increased to 0.81 at the end. During the middle part of the measurement period, there were some very clear days during which the albedo showed strong diurnal variation dropping to below 0.60 during the night. This was due to a low solar elevation and possibly instrument shading. During the night the sun shone from behind the instrument tripod.

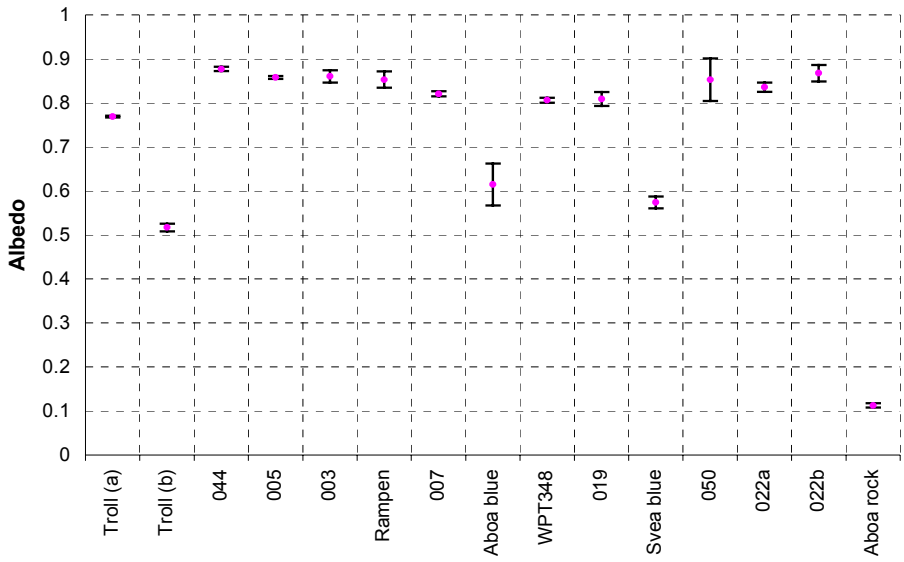

Figure 30. Total albedos (between [300-3000]nm) over different surfaces with standard deviations.

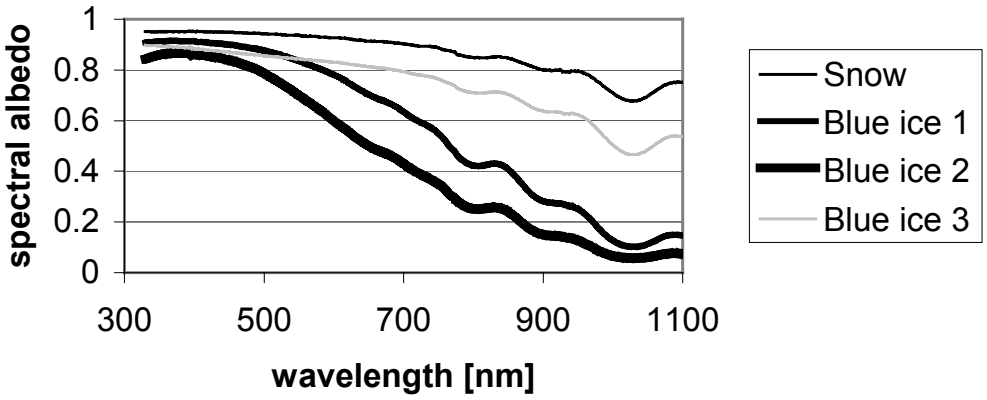

Figure 31. Spectral albedos for four different surfaces. Blue ice 1 was on a slope, blue ice 2 was a melt pool and blue ice 3 was a mixture of very large and very small ice crystals.

The spectral albedos for four different surfaces can be seen in Figure 31. The spectrum for snow is very flat in the visible wavelengths and it has a minimum of 0.63 at 1050 nm. Blue ice 1 and Blue ice 2 show values that drop faster after 500 nm going to around 0.1 at 1050 nm. As can be seen from the figure, the albedo spectrum for Blue ice 3 can be decomposed into a true blue ice part, which is what blue ice 1 and blue ice 2 represent, and a snow part.

The effects of the observed snow characteristics on albedo were studied. None of the snow properties studied correlated very well with the spectral albedos (correlation coefficients were below 0.3). It had been expected that the albedo would follow changes in the snow density, in the crystal size or in the content of impurities (the downwind distance from mountains was used as a proxy for this parameter). Instead the cloudiness showed the strongest correlation (Fig. 32) indicating that the albedo is very much an apparent optical property, i.e. it depends on the prevailing light conditions. The solar altitude did not seem to correlate very well with the albedo, however.

The broadband albedo calculated from measurements made with the LI-1800UW differs from the total albedo measured with the EP-16 (Fig. 34). The reason for this comes from the different spectral ranges of the two instruments; the EP-16 goes much further into the infrared. Downwelling solar radiation E_s can basically be considered to be blackbody radiation, which is described by Planck's law:

$$E_s(\lambda,T) = \frac{2\pi hc^2}{\lambda^5}\frac{1}{e^{\left(\frac{hc}{k_B T\lambda}\right)}-1} \qquad (3)$$

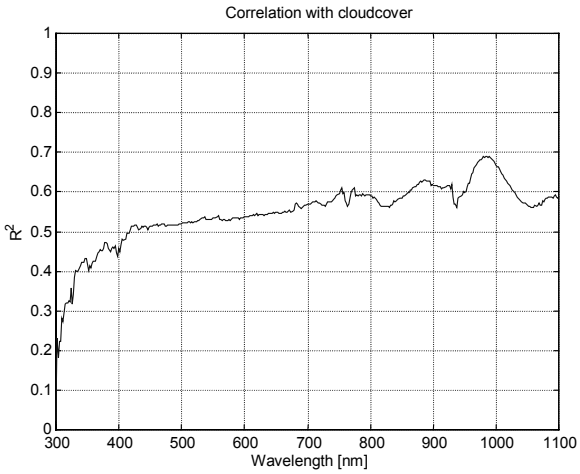

Figure 32. The spectral correlation coefficient between the cloudcover and the spectral albedo.

where T is temperature, λ is wavelength, h is Planck's constant ($6.626 \cdot 10^{-34}$ Js), c is the speed of light ($2.998 \cdot 10^{8}$ m s^{-1}) and k_B is Boltzmann's constant ($1.381 \cdot 10^{-23}$ J K^{-1}). Let us make the assumption that the albedo beyond 1100 nm is negligible. The two different albedos can then be calculated.

$$\alpha_{LI1800} = \frac{E_u}{E_{d1}}$$
$$\alpha_{EP16} = \frac{E_u}{E_{d2}} \qquad (4)$$

The upwelling irradiance E_u is the same for both of the albedos because of the assumption we made. The downwelling irradiances can be calculated from Eq. (3) by integrating over the wavelength ranges $\Delta\lambda_1$=[300,1100] nm and $\Delta\lambda_2$=[300,3000] nm. The ratio of the two albedos is:

$$\frac{\alpha_{EP16}}{\alpha_{LI1800}} = \frac{E_{d1}}{E_{d2}} \approx 0.80 \qquad (5)$$

This is a different figure from the measured value, which was 0.92, but the assumption made was crude and the downwelling radiation is not exactly purely blackbody radiation. It must also be remembered that the spectral irradiance data has not been corrected for cloudcover effects.

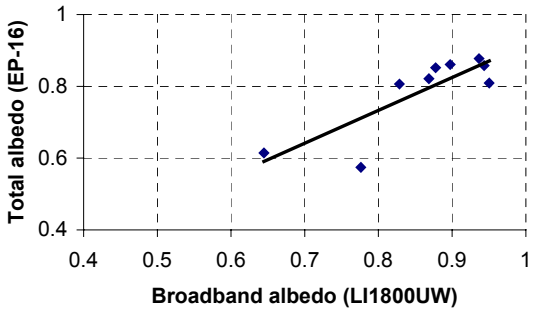

Figure 33. The relation between the total albedo and the broadband albedo. The equation for the line is y=0.92x. The correlation coefficient is 0.70 (n=9).

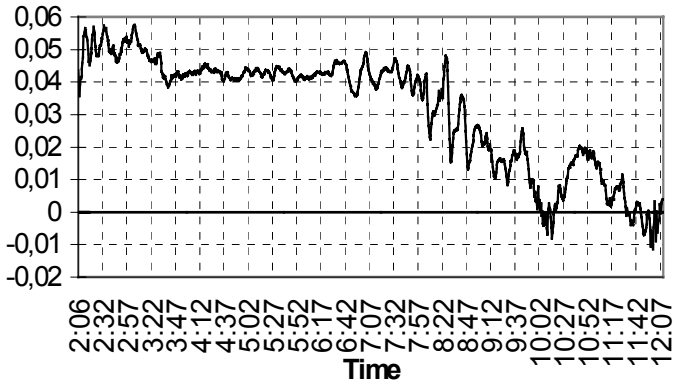

Figure 34. Difference between the albedos measured with the two albedometers simultaneously on the 16th January 2000 at Waypoint 022.

When the two albedometers were used simultaneously, they were observed to show slightly different readings. The difference of the albedos of these two instruments is shown in Figure 34. It is noteworthy that the difference is not constant but decreases with time. The measurement was started during the night in white-out conditions. In the morning there was a little bit of blue sky visible above but neither the sun or the horizon was visible. One of the instruments had a slightly dented skirt but is it possible that this could cause such a difference?

The time series of the difference between the total downwelling and upwelling irradiances measured at Waypoint 022 on the 16 Jan is shown in Figure 35. It can be seen that the albedo difference remains between 0.04 and 0.05 when the irradiance differences are below 10 W m^{-2}. This period coincides with the period of total whiteout. When the blue sky became visible above, the irradiance differences start to fluctuate and the albedo difference approaches zero. The irradiance difference can be explained by ice or snow on the domes, or by partial cloud, i.e. the sun was visible to one instrument and not the other. However, this indicates a problem with automatic pyranoalbedometers. It is not possible to know afterwards in what condition the instrument was during the measurement. It would seem that the dent in the skirt of one of the instruments was not of major consequence.

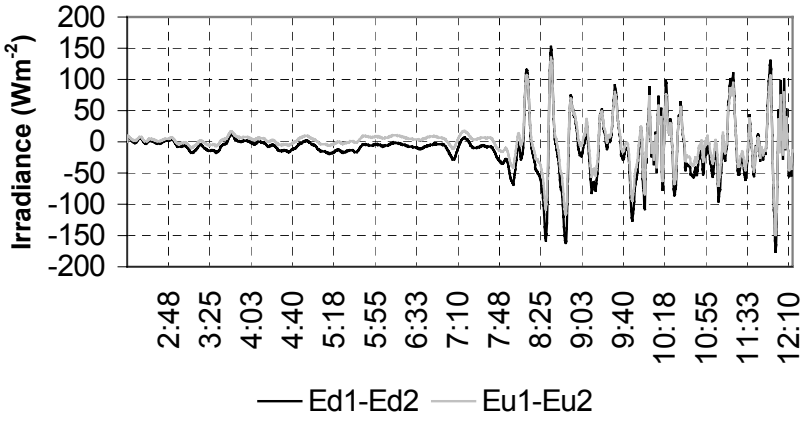

Figure 35. The differences between the downwelling and upwelling irradiances measured using the two instruments on the 16 Jan 2000 at Waypoint 022.

5.4 Bi-directional spectral reflectance measurements

Table 11 gives details on the site location and the general conditions occurring during the data collection events.

Spectral attenuation is obtained from the differences between surface upwelling radiation at a given depth and radiation reflected by the surface. Proportionality between upwelling radiance and downwelling irradiance is assumed (as could occur, for example, if the surface reflectance was approximately Lambertian). Attenuation factors were then defined as A = 1 - T, where T is the transmission factor. Attenuation coefficients for upwelling radiance were calculated using the solution from eq. (2).

Upwelling radiances were integrated over the hemisphere in order to compute the total reflected irradiance. According to Eaton and Dirmhirn (1979), the irradiance received by the instrument is given by:

$$F = {}_0\int^{\pi/2} {}_0\int^{2\pi} I_{(\theta,\alpha,\zeta)} \cos\theta \sin\theta \, d\alpha \, d\theta \qquad (6)$$

Table 11. Site location and measurement type.

			Type of data*		Surface	cloud	mean	time	temp
date	lat (S)	long (W)	Hemis	Atten	sampled**	cover	a.s.z.*** (°)	(GMT)	(°C)
9.12.1999	70°07,033'	5°23,044'	x		fast ice	0/8 - 1/8	53,53	8:15 - 9:06	-3,5
24.12.1999	73°02,043'	13°19,496'		12	s-i	7/8 - 8/8	55,42	13:06 - 17:24	-4,2
2.1.2000	72°57,870'	13°34,890'	x	3	s-i	0/8 - 1/8	81,26	22:03 - 23:36	-6,7
5.1.2000	73°05,222'	13°20,245'		4	s-i	6/8	64,06	17:32 - 18:26	-3,9
6.1.2000	73°03,064'	13°27,622'	x	2	bi	0/8	51,14	13:22 - 14:26	-5,5
7.1.2000	73°03,000'	13°25,000'	x		sh	0/8 - 1/8	82,38	22:47 - 23:13	-8,4
8.1.2000	73°12,500'	13°13,000'	x	4	s-i	3/8	57,24	15:17 - 17:42	-6,7
10.1.2000	73°27,400'	12°33,400'		3	s-i	8/8	59,16	15:48 - 17:18	-5,5
	73°42,965'	12°18,609'		1	s-i	7/8	82,93	23:15 - 23:27	-10,2
13.1.2000	74°28,650'	11°33,030'		3	s-i	8/8	82,17	22:17 - 00:10	-9,1
16.1.2000	74°00,797'	12°00,990'		2	s-i	7/8 - 8/8	53,69	12:16 - 12:33	-4,7
18.1.2000	73°03,000'	13°25,000'		4	sh	0/8	59,87	16:19 - 16:50	-5,1
21.1.2000	73°03,636'	13°21,641'	x		s-i	1/8	53,77	14:01 - 14:11	-6,0
	73°04,057'	13°28,270'	x	6	s-i		59,49	15:11 - 17:03	
	73°02,902'	13°28,109'		1	bi		65,56	17:48 - 17:54	
22.1.2000	73°02,594'	13°24,098'		5	sh	3/8	63,73	16:57 - 17:46	-5,0
	73°02,902'	13°28,109'		4	bi		80,76	21:06 - 21:59	

* 'Hemis' and 'Atten' are for attenuation and hemispherical measurements ; ** 's-i' and 'sh' are semi-infinite and shallow snow, 'bi' is blue ice; *** 'a.s.z'. is solar zenith angle.

where F is the reflected irradiance, θ is the zenith angle of reflected radiance, α is the azimuth angle of reflected radiance, ζ is the solar zenith angle, and I is the reflected radiance over the wavelength range of the solar spectrum. If the reflecting surface is isotropic and homogeneous, $I_{(\theta,\alpha,\zeta)}$ is a constant, and by integrating Eq. (6) we obtain:

$$F = I \int_0^{\pi/2} \int_0^{2\pi} d\alpha \, d(1/2 \sin^2\theta) = \pi I(\lambda) \quad (7)$$

Even if total isotropy does not occur under natural conditions (Eaton and Dirmhirn, 1979), we assume that upwelling and downwelling radiances obtained over snow or ice are equally isotropic.

The numerical integration of the irradiance from Eq. (6) gives:

$$F = \Sigma_\theta \Sigma_\alpha [I_{(\theta,\alpha,\zeta)} \cos\theta \sin\theta \, \Delta\alpha \, \Delta\theta] \quad (8)$$

In greater details, we can divide the methodology applied (Van Wyngaarden, 1984) in four steps. First, it requires to average the radiances at each azimuth, for every depression angle (0, 15, 30, 45, 60, 75, 90°). This step is done for every wavelength sampled (400-900 nm), and then, averaged over all wavelengths. Afterwards, L is plotted for every depression angle sampled. The second step is the computation of the solid angle of each 1° slice (the hemisphere was subdivided in 90 slices of 1°) in the hemisphere of unit radius. The solid angle, A_I, was calculated using the following formula:

$$A_I = 2\pi \sin(I - 0{,}5^\circ) \quad (9)$$

where I varies between 1 and 90°. The term 0.5° is taken off I in order to get the value of the centre point of the solid angle. Step three considers the cosine angle of incidence of each individual beam on the instrument. It consists of calculating the relative contribution (RC_I) of each slice by multiplying the solid angle of each slice by its corresponding cosine factor:

$$RC_I = A_I \cos(I - 0{,}5^\circ) \quad (10)$$

The fourth and final step is the sum of the products of individual radiance values, multiplied by their RC_I and $\Delta\theta$.

Radiance readings for the eight azimuth directions were averaged, yielding seven depression angle point values (Fig. 36). For each sample, linear interpolation is used between the seven point values. From that figure, we can see the influence of both cloud cover and solar elevation angle on radiance. The s15 curve, acquired on semi-infinite snow on 8 Jan 2000, is characterized by uniform radiances (mean value of 472.0 DN with standard deviation of 14.2 DN) along the different depression angles. This reflects the diffuse radiation, according to its 3/8 cloud coverage as opposed to 0/8-1/8 for the other samples. The s15 curve has also lower radiance values through out the depression angles compared to the other samples, which mean radiance values range from 677.1 to 1284.3 DN. In addition, the latter values are more variable, ranging from 91.5 to 131.9 DN. There, for roughly constant sky conditions, the solar elevation angle plays an important role on mean radiance. As solar elevation increases, so does the radiance. This is the case for samples fast, swit, and wpt7, respectively acquired on 9 Dec and 21 Jan and 2 Jan. The sample acquired on blue ice on 6 Jan, has lower values than the fast profile even though its solar elevation is higher (39° compared to 35°).

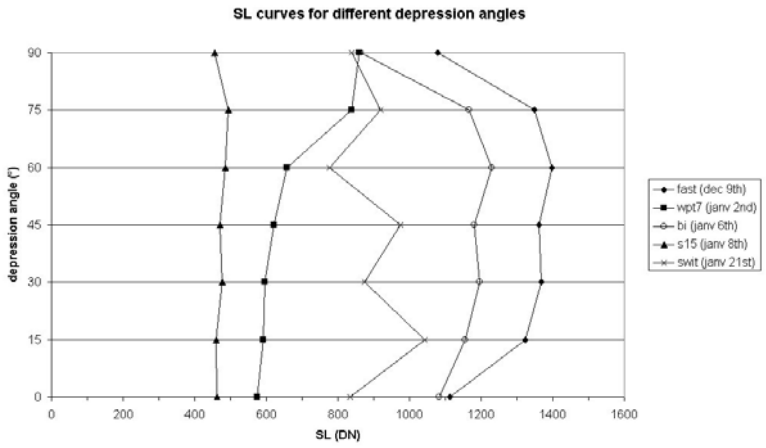

Figure36. SL curves for different depression angles.

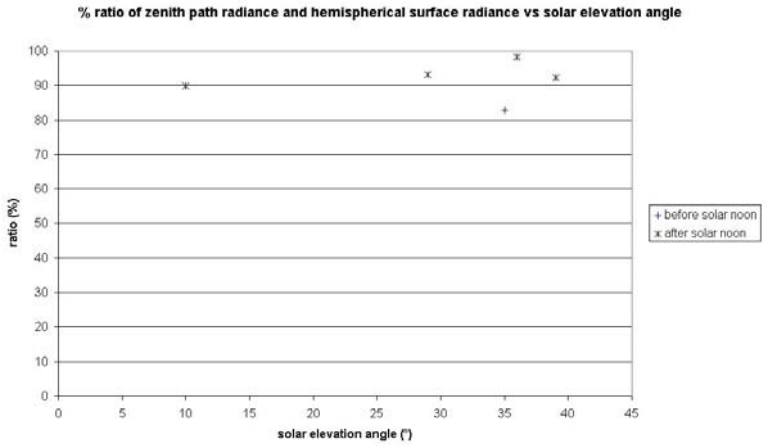

Figure 37. % ratio of zenith path radiance.

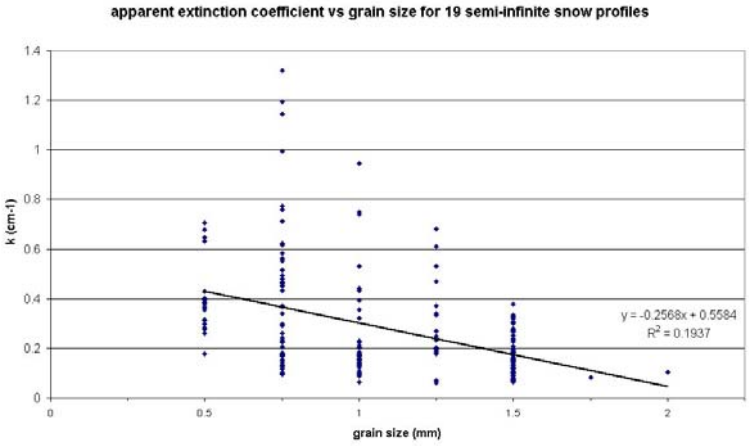

Figure 38. Apparent extinction coefficient.

Table 12. Percentage ratio of the zenith path radiance to the hemispherical radiance.

date	GMT time	solar elevation angle (°)	hemispherical radiance (DN) [1]	zenith path radiance (DN) [2]	ratio: [2] / [1] (%)
9/12/1999	8:15	35	4219.1	3495.7	82.9
2/01/2000	22:03	10	2009.0	1803.3	89.8
6/01/2000	13:22	39	3681.9	3399.5	92.3
8/01/2000	15:17	36	1477.1	1450.5	98.2
21/01/2000	16:42	29	2809.2	2619.8	93.3

The results for 5 (out of 7) samples are listed in Table 12, which shows the percentage ratio of the zenith path radiance to the hemispherical radiance. As expected, the percentage ratio is much higher in the case of diffuse radiation (98.2) than for clear sky conditions (89.8 to 93.3). The average ratio calculated is 0.91, which is in good agreement with van Wyngaarden's measurements (0.93).

This percentage ratio is plotted against solar elevation angle (in degrees) is shown in Figure 37. From those results, correction factors can be obtained by computing the inverse aforementioned ratio. The correction factors determined here are ranging from 101.8 (s15) to 117.1 (fast). Contrary to the results obtained by Eaton and Dirmhirn (1979), the correction factors seem to be unrelated to solar elevation angle.

The effect of snow grain size on the extinction coefficient was verified. The extinction coefficient should decrease as grain size increases (Warren, 1982). The extinction coefficient was estimated for every sampled depth and plotted versus the associated grain size issued from snow pit measurements. The relationship was tested for 19 semi-infinite profiles and the results are presented in Figure 38. The highest extinction coefficient values decrease as the grain size increases, showing a greater penetration of light when the grain size gets bigger, although the all-data correlation is poor. This is possibly due to the fact that the grain sizes attributed to the different profiles were not exactly taken from the sampling site, but from the nearest snowpit.

5.5 Attenuation measurements

As mentioned above, we worked with raw radiance rather than normalized radiance data because of signal saturation problems at the surface (ratio of surface downwelling radiance and radiance reflected by a nominally Lambertian panel (Spectralon)).

Only three data series are presented, i.e. one for each medium. Figure 39 (a-c) present raw un-normalised radiance plotted against wavelength for semi-infinite snow, shallow snow (18.5 cm deep, overlaying a rocky surface), and blue ice profiles. Those profiles were respectively sampled on 24 Dec 1999, 22 Jan 2000, and 6 Jan 2000. By looking at the signal proportional to radiance (SL), we note that the greatest amount of solar radiation is reflected at about 670-680 nm in all three cases. As we go down below the surface, we see a general rapid attenuation in the case of shallow snow (b). In the semi-infinite snow (a) there is a strong blue-shift at greater depths below the surface. This is also the case for blue ice (c).

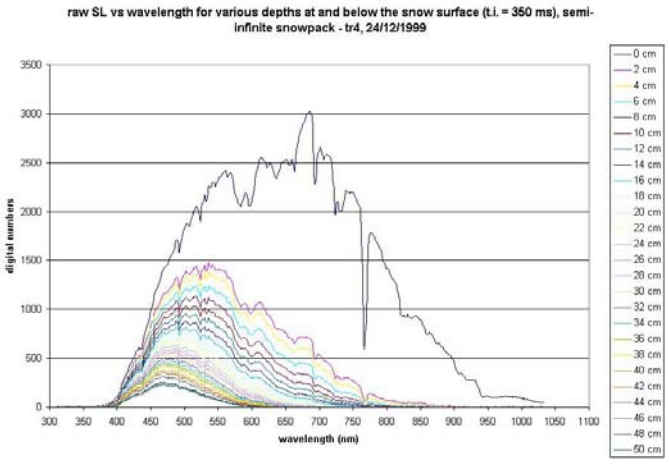

a)

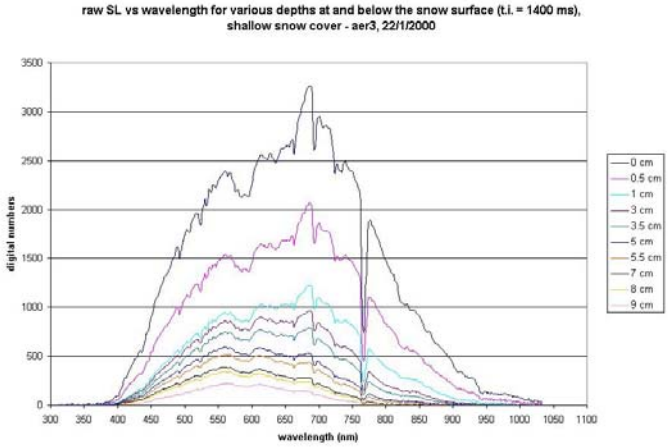

b)

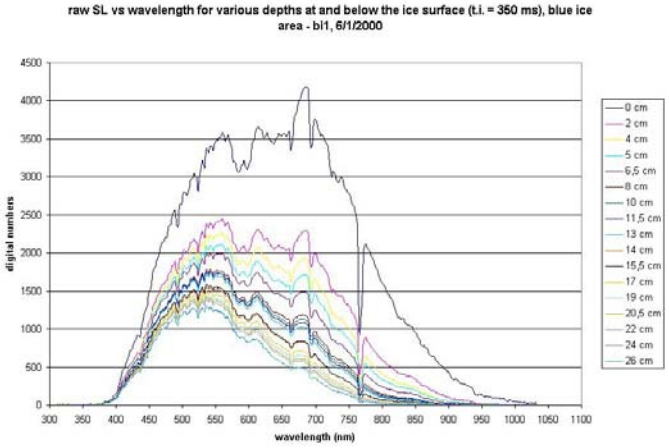

c)

Figure 39. Upwelling raw spectral SL.

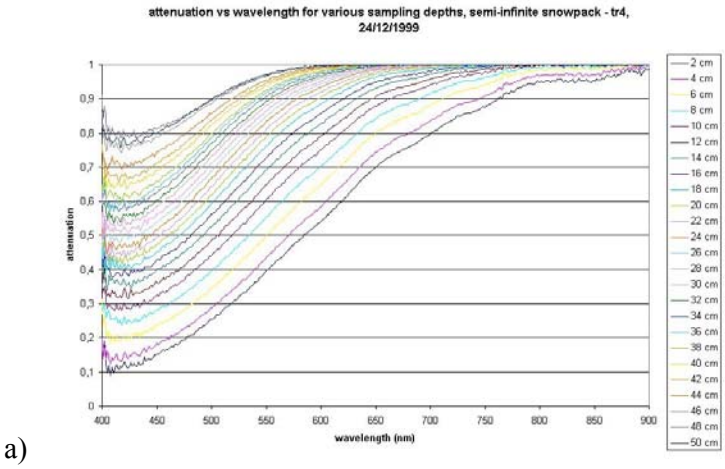

a)

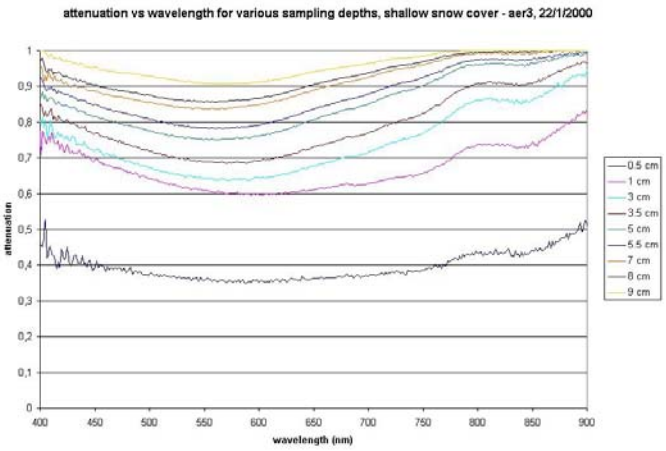

b)

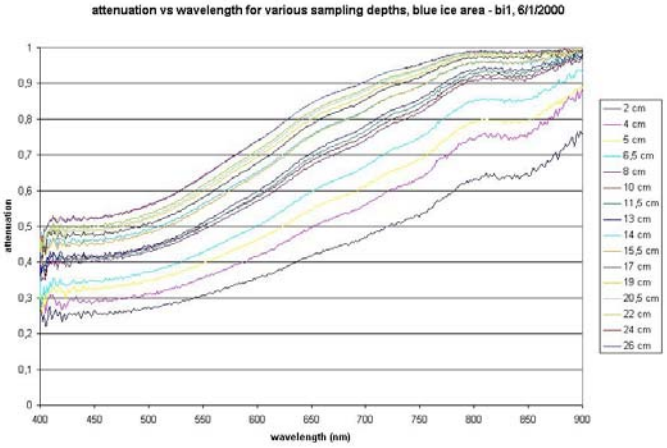

c)

Figure 40. Spectral attenuation in the snowpack.

Light attenuation by the snowpack is plotted against wavelength for the three media (Fig. 40 a-c). From those figures, we can observe that the media plays a significant role for light attenuation. For the semi-infinite snow profile (Fig. 40 a), the attenuation is strongest in the top centimeters of the snowpack, particularly in the near infrared region. As we get deeper, the light is filtered out by the snow, leaving only wavelengths close to 470 nm unextinguished (Brandt and Warren, 1993). The lowest attenuation values are observed in the 420-470 nm spectral region. At blue and shorter wavelengths, the upwelling radiation at 50 cm depth is still about 20 % of the amount measured at the surface, while it is less than 1 % at wavelengths above 600 nm.

In a shallow snow cover (Fig. 40 b), where bottom surface albedo has a great influence on light attenuation, the attenuation is least pronounced at about 550-580 nm and greater at both ends of the solar spectrum. In the longer wavelengths (greater than 750 nm), the attenuation pattern is rather similar to the semi-infinite (Fig. 40 a), although the attenuation rate is somewhat greater than that for the blue ice (Fig. 40 c). At the shorter wavelengths, there is a marked difference between the attenuation rates for respectively deep (Fig. 40 a) and shallow snow (Fig. 40 b). The strongest attenuation takes place at wavelengths greater than 750 nm, and the weakest occurs around 600 nm.

In blue ice light attenuation resembles that of the semi-infinite media, although the attenuation curves have a gentler slope. Indeed, light attenuation is fairly constant in the 400-550 nm range, and rises up to 750-800 nm. There it plateaus, and then rises up again to attain its maximum value at 900 nm. The pattern of lesser attenuation in the shorter wavelength range of the spectrum, as compared to the longer wavelengths, is observed in blue ice. Additionally, the overall rate of attenuation is much smaller for blue ice than for snow.

The decline in radiation intensity with depth varies with environment and also with wavelength (Fig. 41 a-c). At short wavelengths, the decline in radiation intensity with depth is much more gradual than at greater wavelengths. This is the case for all environments.

To study the appropriateness of assuming exponentially decaying light attenuation, graphs of 'ln (L_z/L_o) versus depth', for 470 nm, were produced (Fig 42). This wavelength was chosen since at this particular wavelength, the transmission is largest (attenuation is lowest). The good correlation implies quite homogeneous media, although there are large differences in b values for point pairs, in particular from the origin to the first point. This might be related to density variations (change of material compaction) between the surface, and deeper down or it might be an instrumental artifact (due to ln(1) which is 0). Considering all profiles for each media, the averaged extinction coefficients at 470 nm were 0.11 cm^{-1} for semi-infinite snow, 0.41 cm^{-1} for shallow snow, and 0.036 cm^{-1} for blue ice. These are in accordance with the results of Grenfell (1979), Grenfell and Maykut (1977), and Liljequist (1956).

Figure 43 (a-c), presents extinction coefficients for every depth-profile acquired in respectively semi-infinite, shallow snowpack, and blue ice media. The extinction coefficients extracted for the three media show similar pattern in the 750-900 nm range.

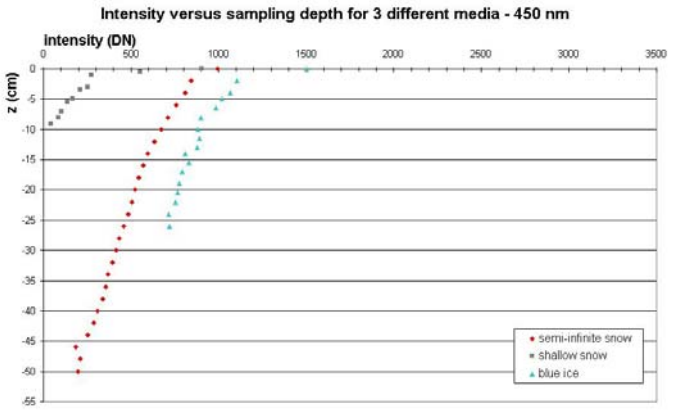

a)

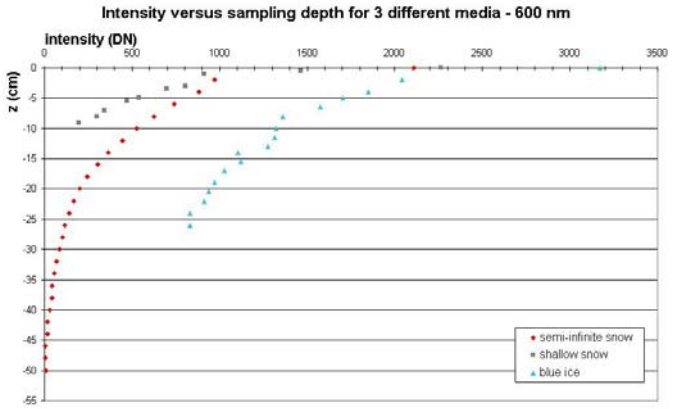

b)

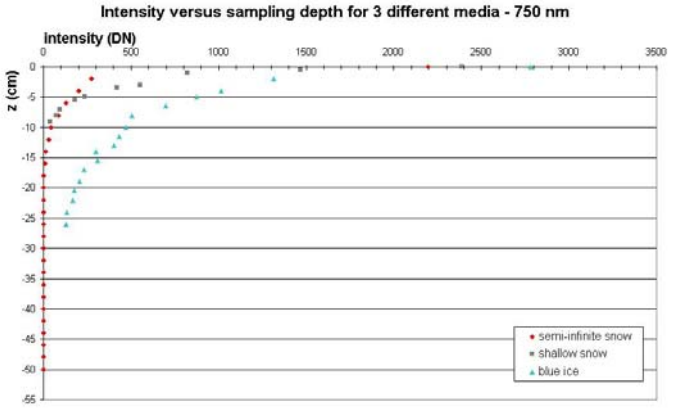

c)

Figure 41. Intensity vs sampling depth.

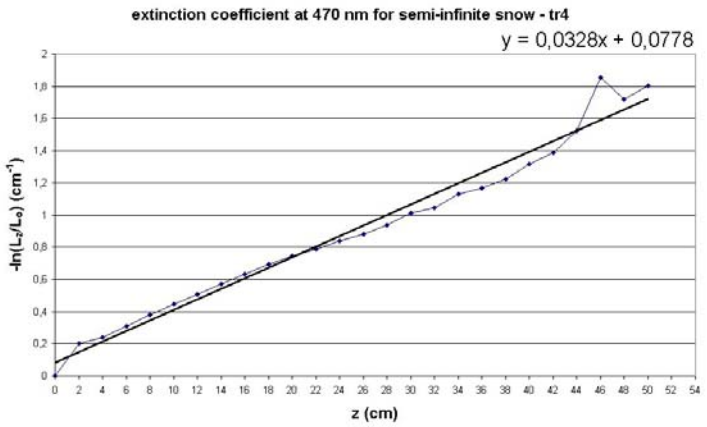

a)

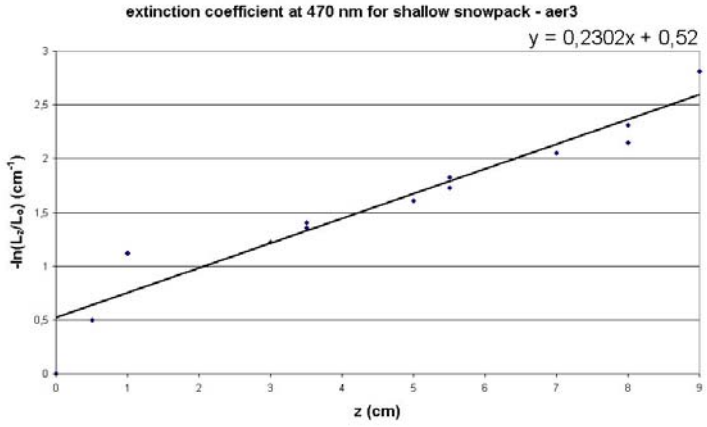

b)

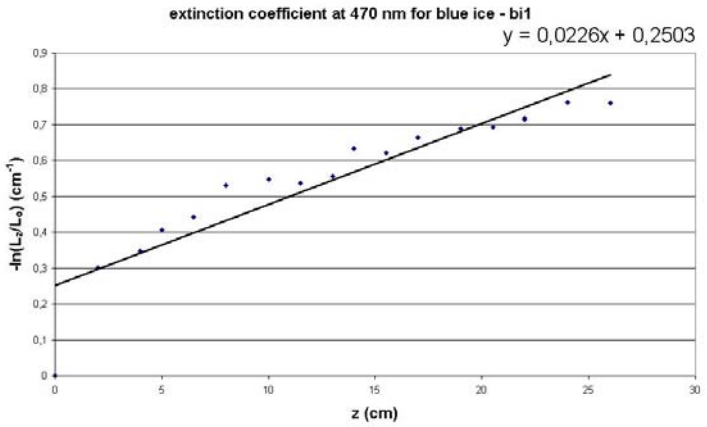

c)

Figure 42. Extinction coefficients at 470 nm.

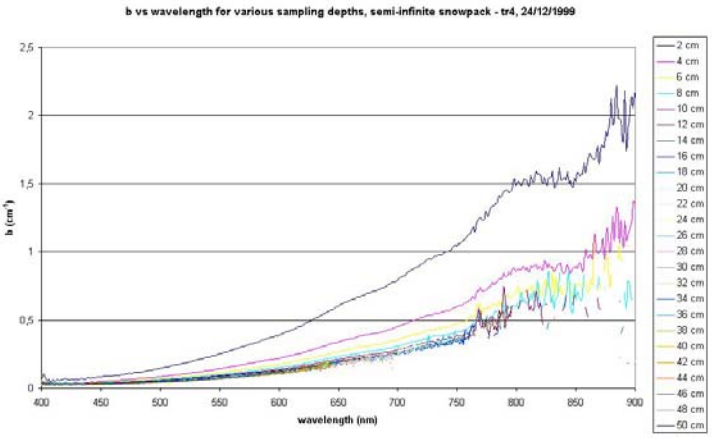

a)

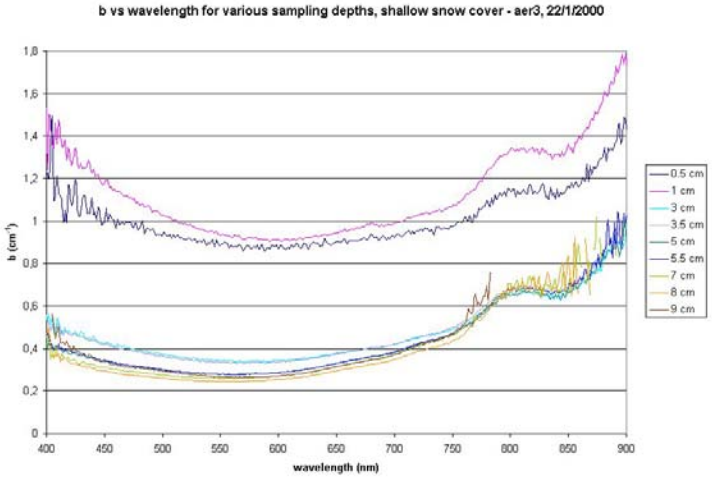

b)

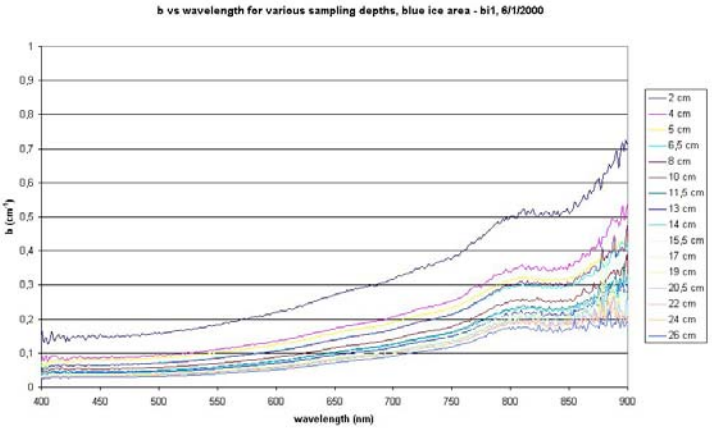

c)

Figure 43. Extinction coefficient b vs wavelength.

In deep snow, one can observe attenuation coefficient values ranging from 0.025 to 2 cm^{-1}. The highest extinction coefficient (0.06-2 cm^{-1}) is found closer to the surface. With increasing depth (10 cm and deeper), it reaches asymptotic value (wavelength-dependant), which indicates a more constant light attenuation. The 10 cm curve (Fig. 43) in the tr4 profile shows that there is less variations and the attenuation coefficient ranges between 0.035 and 0.7 cm^{-1}. The extinction coefficient in shallow snow is strongest close to the surface with attenuation coefficient values of about 0.9 to 1.7 cm^{-1}. At both ends of the solar spectrum, the extinction is more pronounced (1.3-1.7 cm^{-1}). The weakest b (0.9 cm^{-1} for less than 1 cm depths) values are observed around 570-580 nm. The 3-9 cm curves' pattern is similar to the surface ones, but with b values ranging from 0.3-1 cm^{-1}. The extinction coefficient in blue ice shows only slight variations in the visible: 0.025-0.15 cm^{-1} at 400 nm, and 0.09-0.30 cm^{-1} at 700 nm. From the visible to near infrared, the attenuation coefficient increases progressively, showing higher values in the 750-900 nm range. The top profiles have higher attenuation coefficient values, differing (at all wavelengths) from other depth-profiles of at least 0.1 cm^{-1}.

The extinction coefficients were also determined as averages for every depth sampled in each profile. From Figure 44, we can notice that blue ice is more transparent to solar radiation than snow, although blue ice and semi-infinite snow has b values in the same order of magnitude (about 0.035 cm^{-1}) in the 400-500 nm spectral region. b values of the s-i profile increase almost steadily between 500-750 nm, and it catches up the shallow snow profile. The latter present considerably higher b values in the visible range (compared to s-i and bi).

5.6 Helicopterborne spectroradiometry

Helicopter borne measurements were made using an ASD spectroradiometer with the wavelength range 300-2500 nm. The spectroradiometer was mounted in the rear seat of the helicopter and its fibre optics cable was attached to the landing gear on the left side. This arrangement allowed unobstructed view of the surface below the helicopter.

Typically the instrument requires a warm up time of about 30 minutes to ensure adequate stability for this type of measurement. The instrument was optimized against a Spectralon reference panel that also served as white reference. During the flights 25 spectra were sampled and averaged to give outputs at five-second intervals along the flight line. The output is written straight to the hard disc of the computer controlling the instrument.

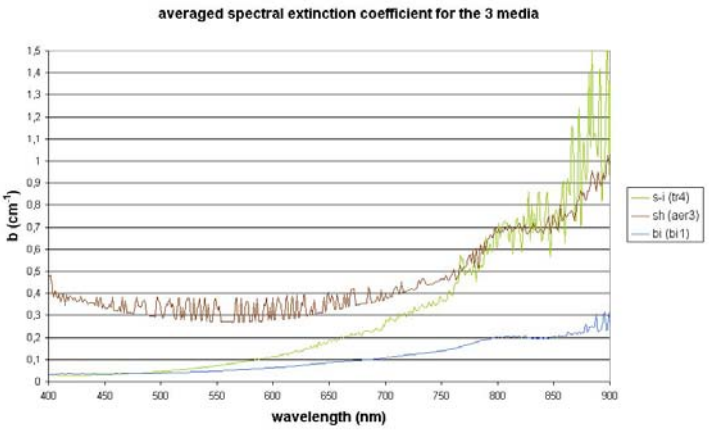

Figure 44. Averaged spectral extinction coefficient for three media.

6. Ice observations

6.1 Sea ice

Originally it was planned that the sea ice work would utilise the Russia MI-8 helicopters from the R/V Akademik Fedorov. Unfortunately they where not available for this role and so the sea ice work shrunk from an extensive survey that would have started already at the marginal ice zone, to only three fast ice points located close to the offloading places in the direct vicinity of the ice shelf edge.

The snow measurements above the sea ice gave some valuable information together with other snow measurements done in Dronning Maud Land. FINNARP has made sea ice research also earlier in the same area (Kosloff, 1991; Kosloff et al., 1997).

Two of the sea ice sites were situated near the Norwegian unloading place located 220 km from their research station Troll (72° 01'S, 2° 32'E) which is several hundred kilometres further east from the Finnish unloading place Ramppi. One sea ice site was in the front of Ramppi. Sea ice measurement sites are listed in Table 13. Sea ice and seawater samples were taken only from stations 1 and 2. At station 3 ice was too thick to drill through. The location of station 3 was poorly decided in the front of the vessel. In all three sites snow properties i.e. temperature, density, pH, conductivity and salinity were measured, at station 3 dielectric constant also. Conductivity, pH and salinity were measured from melted samples. Sea ice samples were taken with Kovacs ice drill. Snow measurements were made in a similar way to those made in snow pits. From sea ice samples some thin sections have been made to determine the crystal size and orientation.

Sea ice measurements were made in the middle of the melting season between December 9-15. Table 14 show ice thickness (H), free board (fb), salinity of seawater (S), pH of seawater (pH) and conductivity of seawater (κ) and Table 15 show the snow measurements: snow thickness (h), density (ρ), surface dielectric constant (ε_r), salinity (S), pH (pH) and conductivity (κ). The average snow depth was 21 cm, the average snow density 386±14 kg m^{-3}, the average salinity of snow 1.3±0.3 ppt, the average pH 7.4±0.3 and the average conductivity 2.7±0.6 mS cm^{-1}. In the station 3 the real part of dielectric constant was 2.86. It was higher than the values in the continent because of salinity of snow. In Figure 45 are seen snow temperature profiles from three different sites.

Table 13. Sea ice stations.

Site	Date	Time (UTC)	Latitude	Longitude	Air temp. °C	Cloud cover
1. Near Troll	9. Dec 1999	7:38	70º 07.033' S	05º 23.044' E	-3.5	1/8
2. Troll	10. Dec 1999	13:15	70º 06.967' S	05º 20.666' E	-1.1	8/8
3. Ramppi	15. Dec 1999	7:50	72º 29.275' S	16º 31.566' W	-3.1	8/8

Table 14. Sea ice measurements.

Station	H (cm)	fb (cm)	S (ppt)	pH	κ (mS cm^{-1})
1.	138	9	30.5	7.9	49
2.	90	8	32	7.9	52

Table 15. Snow measurements on the sea ice.

Station	h (cm)	ρ (kg m^{-3})	ε_r	S (ppt)	pH	κ (mS cm^{-1})
1.	17	332	-	1.4	7.3	2.9
2.	20	403	-	0.5	7.5	1.3
3.	25	413	2.86	2	7.5	3.9

6.2 Blue ice

6.2.1 Blue ice studies at Aboa

Some low altitude blue ice measurements were made in 1999/2000 near Basen nunatak (about 250 m a.s.l.) and also in Heimefrontfjella near the Svea base (1250 m a.s.l.). Near Basen ice temperature profiles were measured once and some radar profiles and radiation measurements were made. Also few ice samples were taken and thin sections for later ice crystal analyses were made. Few ice samples were taken from cryoconite holes that have been formed when some

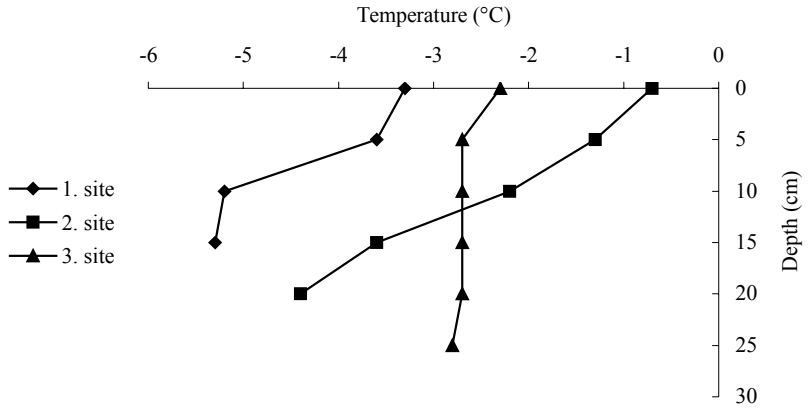

Figure 45. Temperature profiles of snow cover above the sea ice in three different sites.

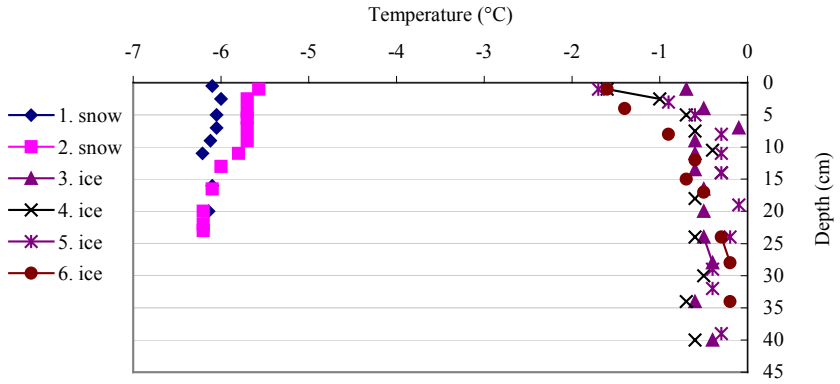

Figure 46. Temperature profiles from the low altitude blue ice area near Basen and from snow cover next to it.

rocks have melted from the surface inside the ice (Bintanja, 1999). Usually rocks sink some decimetres. Near Svea base in Heimefrontfjella some blue ice samples were collected and radiation measurements were made.

Temperature profiles were taken January 26 near Basen are seen in Figure 46. First two are from snow next to the frozen lake and four are from blue ice. Snow temperatures are 4-6 °C lower than temperatures in the ice. Temperatures were measured from the hole made with motored hand drill.

During the season 2000/2001 weather station was left in a low altitude blue ice area (about 250 m a.s.l.) near Basen nunatak for a period January 16-28. It measured temperatures of 1.5 m and 2.5 m, wind speed, wind direction and ice temperatures in 0.1 m and 0.4 m depth. The blue ice area was mapped around with hand-held GPS and several digital images were taken from helicopter.

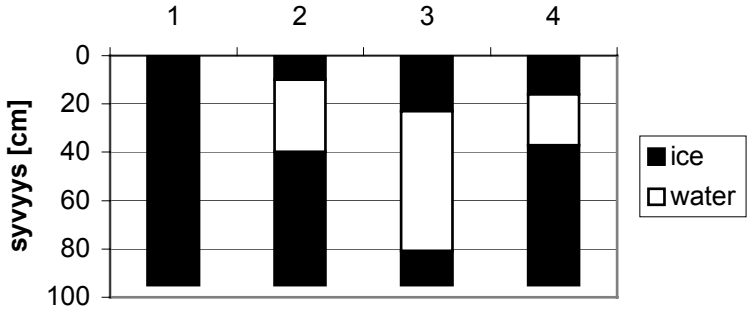

Figure 47. The holes drilled in blue ice showing the depth and thickness of the water layer.

6.2.2 Blue ice studies in 2000/2001 at SANAE 4

Subsurface melting was observed in a low altitude blue ice field close to the SANAE 4 Antarctic research station. There was an average of 36.3 cm of liquid water below an average of 16.3cm of ice. Three out of four holes drilled in this field contained water. The fourth hole was drilled to a depth of 95 cm without finding water. The pH of the ice crystals in a hole containing water was 5.9 and the conductivity was 11.1 μS. The holes drilled are schematically illustrated in Figure 47.

These holes were drilled relatively close to the mountain in a blue ice area that was definitely formed by the mountain. This means that most probably the water is meltwater runoff rather than subsurface melting.

7. Conclusions

Seasonal snow investigations were made in Dronning Maud Land within the 'Seasonal Snow in Antarctica' project. Scientists working for this project took part in the FINNARP 99 and FINNARP 2000 expeditions. Measurements were made in the vicinity of the Finnish Antarctic research station Aboa and the South African research station SANAE 4.

According to measurements the snow cover of the area can be divided to five zones; 1) sea ice, 82) the seaward edge of the ice shelf, 3) the inner parts of ice shelf, 4) the glaciers above the grounding line and 5) the local topographic highs. On the ice shelf elevation is quite equal (about 70 m a.s.l.) but above the grounding line it starts to increase steeper up to 1000 m a.s.l. Topographic features near the grounding line block partly the moist air masses coming from the Southern Ocean (Bromwich, 1988). Ice domes and ice rises are locally high points rising from the ice sheet. They are not so much exposed to katabatic winds.

The data taken during the austral summer 1999-2000, showed that the attenuation by the snowpack is higher than that of the blue ice. In the case of shallow snowpack, the underlying surface controls the radiation pattern.

The irradiance data showed that, in the case of a partly covered sky, the ratio between the zenith path radiance to the hemispherical radiance is much higher due to diffuse radiation. The correction factors computed were not related to the solar elevation angle. This goes along with Wan Wyngaarden's results (1984), but is opposed to those found by Eaton and Dirhhirn (1979).

8. References

Bintanja, R. 1999. On the glaciological, meteorological, and climatological significance of Antarctic blue ice areas. Reviews of Geophysics, Vol. 37, No. 3, p. 337-359.

Brandt, R.E. and S. G. Warren, 1993. Solar-heating rates and temperature profiles in Antarctic snow and ice. Journal of Glaciology, vol. 39, no. 131, p. 99-110.

Van den Broeke, M.R., J-G Winther, E. Isaksson, J.F. Pinglot, L. Karlöf, T. Eiken and L. Conrads. 1999. Climate variables along a traverse line in Dronning Maud Land, East Antarctica. Journal of Glaciology, Vol.45, No. 150, p. 295-302.

Bromwich, D.H., R.I. Cullather and M.L. Van Woert. 1998. Antarctic precipitation and its contribution to the global sea-level budget. Annals of Glaciology 27, p. 220-226.

Bromwich, D.H. 1988. Snowfall in high southern latitudes. Reviews of Geophysics, Vol. 26, No. 1, p. 149-168.

Colbeck, S., E. Akitaya, R. Armstrong, H. Gubler, J. Lafeuille, K. Lied, D. McClung and E. Morris. 1990. The International Classification for Seasonal Snow on the Ground, 23 p.

Dahe, Q., N.W. Young and R.J. Thwaites. 1988. Growth rate of crystals within the surface-snow/firn layer in Wilkes Land, East Antarctica. Annals of Glaciology 11, p. 121-125.

Eaton, F.D. and Dirmhirn, I. 1979. Reflected irradiance indicatrices of natural surfaces and their effect on albedo. Applied Optics, vol. 18, no. 7, p.994-1008.

Goodwin, I.D. 1991. Snow-accumulation variability from seasonal surface observations and firn-core stratigraphy, eastern Wilkes Land, Antarctica. Journal of Glaciology,Vol.37, No. 127, p. 383-387.

Goodwin, I.D., M. Higman, I. Allison and R. Jaiwen. 1994. Accumulation variation in eastern Kemp Land, Antarctica. Annals of Glaciology 20, p. 202-206.

Granberg, H. B., 2002. Seasonal Snow in Antarctica, Automatic Snow Sensors Tech. Report, CARTEL, Université de Sherbrooke.

Grenfell, T.C. and G. A. Maykut, 1977. The optical properties of ice and snow in the Arctic basin. Journal of Glaciology, vol. 18, no. 80, p. 445-463.

Grenfell, T.C. 1979. The effects of ice thickness on the exchange of solar radiation over the polar oceans. Journal of Glaciology, vol. 22, no. 87, p. 305-320.

Hallikainen, M. and D.P. Winebrenner. 1992. The physical basis for sea ice remote sensing. In Microwave remote sensing of sea ice, Geophysical Monograph 68, p. 29-46.

Holmlund, P. and J.-O. Näslund. 1994. The glacially sculptured landscape in Dronning Maud Land, Antarctica, formed by wet-based mountain glaciation and not by the present ice sheet. Boreas, Vol. 23, p. 139-148.

Isaksson, E. and W. Karlén. 1994. Spatial and temporal patterns in snow accumulation, western Dronning Maud Land, Antarctica. Journal of Glaciology, Vol. 40, No.135, p. 399-409.

Jeffries, M.O., B. Hurst-Cushing, H.R. Krouse and T. Maksym. 1998. The role of snow in the thickening and mass budget of first-year floes in the eastern Pacific sector of the Antarctic pack ice. Report UAG R-327. Geophysical Institute, University of Alaska Fairbanks. 34p.

Kojima, K. 1964. Densification of snow in Antarctica. Antarctic Snow and Ice Studies, Antarctic Research Series Vol. 2, p.157-218, American Geophysical Union.

Kosloff, P. 1991. Structural Characteristics of Weddell Sea Ice during the First Leg of the FINNARP-89. FINNARP-89 Symposium report No 1, p. 48-52.

Kosloff, P., S. Kivimaa and H. Grönvall. 1997. Remote sensing and sea ice. Antarctic Reports of

Finland Report No 6, p. 28-29.

Kulkarni, A.V., 1986. A field study of the visible and near-infrared spectral reflectance and attenuation of solar radiation by snow. Masters thesis, Department of Geography, McGill university, Montreal,

Kärkäs, E. 2000. Kesäaikaisen lumipeitteen fysikaaliset ominaisuudet Kuningatar Maudin maalla, Etelämantereella. Master of Science thesis. Department of Geophysics, University of Helsinki. 96p.

Liljequist, G. H. 1956. Short-wave radiation. Norwegian/British/Swedish Antarctic Expeditions 1949-1952, vol. II (Meteorology), part 1 (Energy exchange of an Antarctic snow-field), p. 1-110.

Massom, R.A., M. R. Drinkwater and C. Haas. 1997. Winter snow cover on sea ice in Weddell Sea. Journal of geophysical research, 102(C1), p. 1101-1117.

Mosley-Thompson, E., P.D. Kruss, L.G. Thompson, M. Pourchet, and P. Grootes. 1985. Snow stratigraphic record at South Pole: Potential for paleoclimatic reconstruction. Annals of Glaciology 7, p. 26-33.

Paterson, W.S.B. 1994. The physics of glaciers. 3rd edition, 480p.

Pihkala, P. and E. Spring. 1985. A practical method for photographing snow samples. Report Series in Geophysics No 20. University of Helsinki, Department of Geophysics, 11p.

Sihvola, A. and M. Tikri, 1986. Snow fork for the field determination of the density and wetness profiles of a snow pack, IEEE Trans. Geosci. Remote Sensing, GE –24 , p. 717-720.

Ulaby, F. T. 1986. Microwave remote sensing active and passive. Vol. 3: From theory to applications, p. 2017-2115.

Virta, J. and A. Blanco. 1995. Correction of measured underwater spectral irradiance to the variation of some external effects with examples, in Pulkkinen, K. (ed.), Proceedings of the 2nd Finnish-Estonian seminar on underwater optics with applications, Helsinki, 10-12 April 1995. University of Helsinki, Department of Geophysics, Report Series in Geophysics 32, p. 93-100.

Wadhams, P. 1998. Sea ice morphology. In Physics of ice-covered seas. Vol 1, p. 231-288. Editor M. Leppäranta. Helsinki University Press, p. 231-288.

Warren, S. G., 1982. Optical Properties of Snow, Reviews of Geophysics and Space Physics, Vol. 20, No. 1, p. 67-89.

Van Wyngaarden, R. 1984. Observations on the relationship between hemispherical surface reflectance and zenith path reflectance over snow at Schefferville, P.Q. Department of Geography, McGill University, Montréal, 18 p.

9. Appendix A

Snow pit data for the 1999 / 2000 and 2000 / 2001 from the region surrounding Aboa.

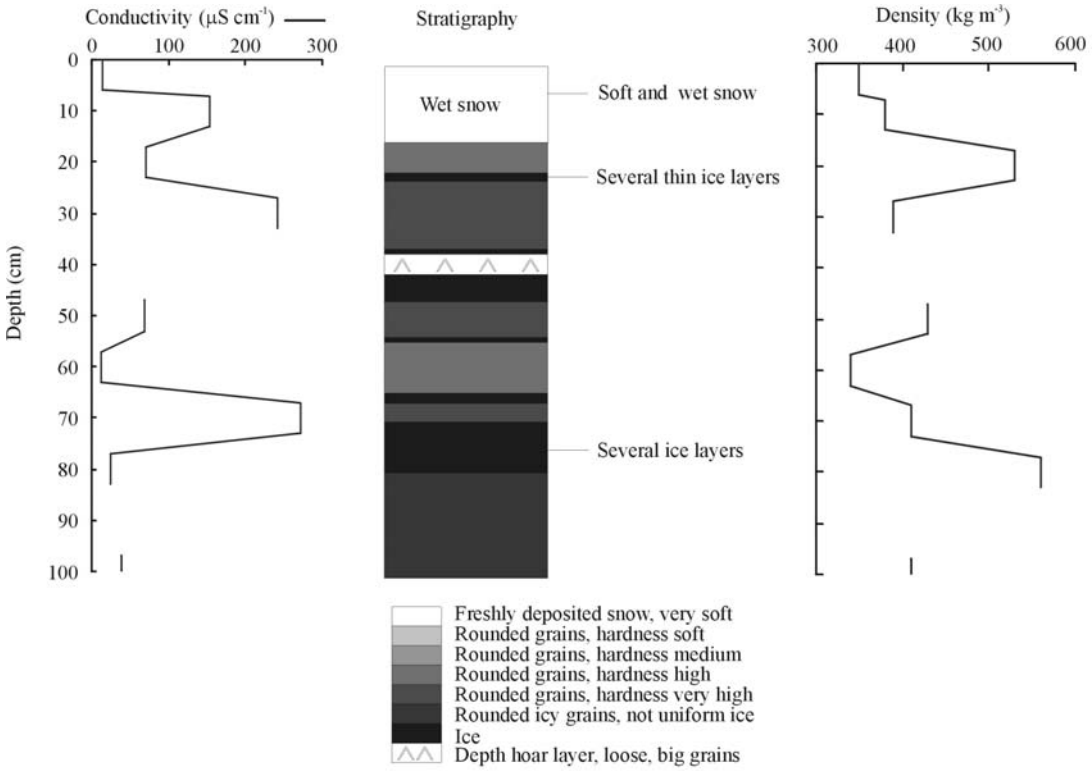

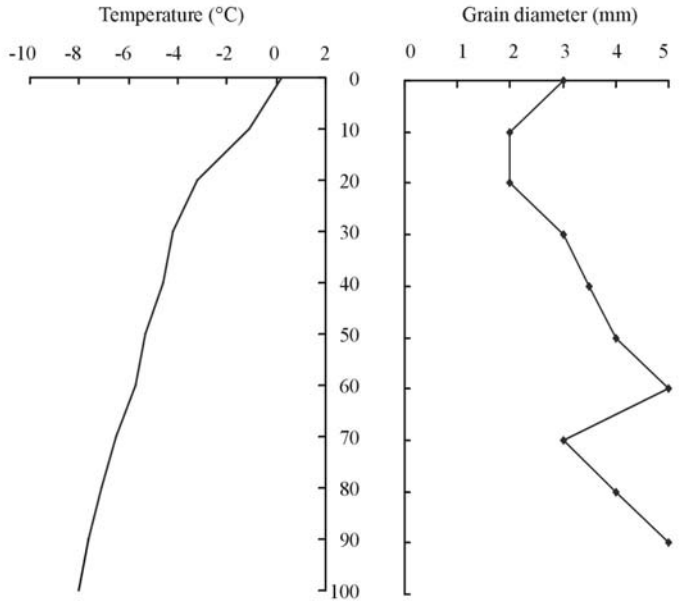

Snow site 1
Date: 26 Dec 1999
Coordinates: 72° 32.0'S, 16° 34.0'W

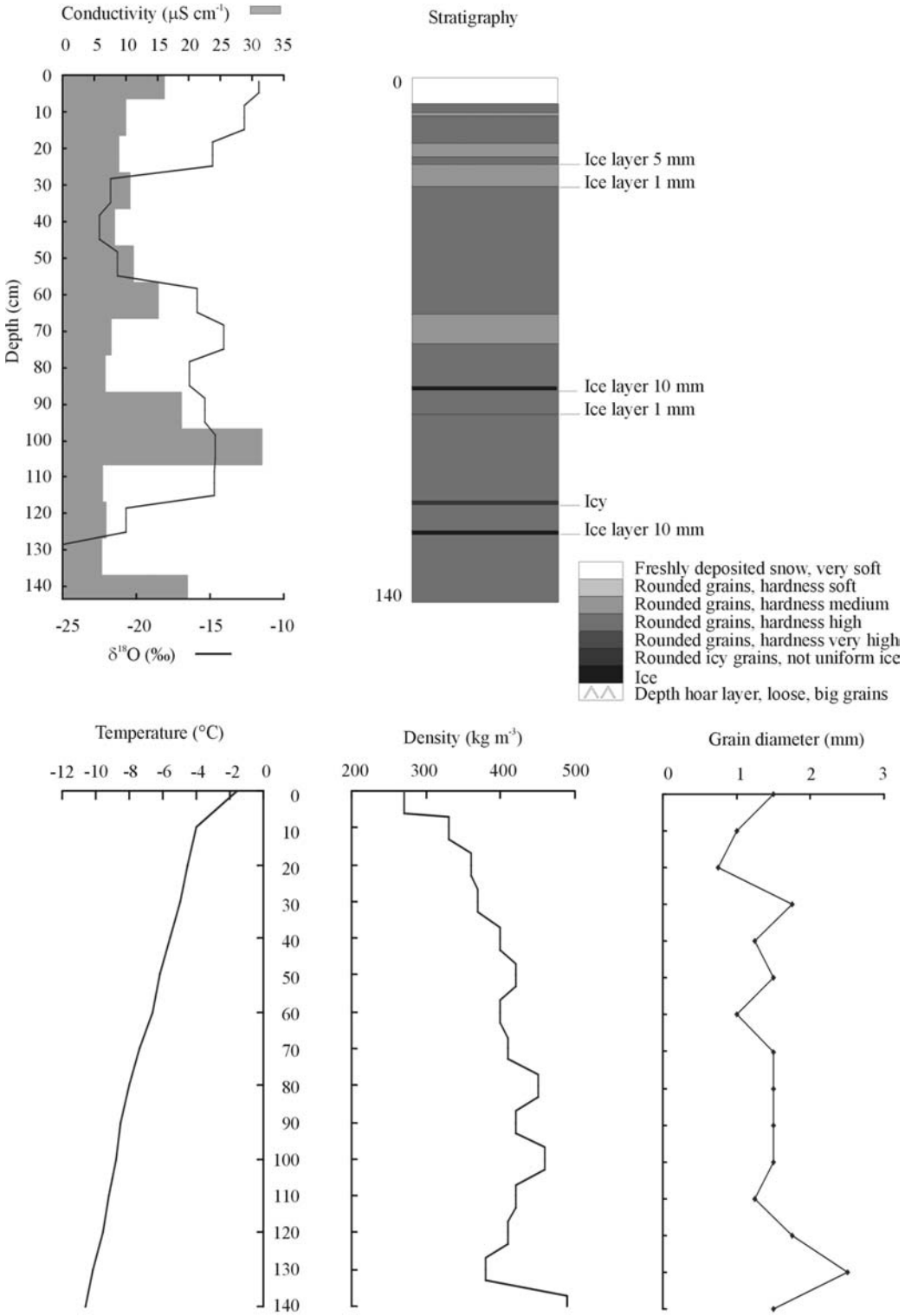

Snow site 2
Date: 18 Jan 2000
Coordinates: 72°36.6'S 16° 18.6'W

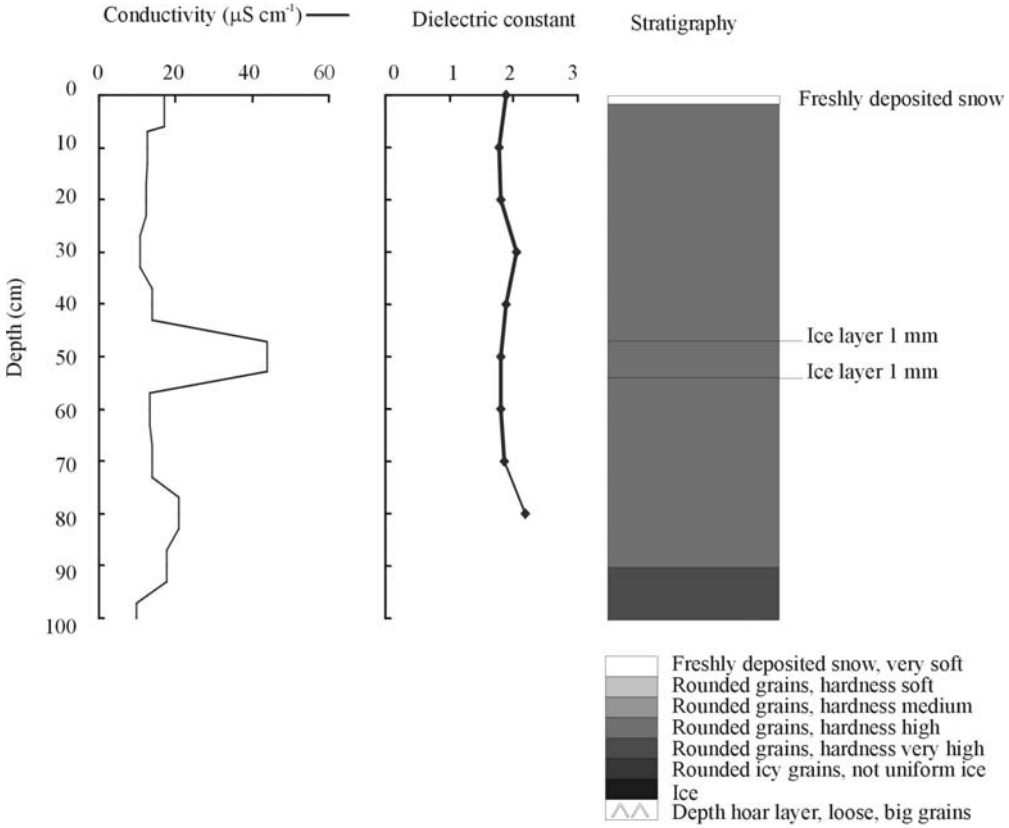

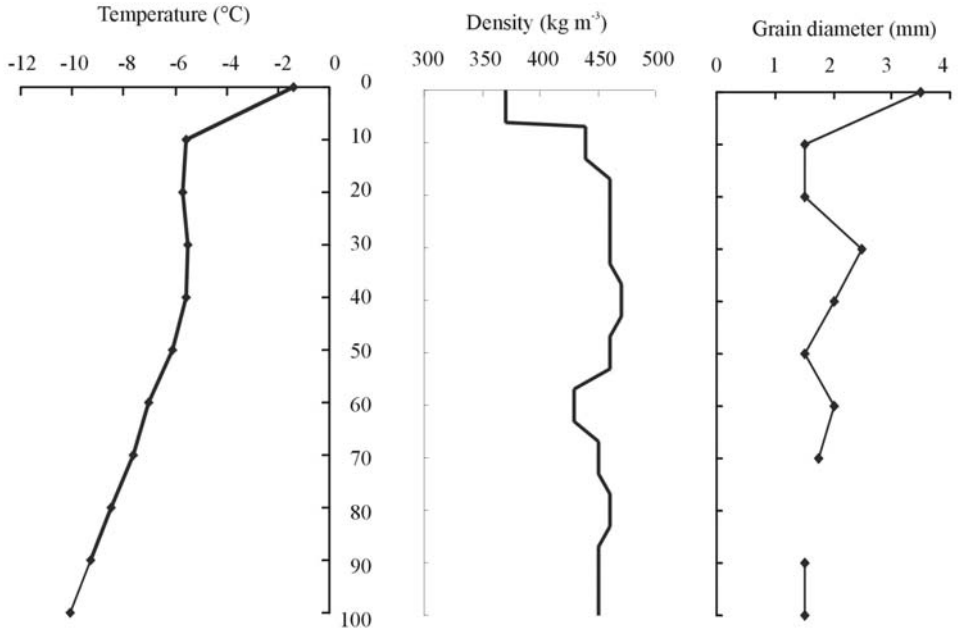

Snow site 3a
Date: 26 Dec 1999
Coordinates: 72° 40.0'S, 16° 41.9'W

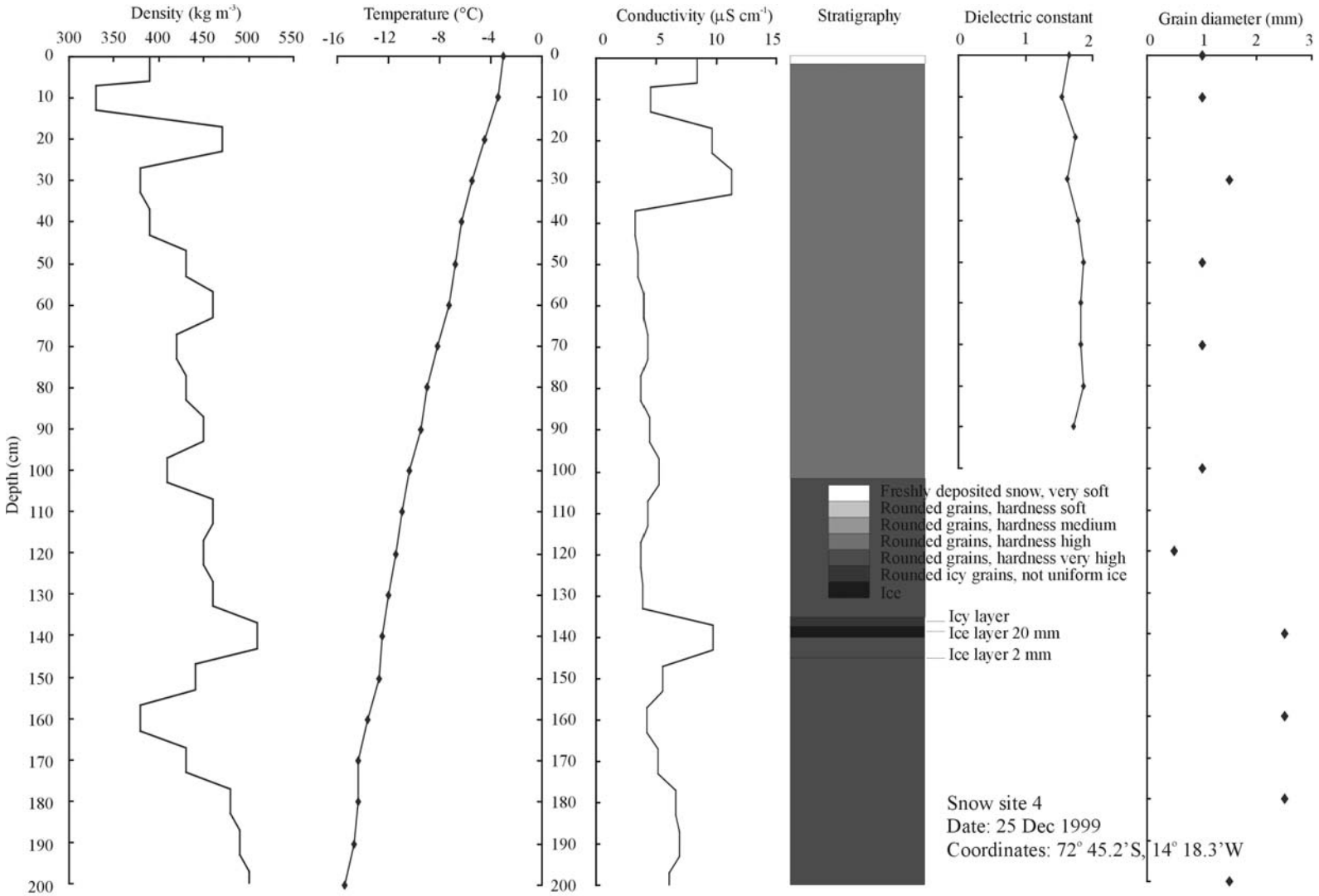
Density (kg m-3)
300 350 400 450 500 550
Temperature (°C)
-16 -12 -8 -4 0
Conductivity (µS cm-1)
0 5 10 15
Stratigraphy
Dielectric constant
0 1 2
Grain diameter (mm)
0 1 2 3
Depth (cm)
0 10 20 30 40 50 60 70 80 90 100 110 120 130 140 150 160 170 180 190 200
Freshly deposited snow, very soft
Rounded grains, hardness soft
Rounded grains, hardness medium
Rounded grains, hardness high
Rounded grains, hardness very high
Rounded icy grains, not uniform ice
Ice
Icy layer
Ice layer 20 mm
Ice layer 2 mm
Snow site 4
Date: 25 Dec 1999
Coordinates: 72° 45.2'S, 14° 18.3'W

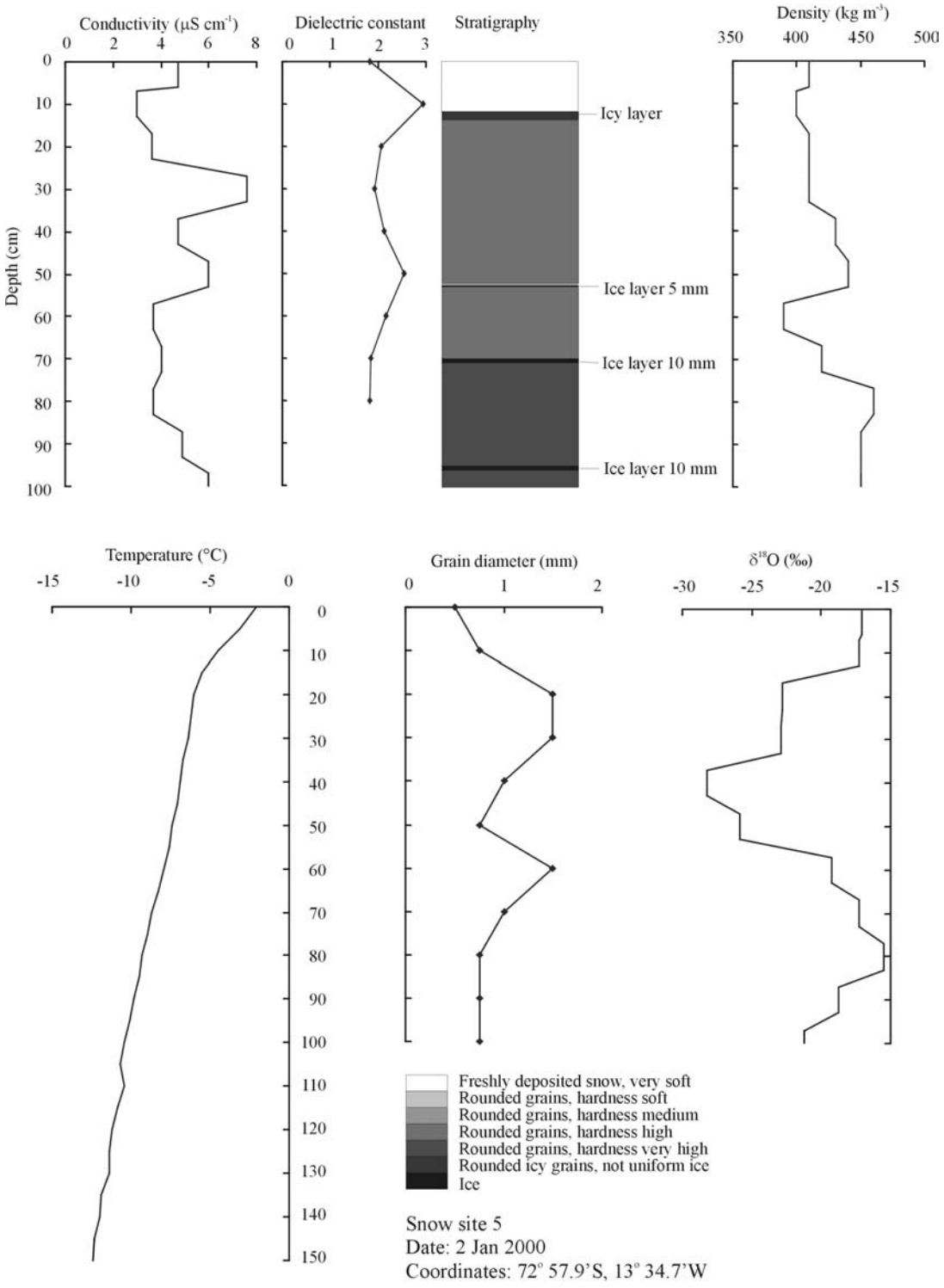
Conductivity (μS cm-1)
0 2 4 6 8
Dielectric constant
0 1 2 3
Stratigraphy
Density (kg m-3)
350 400 450 500
Depth (cm)
0 10 20 30 40 50 60 70 80 90 100
Icy layer
Ice layer 5 mm
Ice layer 10 mm
Ice layer 10 mm
Temperature (°C)
-15 -10 -5 0
Grain diameter (mm)
0 1 2
δ18O (‰)
-30 -25 -20 -15
0 10 20 30 40 50 60 70 80 90 100 110 120 130 140 150
Freshly deposited snow, very soft
Rounded grains, hardness soft
Rounded grains, hardness medium
Rounded grains, hardness high
Rounded grains, hardness very high
Rounded icy grains, not uniform ice
Ice
Snow site 5
Date: 2 Jan 2000
Coordinates: 72° 57.9'S, 13° 34.7'W

Density (kg m-3)
200
300
400
500
Depth (cm)
0
10
20
30
40
50
60
70
80
90
100
110
120
130
140
150
160
170
180
190
200
Stratigraphy
Ice layer 1 mm
Ice layer 1 mm
Ice layer 1 mm
Ice layer 2 mm
Ice layer 1 mm
Ice layer 1-10 mm
Freshly deposited snow, very soft
Rounded grains, hardness soft
Rounded grains, hardness medium
Rounded grains, hardness high
Rounded grains, hardness very high
Rounded icy grains, not uniform ice
Ice
Grain diameter (mm)
0
1
2
3
Temperature (°C)
0
-5
-10
-15
-20
Snow site 6
Date: 24 Dec 1999
Coordinates: 73° 02.0'S, 13° 19.5'W

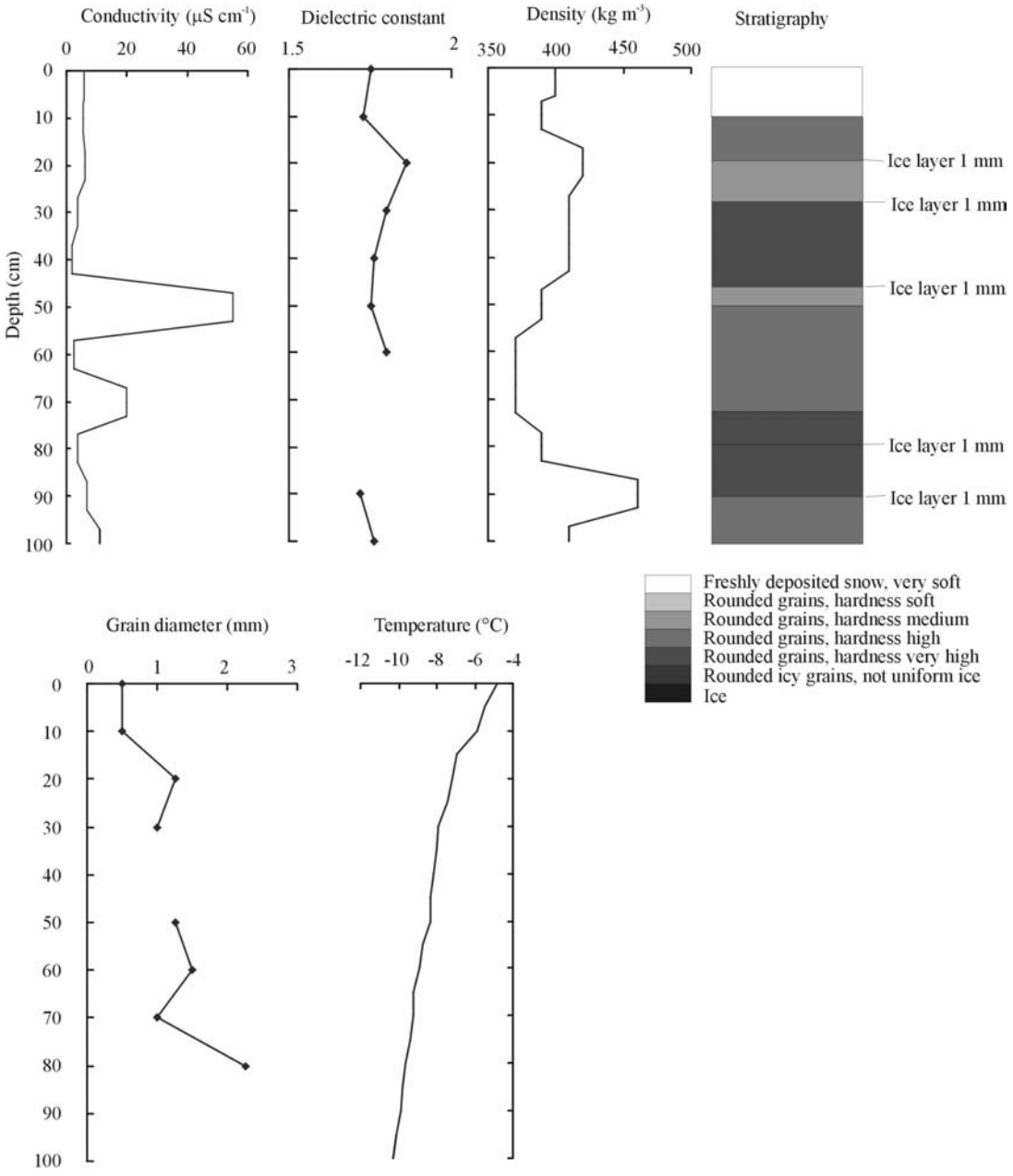

Snow site 7
Date: 3 Jan 2000
Coordinates: 73° 03.6'S, 13° 21.8'W

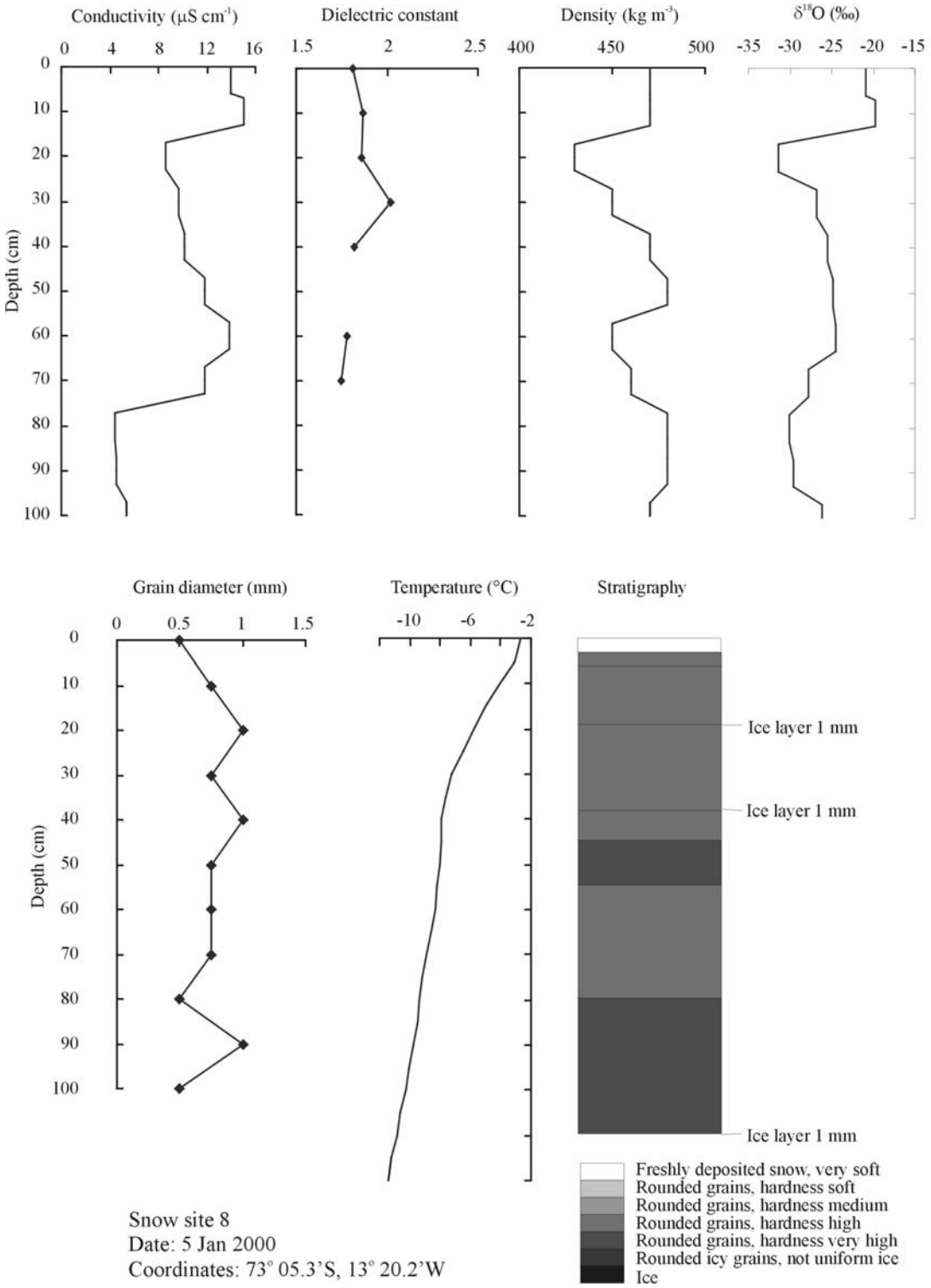
Conductivity (μS cm-1)
Dielectric constant
Density (kg m-3)
δ18O (‰)
Depth (cm)
Grain diameter (mm)
Temperature (°C)
Stratigraphy
Ice layer 1 mm
Ice layer 1 mm
Ice layer 1 mm
Freshly deposited snow, very soft
Rounded grains, hardness soft
Rounded grains, hardness medium
Rounded grains, hardness high
Rounded grains, hardness very high
Rounded icy grains, not uniform ice
Ice
Snow site 8
Date: 5 Jan 2000
Coordinates: 73° 05.3'S, 13° 20.2'W

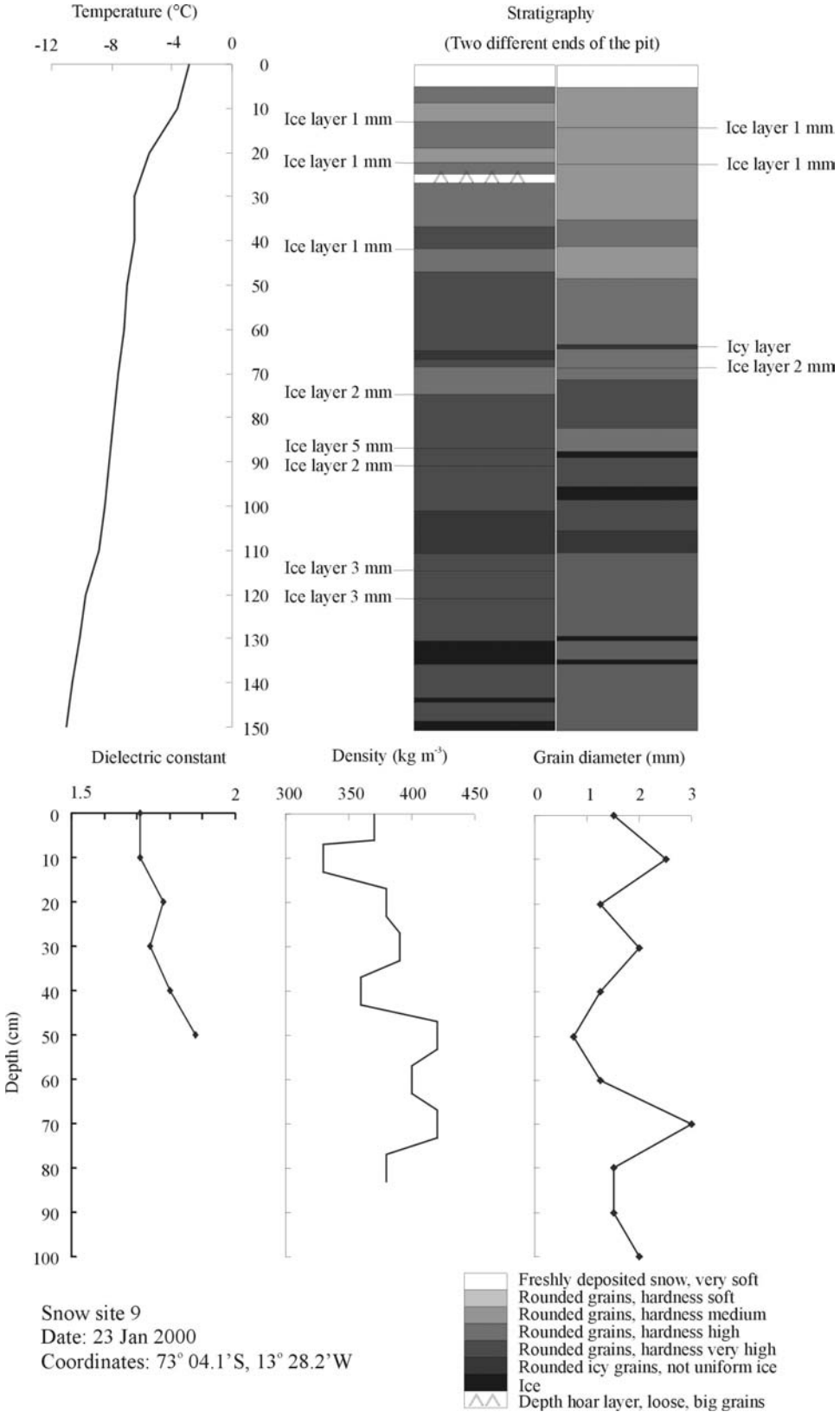
Temperature (°C)
-12
-8
-4
0
Stratigraphy
(Two different ends of the pit)
0
10
20
30
40
50
60
70
80
90
100
110
120
130
140
150
Ice layer 1 mm
Ice layer 1 mm
Ice layer 1 mm
Ice layer 2 mm
Ice layer 5 mm
Ice layer 2 mm
Ice layer 3 mm
Ice layer 3 mm
Ice layer 1 mm
Ice layer 1 mm
Icy layer
Ice layer 2 mm
Dielectric constant
1.5
2
Density (kg m-3)
300
350
400
450
Grain diameter (mm)
0
1
2
3
Depth (cm)
Freshly deposited snow, very soft
Rounded grains, hardness soft
Rounded grains, hardness medium
Rounded grains, hardness high
Rounded grains, hardness very high
Rounded icy grains, not uniform ice
Ice
Depth hoar layer, loose, big grains
Snow site 9
Date: 23 Jan 2000
Coordinates: 73° 04.1'S, 13° 28.2'W

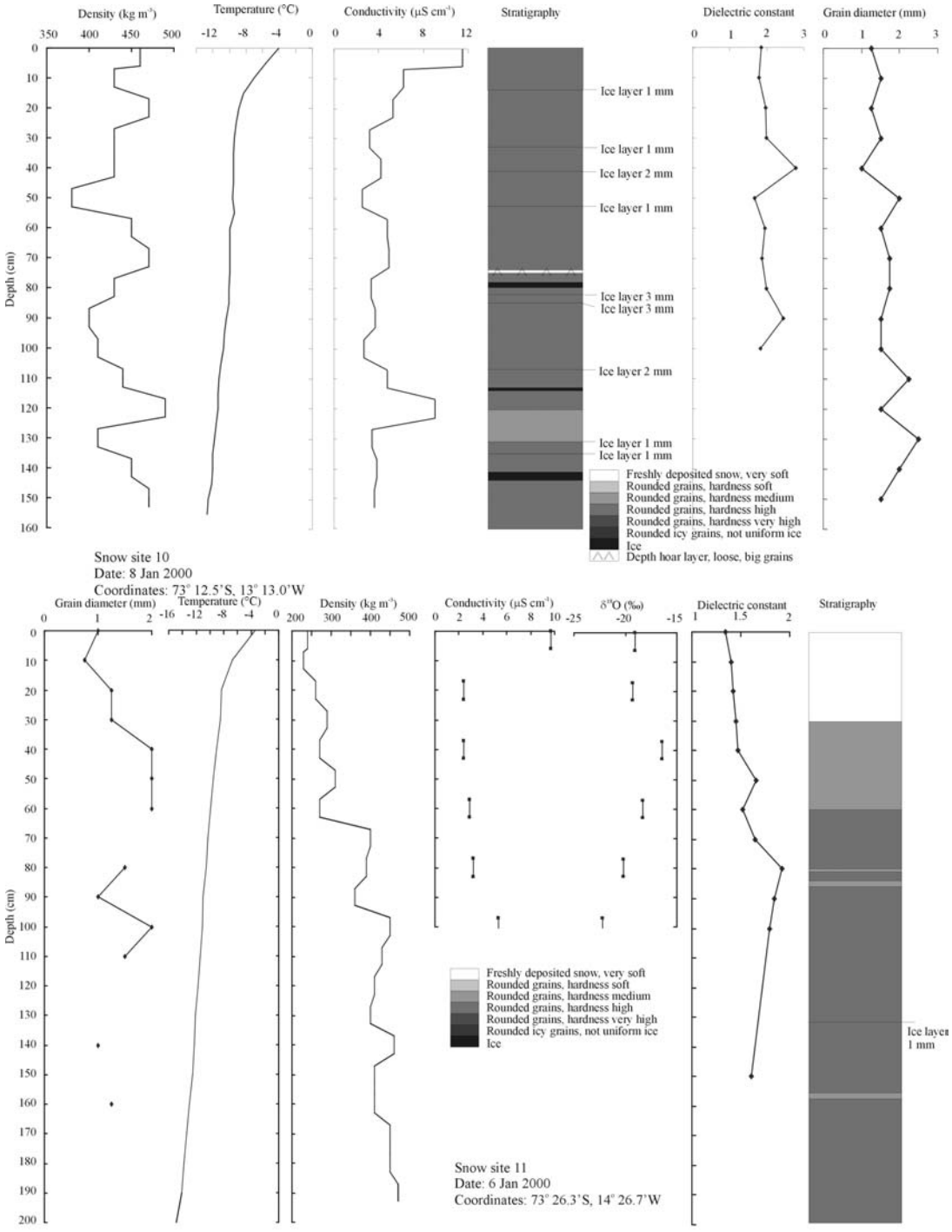
Density (kg m-3)
Temperature (°C)
Conductivity (µS cm-1)
Stratigraphy
Dielectric constant
Grain diameter (mm)
Depth (cm)
Ice layer 1 mm
Ice layer 1 mm
Ice layer 2 mm
Ice layer 1 mm
Ice layer 3 mm
Ice layer 3 mm
Ice layer 2 mm
Ice layer 1 mm
Ice layer 1 mm
Freshly deposited snow, very soft
Rounded grains, hardness soft
Rounded grains, hardness medium
Rounded grains, hardness high
Rounded grains, hardness very high
Rounded icy grains, not uniform ice
Ice
Depth hoar layer, loose, big grains
Snow site 10
Date: 8 Jan 2000
Coordinates: 73° 12.5'S, 13° 13.0'W
Grain diameter (mm)
Temperature (°C)
Density (kg m-3)
Conductivity (µS cm-1)
δ18O (‰)
Dielectric constant
Stratigraphy
Depth (cm)
Freshly deposited snow, very soft
Rounded grains, hardness soft
Rounded grains, hardness medium
Rounded grains, hardness high
Rounded grains, hardness very high
Rounded icy grains, not uniform ice
Ice
Ice layer
1 mm
Snow site 11
Date: 6 Jan 2000
Coordinates: 73° 26.3'S, 14° 26.7'W

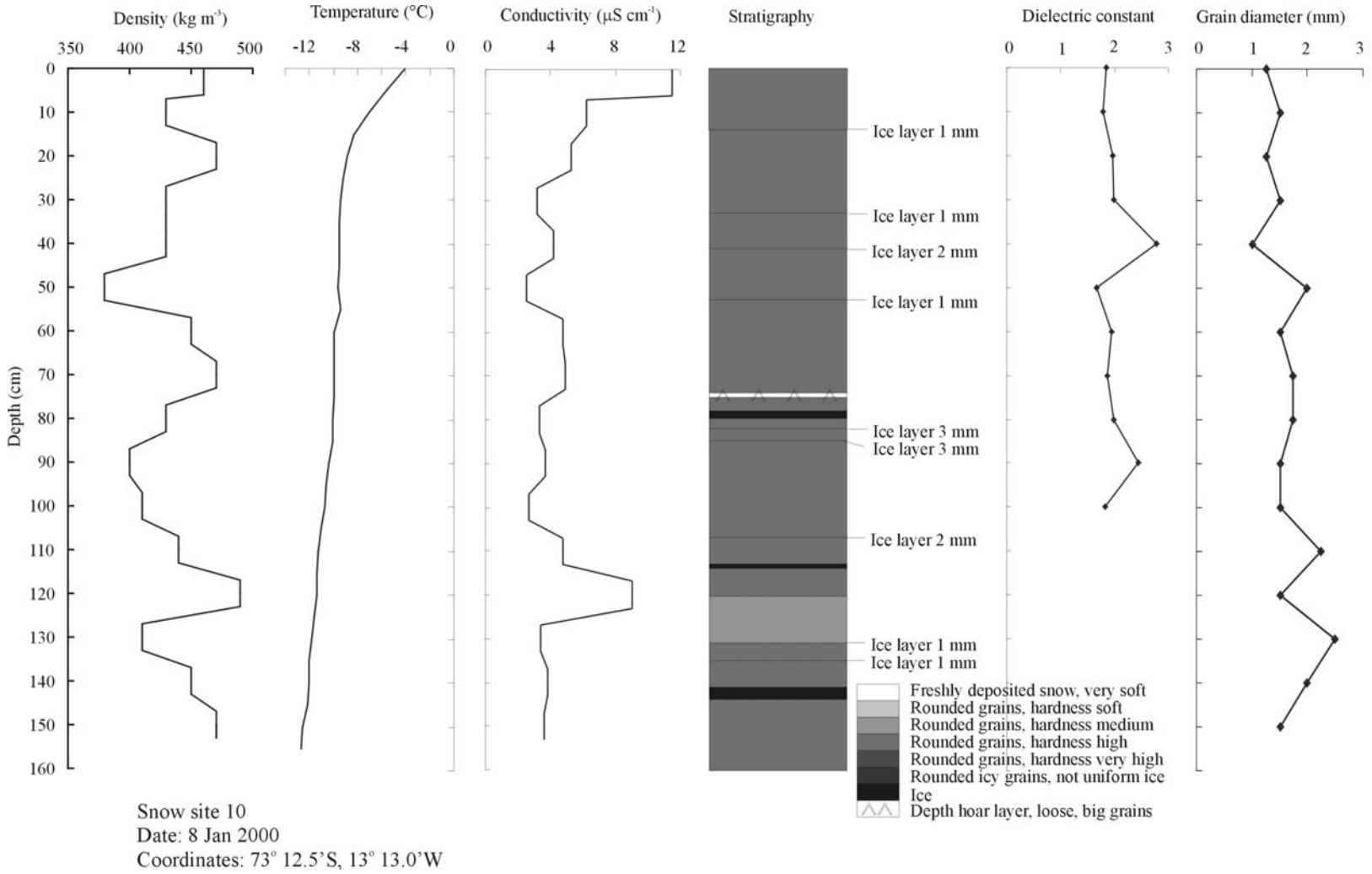

Snow site 10
Date: 8 Jan 2000
Coordinates: 73° 12.5'S, 13° 13.0'W

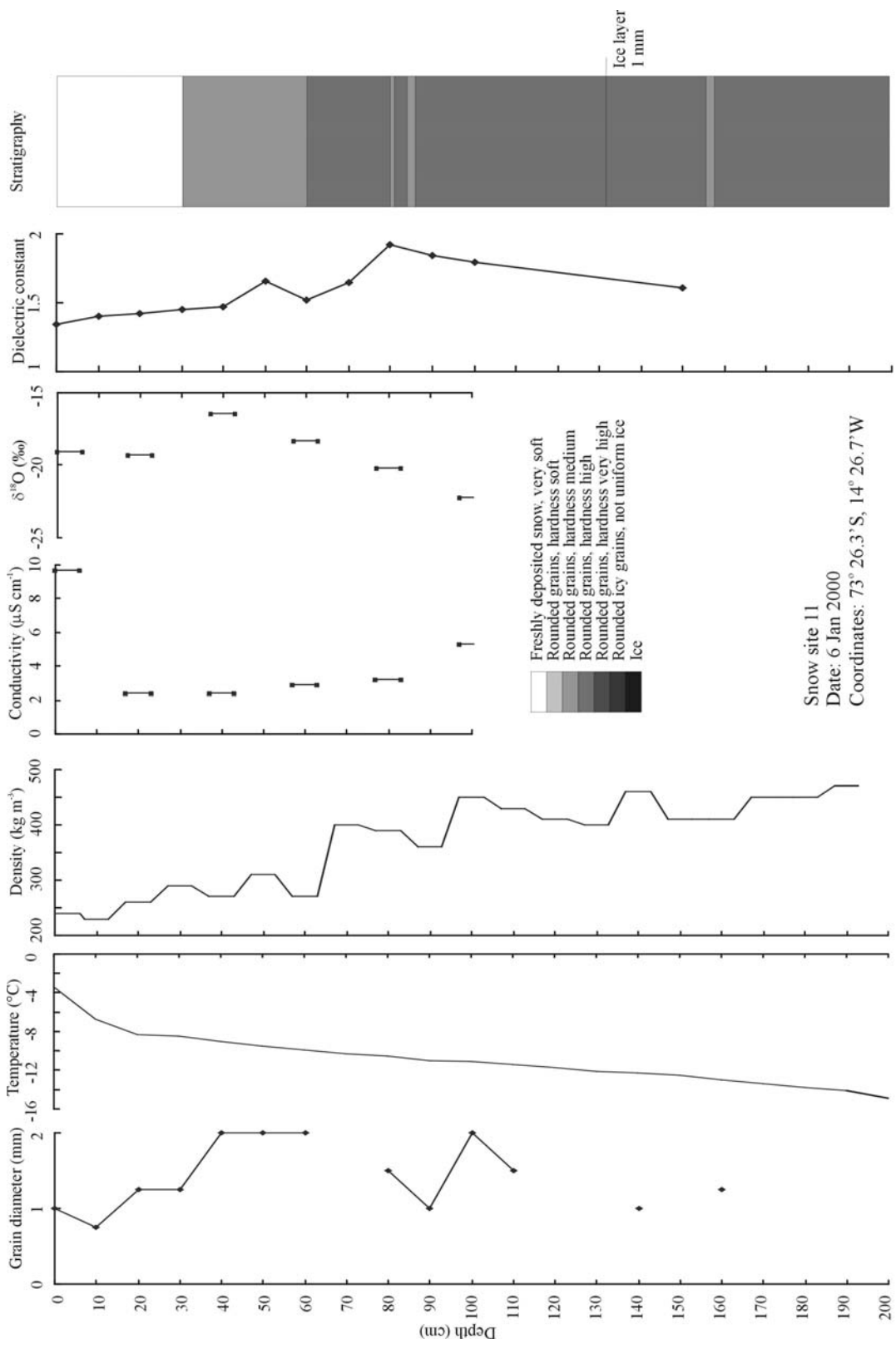
Grain diameter (mm)
Temperature (°C)
Density (kg m-3)
Conductivity (µS cm-1)
δ18O (‰)
Dielectric constant
Stratigraphy
Ice layer
1 mm
Depth (cm)
Freshly deposited snow, very soft
Rounded grains, hardness soft
Rounded grains, hardness medium
Rounded grains, hardness high
Rounded grains, hardness very high
Rounded icy grains, not uniform ice
Ice
Snow site 11
Date: 6 Jan 2000
Coordinates: 73° 26.3'S, 14° 26.7'W

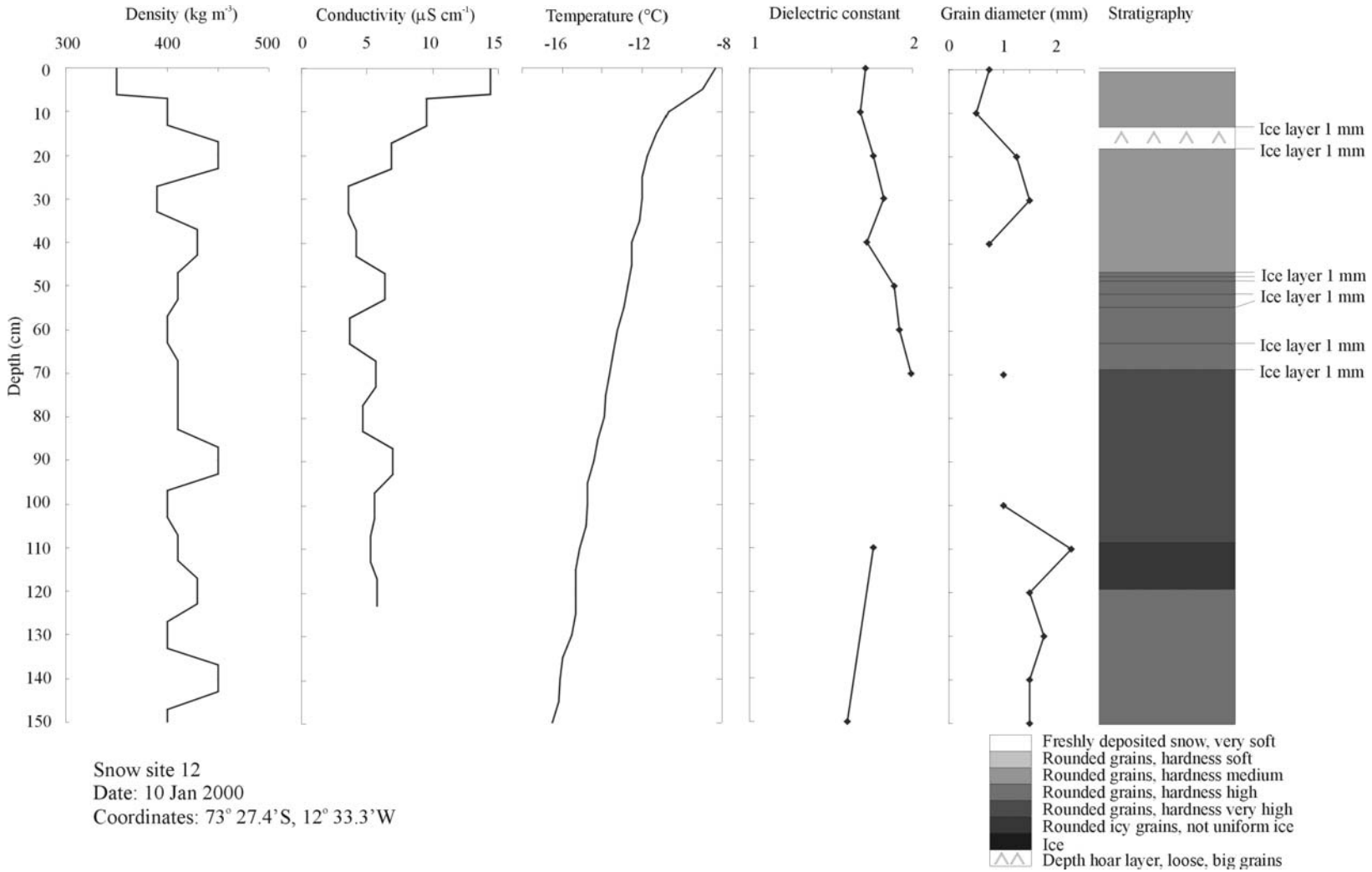

Snow site 12
Date: 10 Jan 2000
Coordinates: 73° 27.4'S, 12° 33.3'W

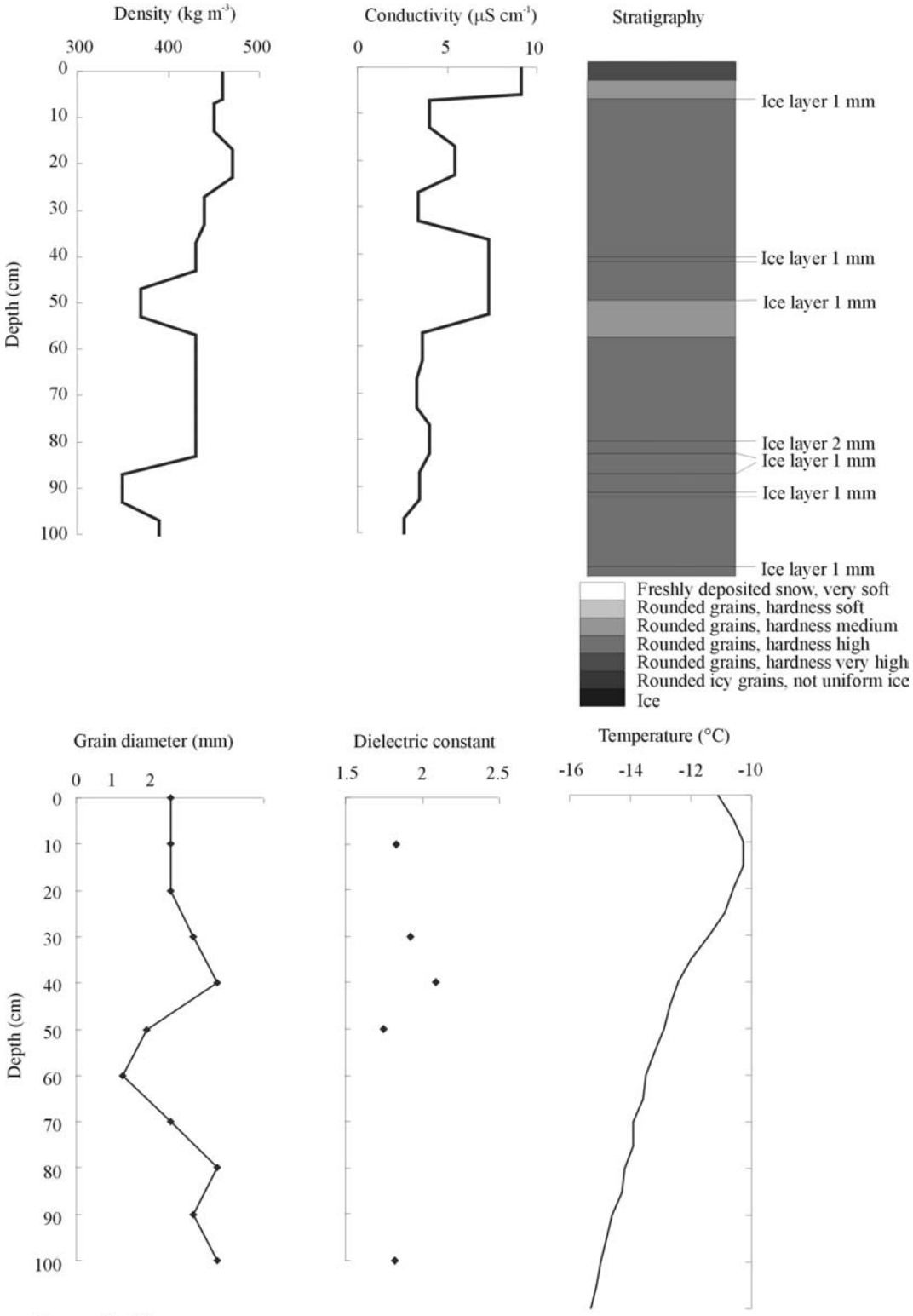

Snow site 13
Date: 10 Jan 2000 at 22:35 (UTC)
Coordinates: 73° 43.0'S, 12° 18.6'W

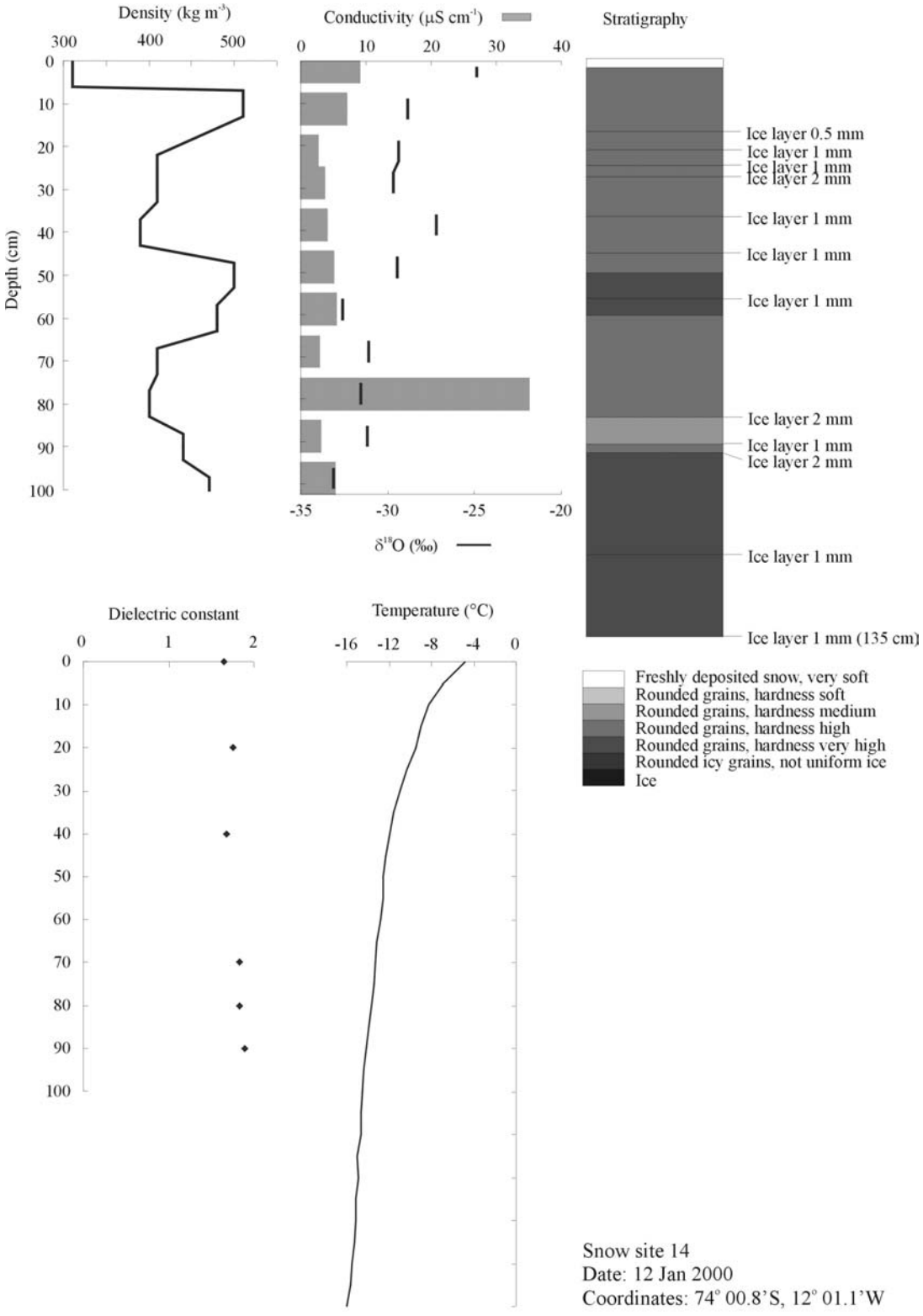

Snow site 14
Date: 12 Jan 2000
Coordinates: 74° 00.8'S, 12° 01.1'W

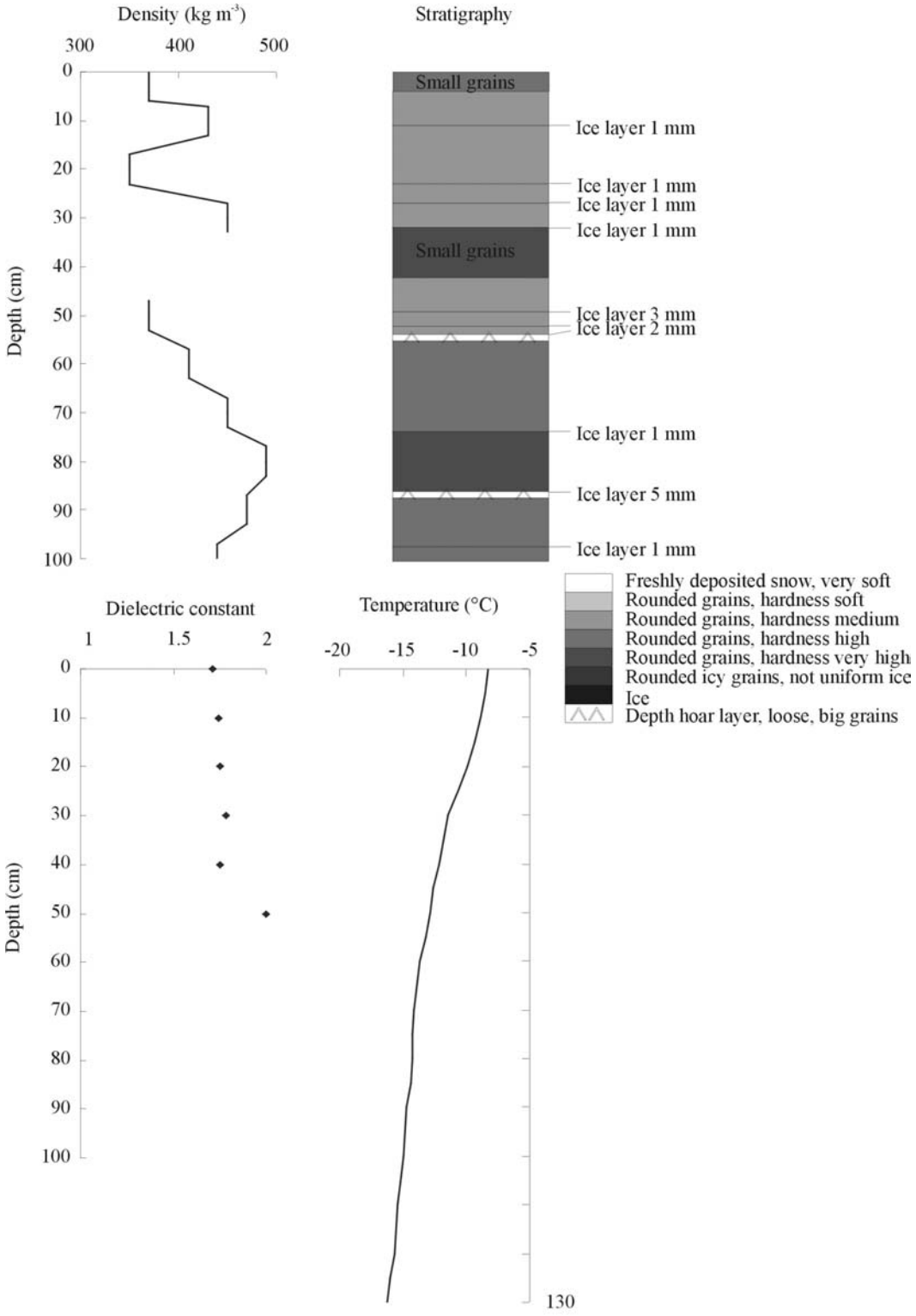

Snow site 15
Date: 12 Jan 2000 at 21:15 (UTC)
Coordinates: 74° 13.9'S, 11° 48.0'W

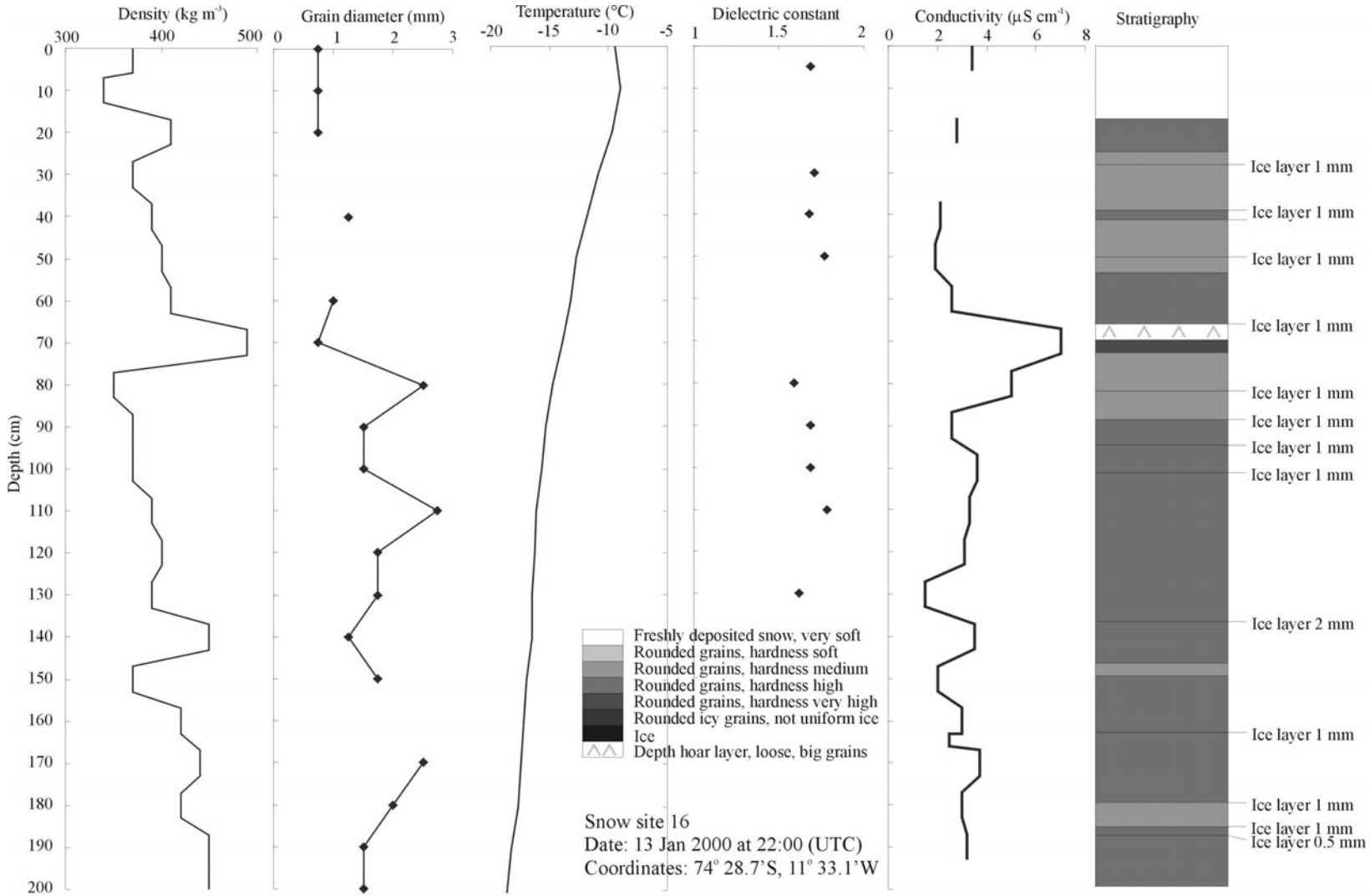
Density (kg m-3)
300
400
500
Grain diameter (mm)
0
1
2
3
Temperature (°C)
-20
-15
-10
-5
Dielectric constant
1
1.5
2
Conductivity (µS cm-3)
0
2
4
6
8
Stratigraphy
Depth (cm)
0
10
20
30
40
50
60
70
80
90
100
110
120
130
140
150
160
170
180
190
200
Freshly deposited snow, very soft
Rounded grains, hardness soft
Rounded grains, hardness medium
Rounded grains, hardness high
Rounded grains, hardness very high
Rounded icy grains, not uniform ice
Ice
Depth hoar layer, loose, big grains
Snow site 16
Date: 13 Jan 2000 at 22:00 (UTC)
Coordinates: 74° 28.7'S, 11° 33.1'W
Ice layer 1 mm
Ice layer 1 mm
Ice layer 1 mm
Ice layer 1 mm
Ice layer 1 mm
Ice layer 1 mm
Ice layer 1 mm
Ice layer 1 mm
Ice layer 2 mm
Ice layer 1 mm
Ice layer 1 mm
Ice layer 1 mm
Ice layer 0.5 mm

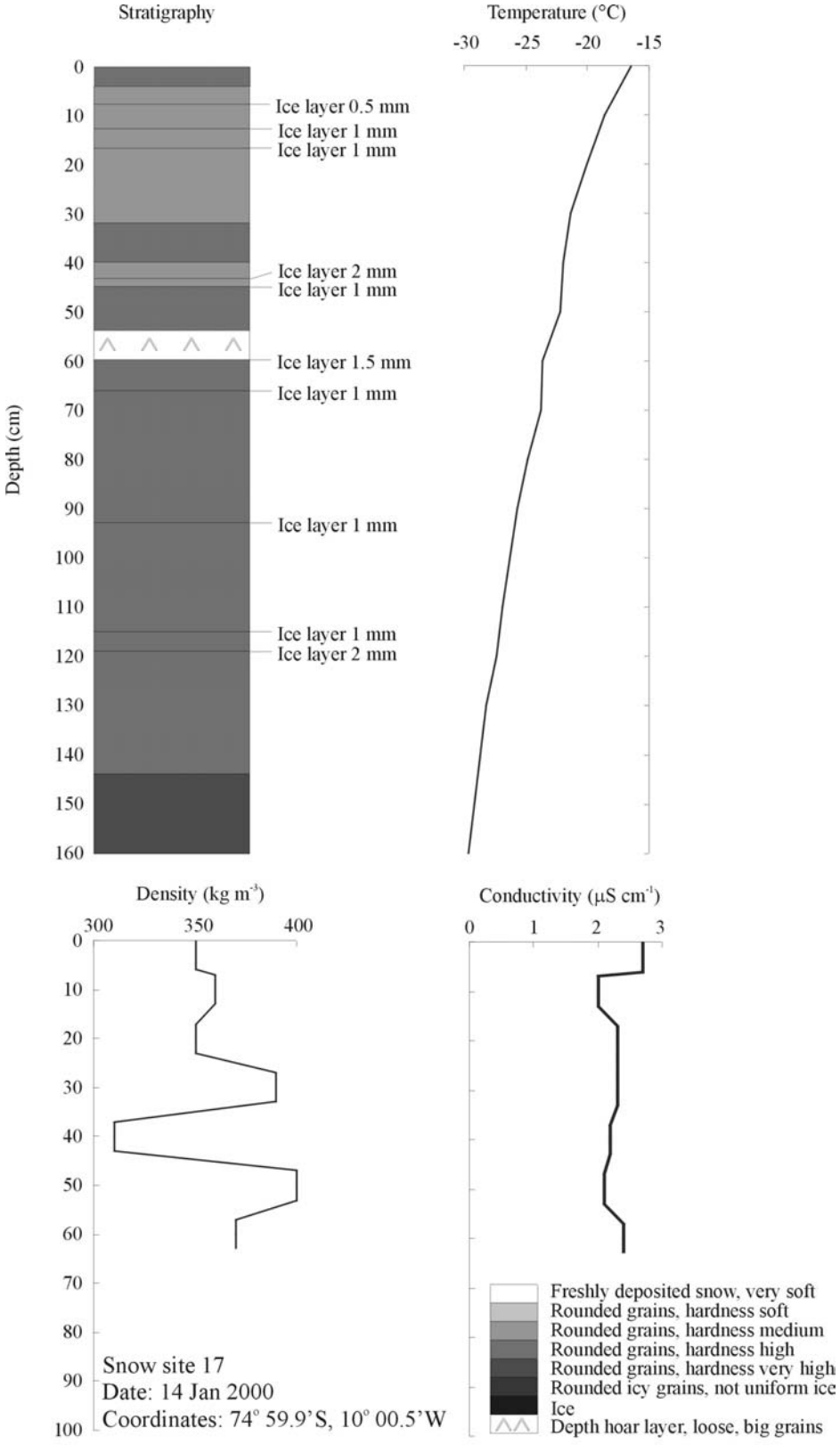
Stratigraphy
Temperature (°C)
-30
-25
-20
-15
Depth (cm)
0
10
20
30
40
50
60
70
80
90
100
110
120
130
140
150
160
Ice layer 0.5 mm
Ice layer 1 mm
Ice layer 1 mm
Ice layer 2 mm
Ice layer 1 mm
Ice layer 1.5 mm
Ice layer 1 mm
Ice layer 1 mm
Ice layer 1 mm
Ice layer 2 mm
Density (kg m-3)
300
350
400
Conductivity (µS cm-1)
0
1
2
3
Snow site 17
Date: 14 Jan 2000
Coordinates: 74° 59.9'S, 10° 00.5'W
Freshly deposited snow, very soft
Rounded grains, hardness soft
Rounded grains, hardness medium
Rounded grains, hardness high
Rounded grains, hardness very high
Rounded icy grains, not uniform ice
Ice
Depth hoar layer, loose, big grains

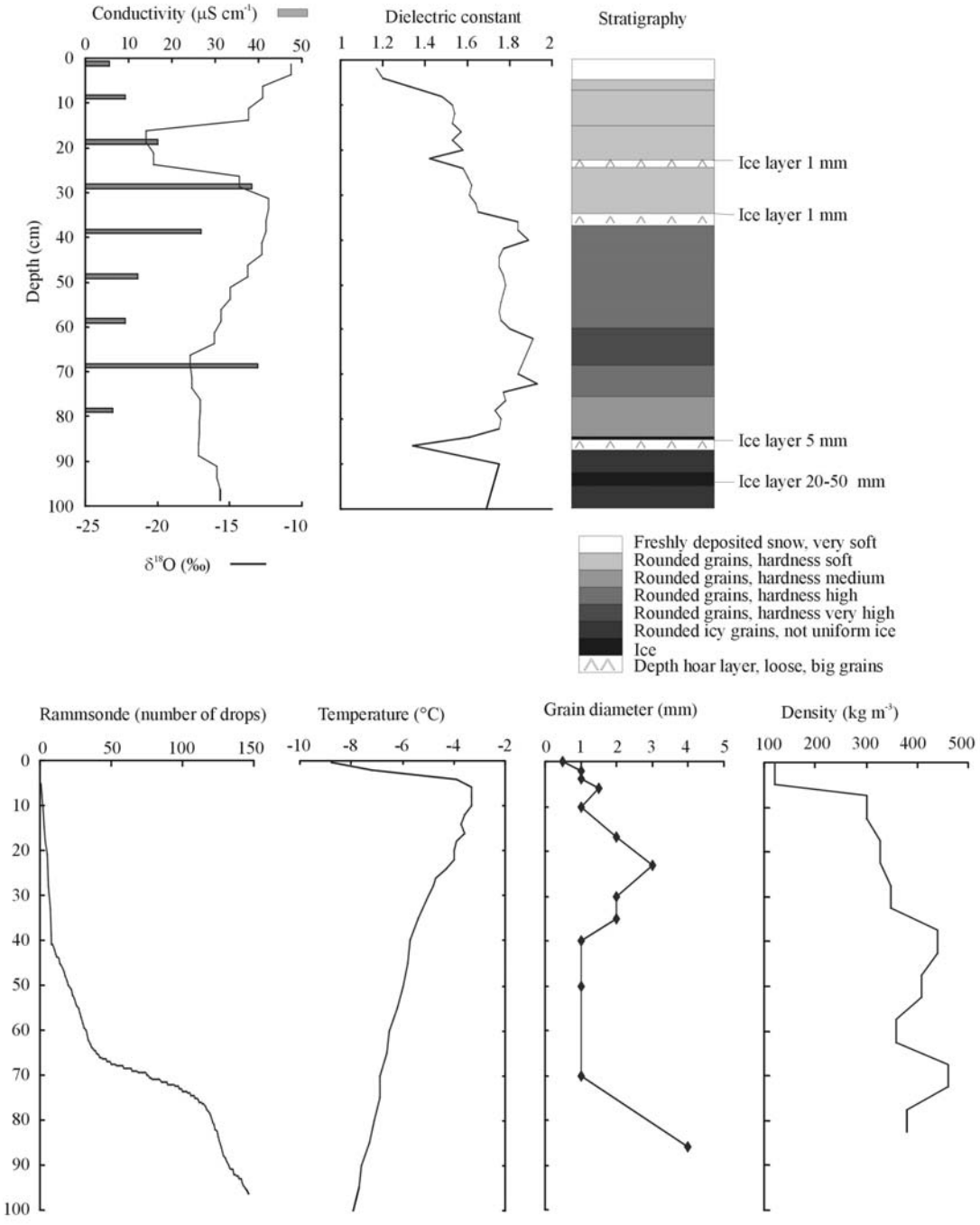

Snow site 1
Date: 30 Jan 2001
Coordinates: 72° 32.0'S, 16° 34.0'W

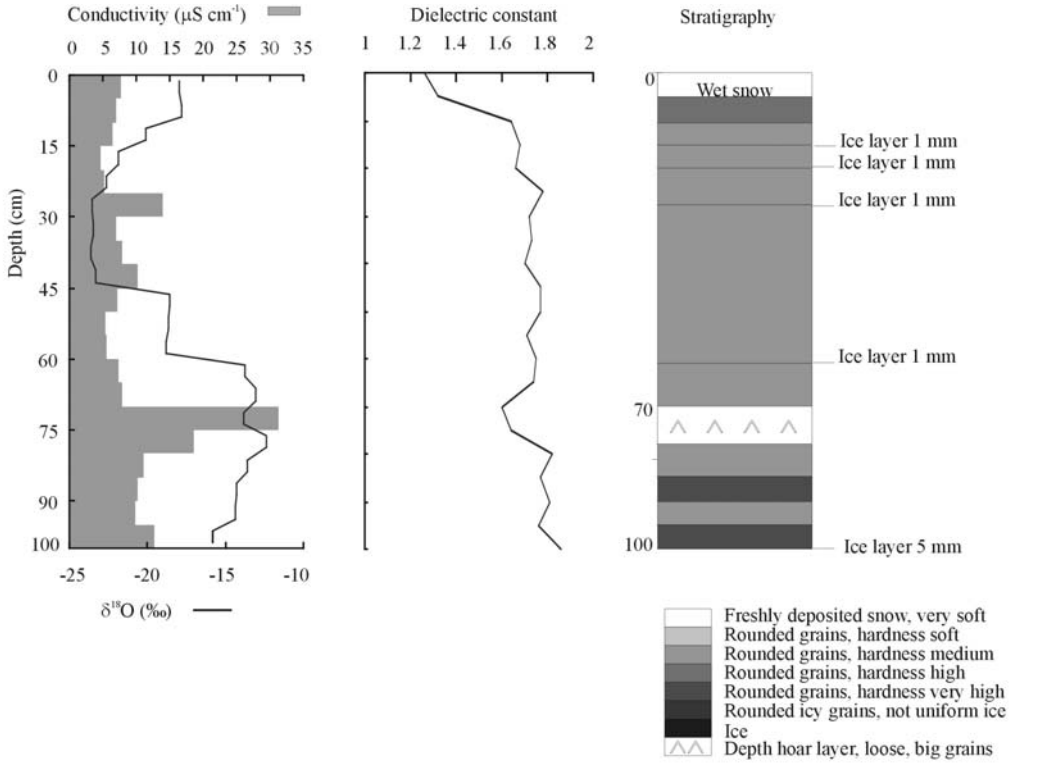

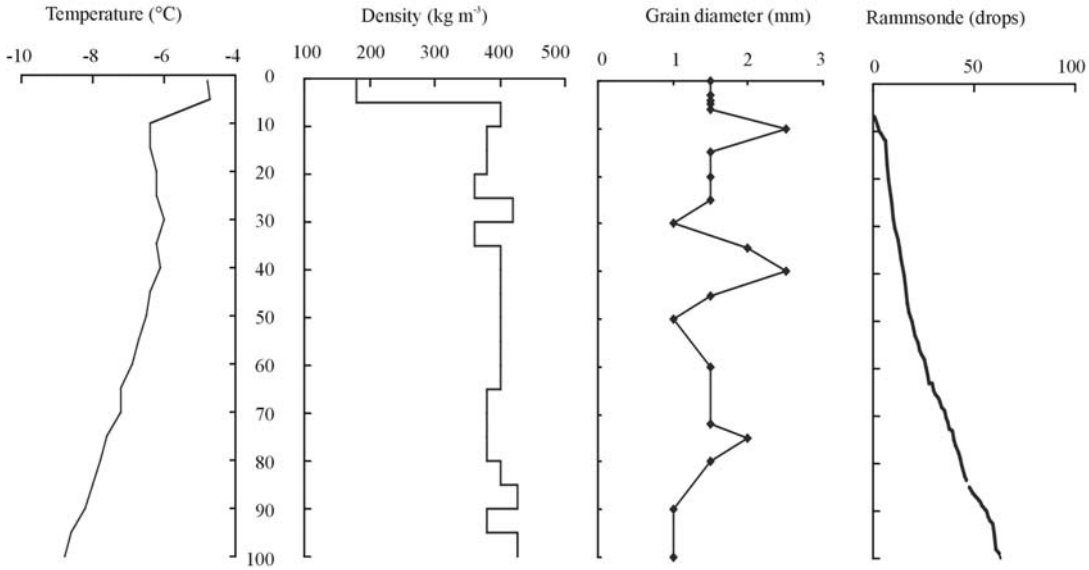

Snow site 2
Date: 20 Jan 2001
Coordinates: 72° 36.6'S, 16° 18.5'W

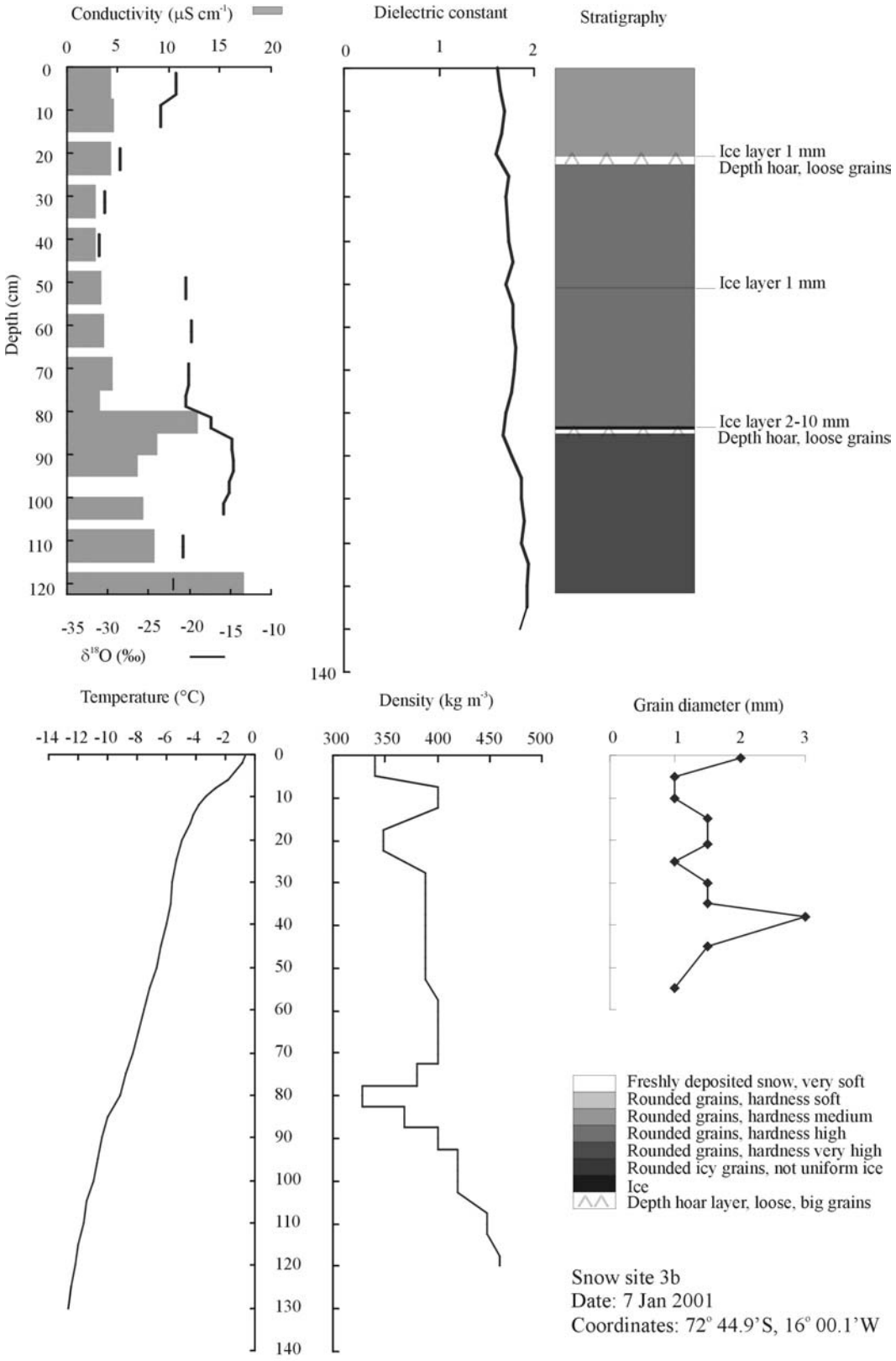
Conductivity (µS cm-1)
Dielectric constant
Stratigraphy
Depth (cm)
δ18O (‰)
Ice layer 1 mm
Depth hoar, loose grains
Ice layer 1 mm
Ice layer 2-10 mm
Depth hoar, loose grains
Temperature (°C)
Density (kg m-3)
Grain diameter (mm)
Freshly deposited snow, very soft
Rounded grains, hardness soft
Rounded grains, hardness medium
Rounded grains, hardness high
Rounded grains, hardness very high
Rounded icy grains, not uniform ice
Ice
Depth hoar layer, loose, big grains
Snow site 3b
Date: 7 Jan 2001
Coordinates: 72° 44.9'S, 16° 00.1'W

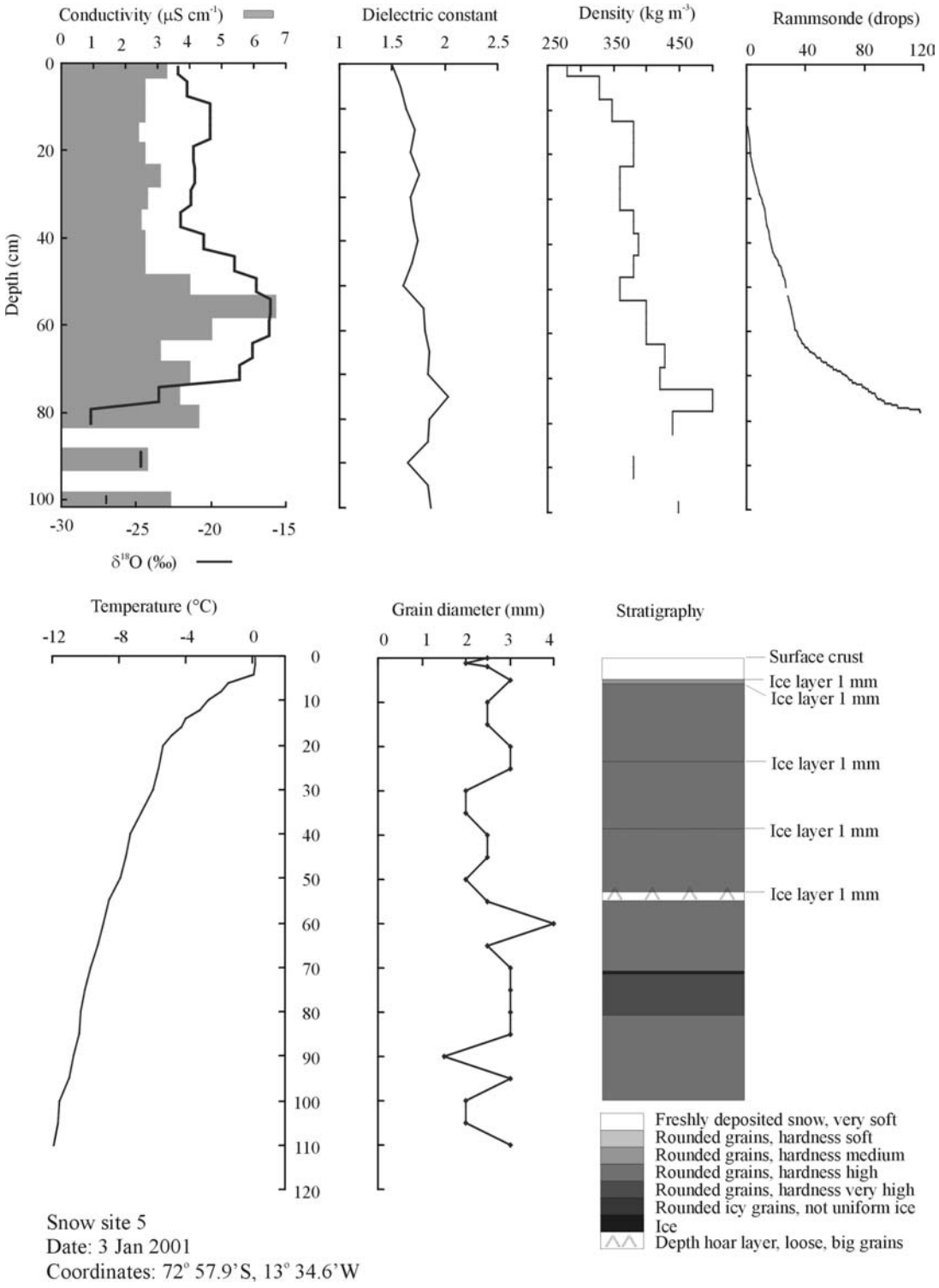
Conductivity (μS cm-1)
Dielectric constant
Density (kg m-3)
Rammsonde (drops)
Depth (cm)
δ18O (‰)
Temperature (°C)
Grain diameter (mm)
Stratigraphy
Surface crust
Ice layer 1 mm
Ice layer 1 mm
Ice layer 1 mm
Ice layer 1 mm
Ice layer 1 mm
Freshly deposited snow, very soft
Rounded grains, hardness soft
Rounded grains, hardness medium
Rounded grains, hardness high
Rounded grains, hardness very high
Rounded icy grains, not uniform ice
Ice
Depth hoar layer, loose, big grains
Snow site 5
Date: 3 Jan 2001
Coordinates: 72° 57.9'S, 13° 34.6'W

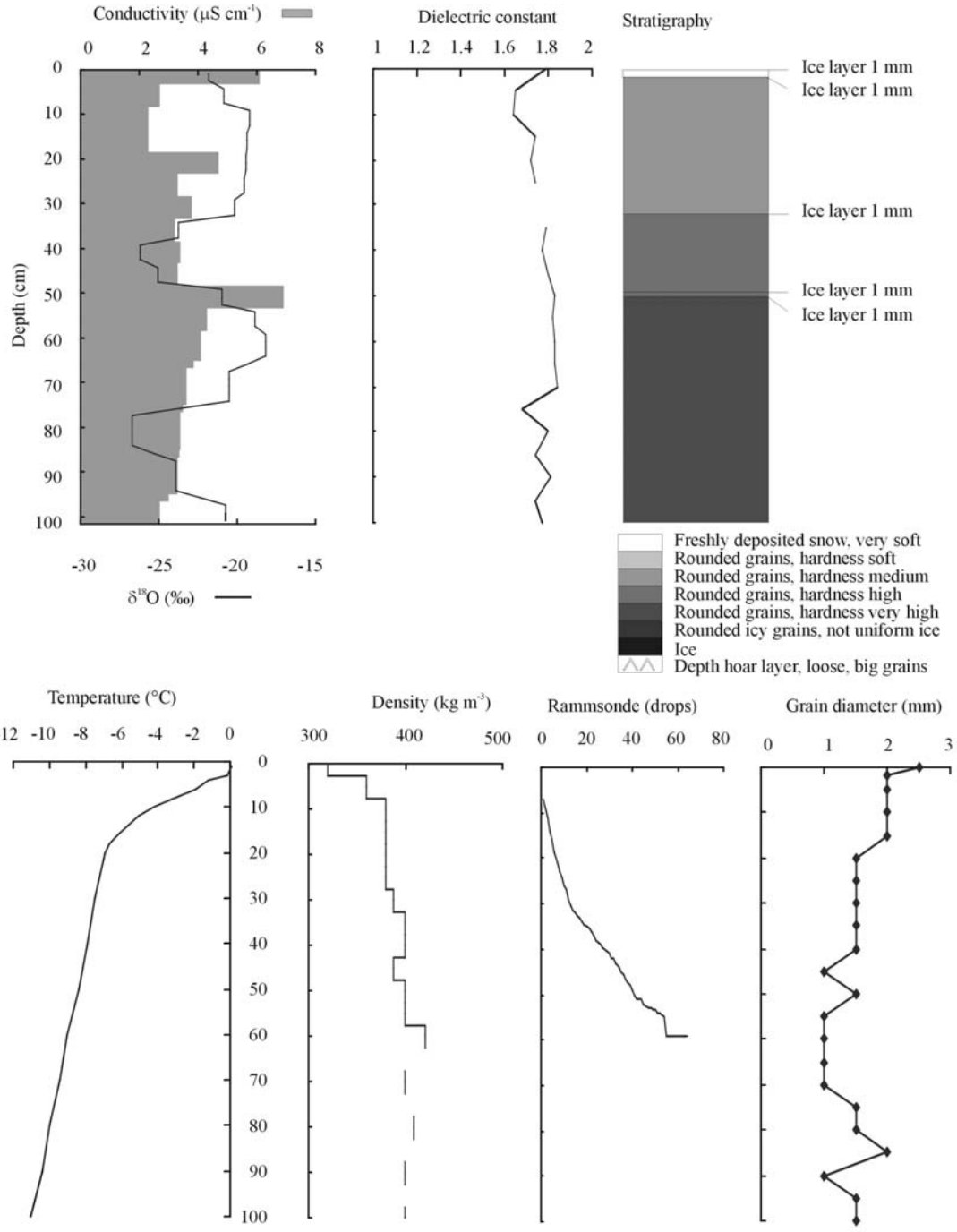

Snow site 9
Date: 29 Dec 2000
Coordinates: 73° 04.1'S, 13° 28.3'W

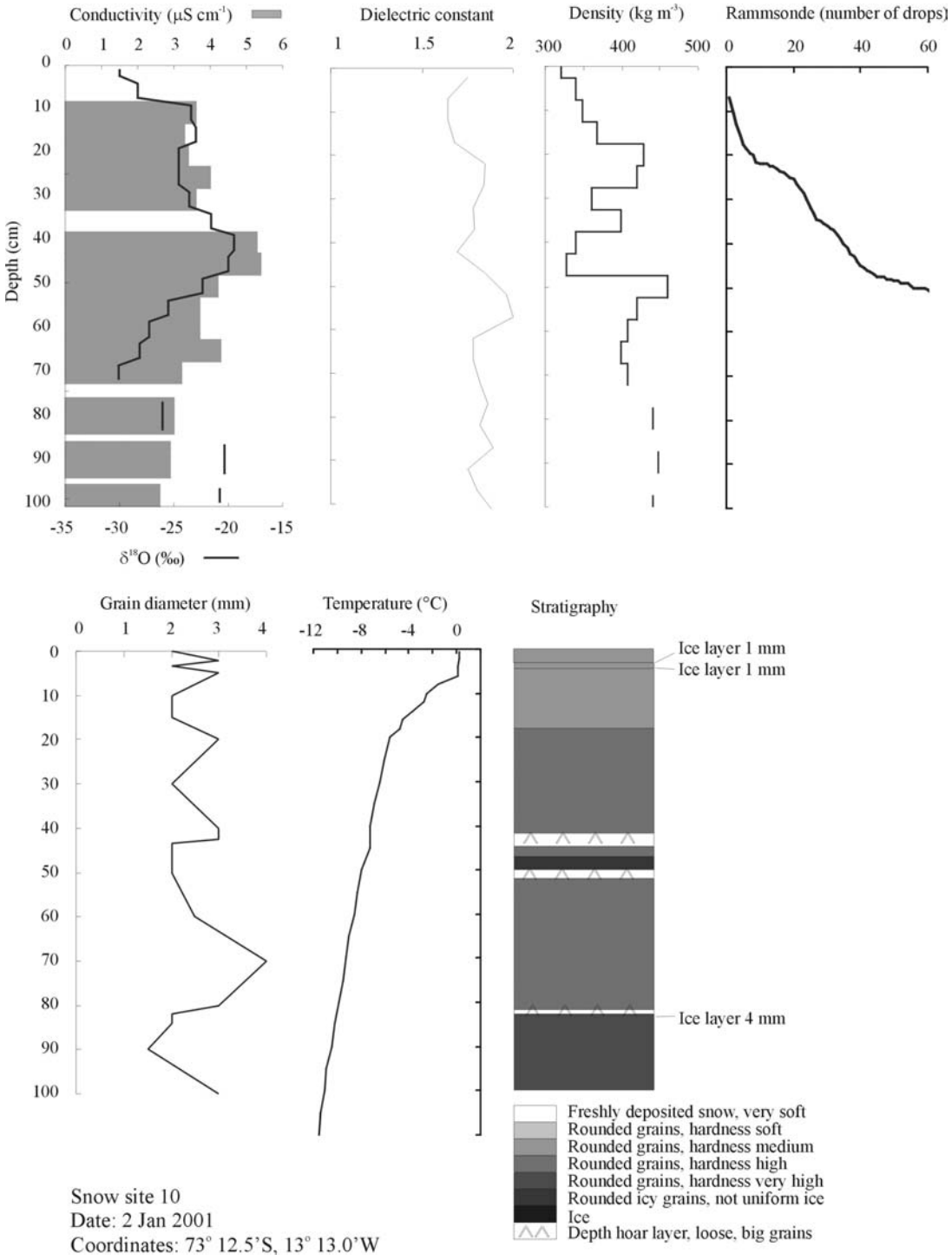
Conductivity (µS cm-1)
Dielectric constant
Density (kg m-3)
Rammsonde (number of drops)
Depth (cm)
δ18O (‰)
Grain diameter (mm)
Temperature (°C)
Stratigraphy
Ice layer 1 mm
Ice layer 1 mm
Ice layer 4 mm
Freshly deposited snow, very soft
Rounded grains, hardness soft
Rounded grains, hardness medium
Rounded grains, hardness high
Rounded grains, hardness very high
Rounded icy grains, not uniform ice
Ice
Depth hoar layer, loose, big grains
Snow site 10
Date: 2 Jan 2001
Coordinates: 73° 12.5'S, 13° 13.0'W

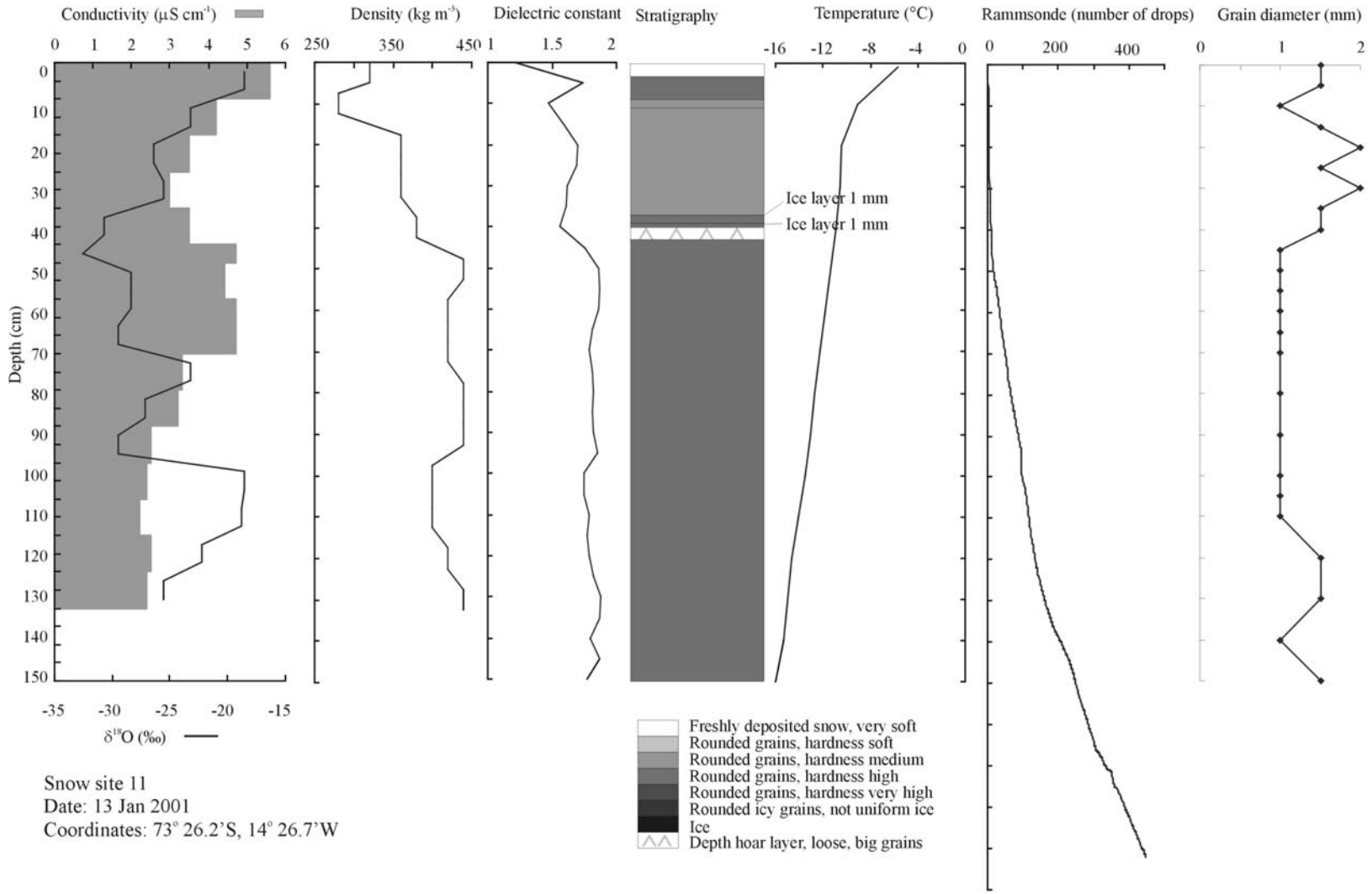
Conductivity (µS cm-1)
Density (kg m-3)
Dielectric constant
Stratigraphy
Temperature (°C)
Rammsonde (number of drops)
Grain diameter (mm)
Depth (cm)
δ18O (‰)
Ice layer 1 mm
Ice layer 1 mm
Freshly deposited snow, very soft
Rounded grains, hardness soft
Rounded grains, hardness medium
Rounded grains, hardness high
Rounded grains, hardness very high
Rounded icy grains, not uniform ice
Ice
Depth hoar layer, loose, big grains
Snow site 11
Date: 13 Jan 2001
Coordinates: 73° 26.2'S, 14° 26.7'W

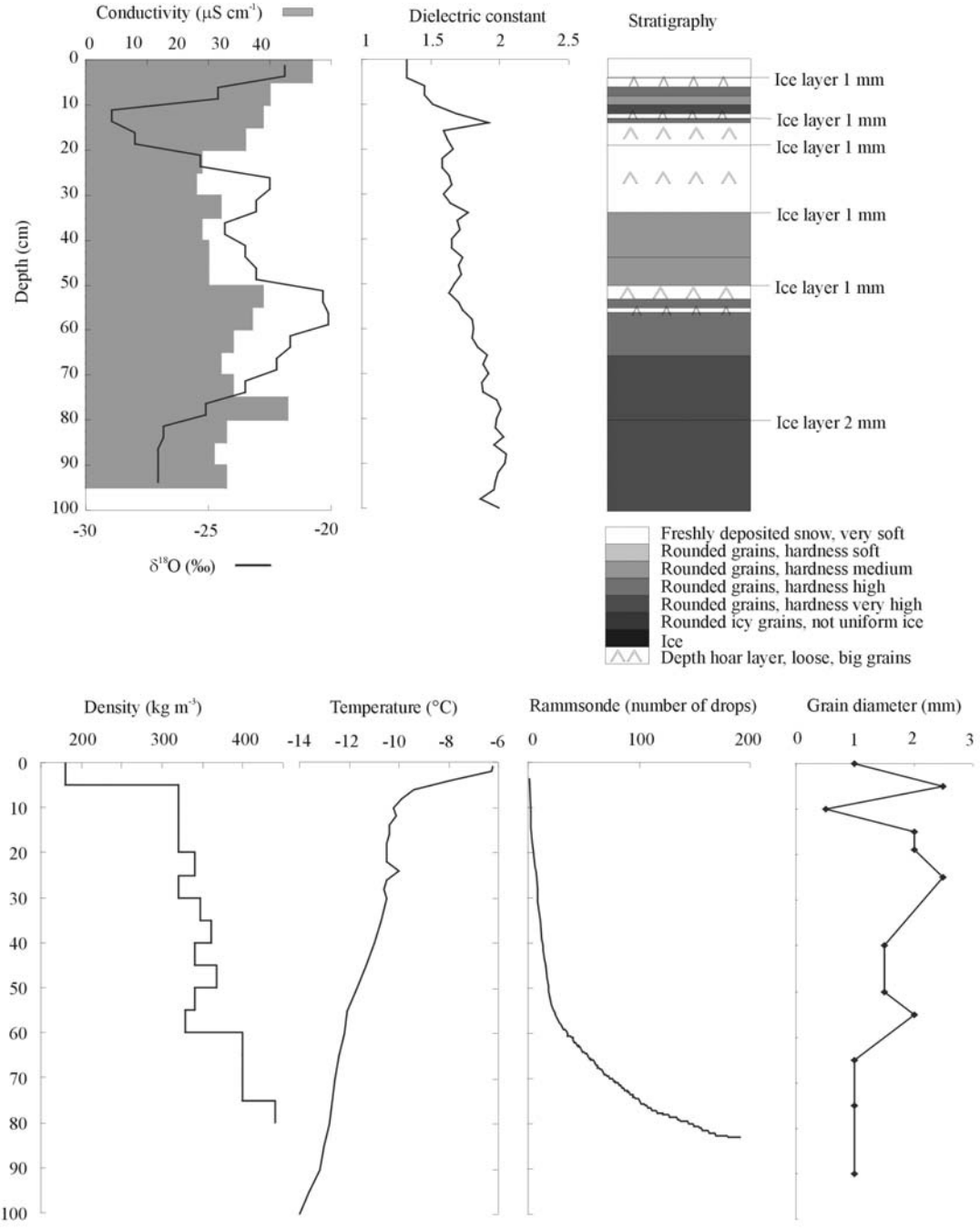

Snow site 12
Date: 24 Jan 2001
Coordinates: 73° 27.4'S, 12° 33.3'W

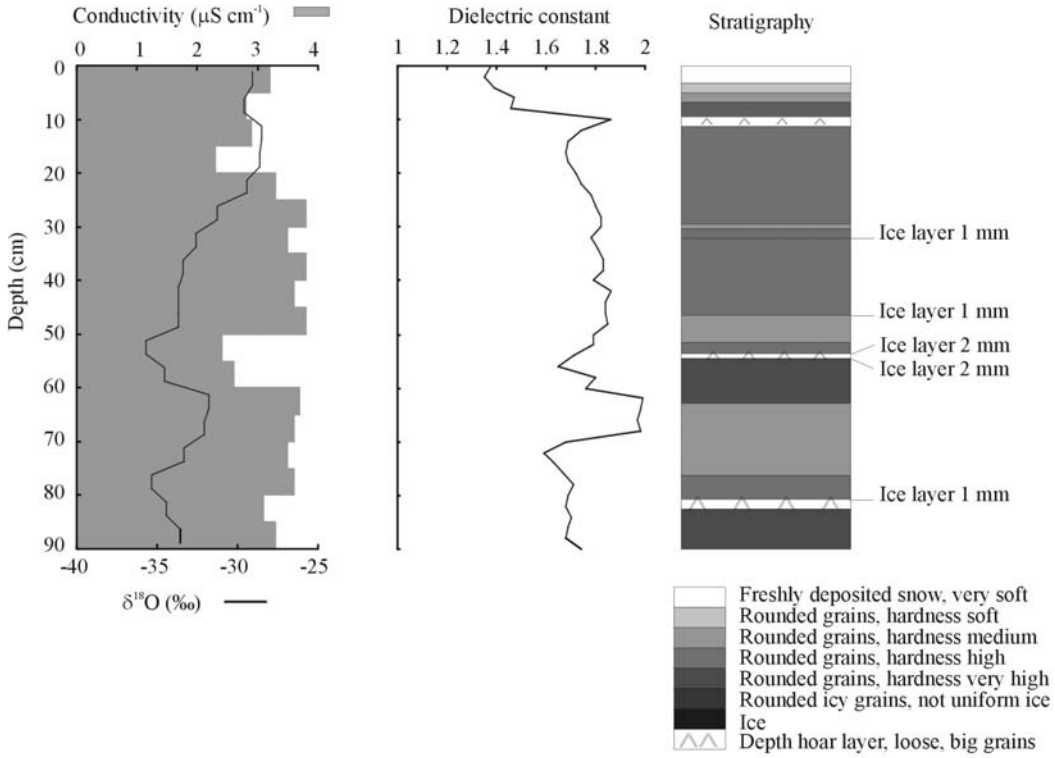

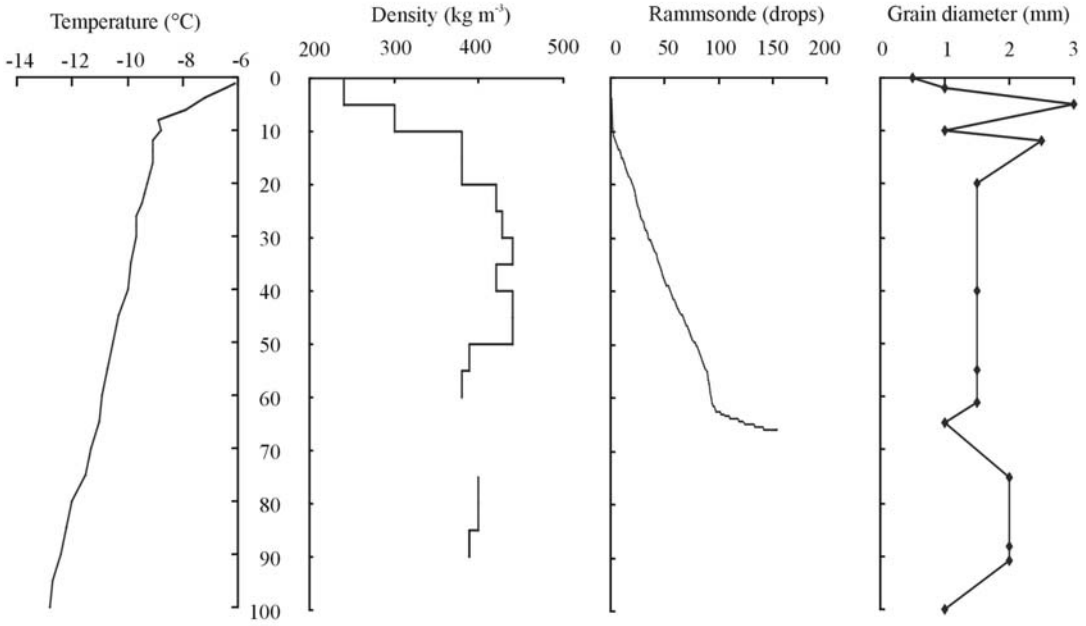

Snow site 14
Date: 23 Jan 2001
Coordinates: 74° 00.8'S, 12° 01.1'W

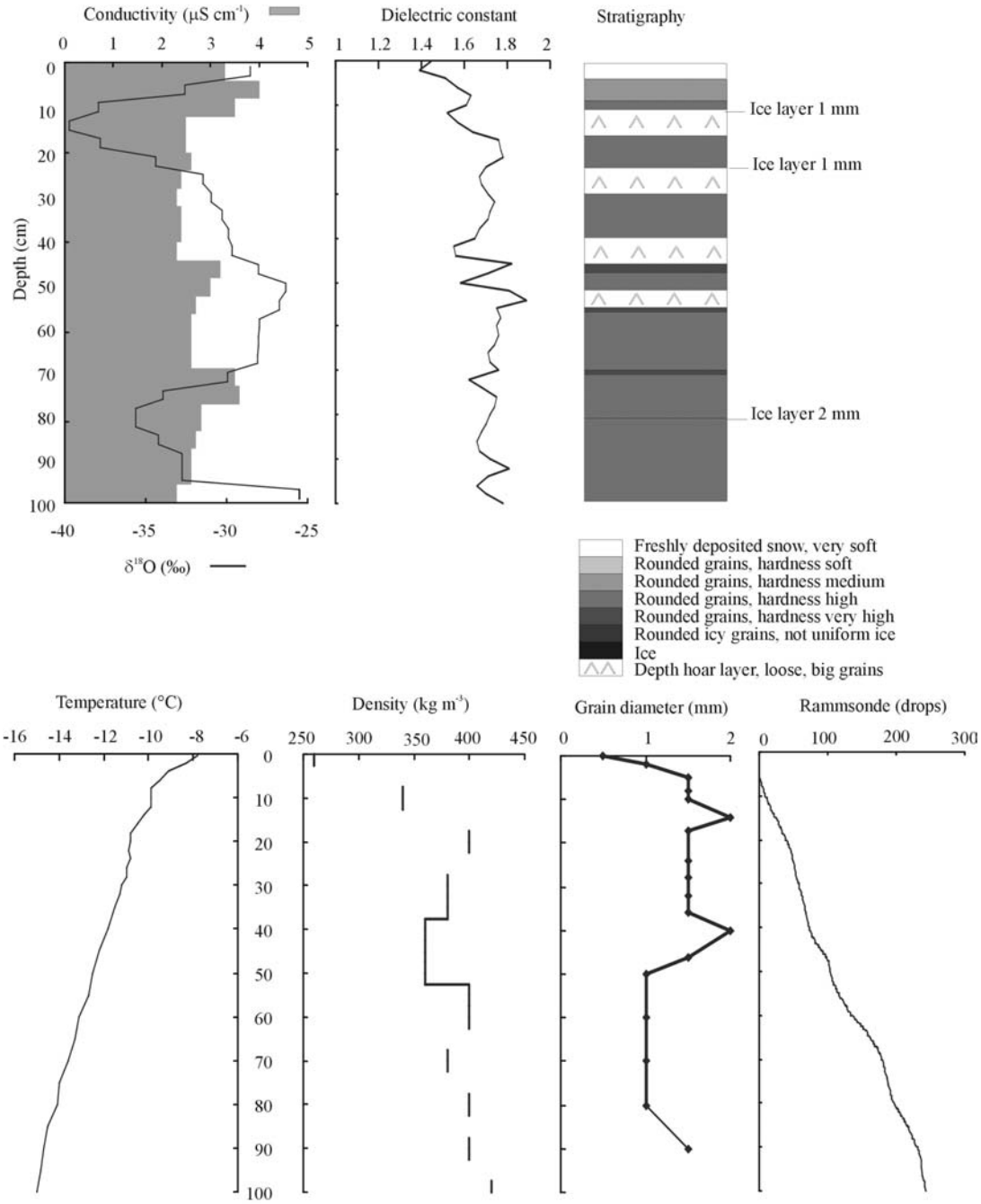

Snow site 16
Date: 22 Jan 2001
Coordinates: 74° 28.7'S, 11° 33.1'W

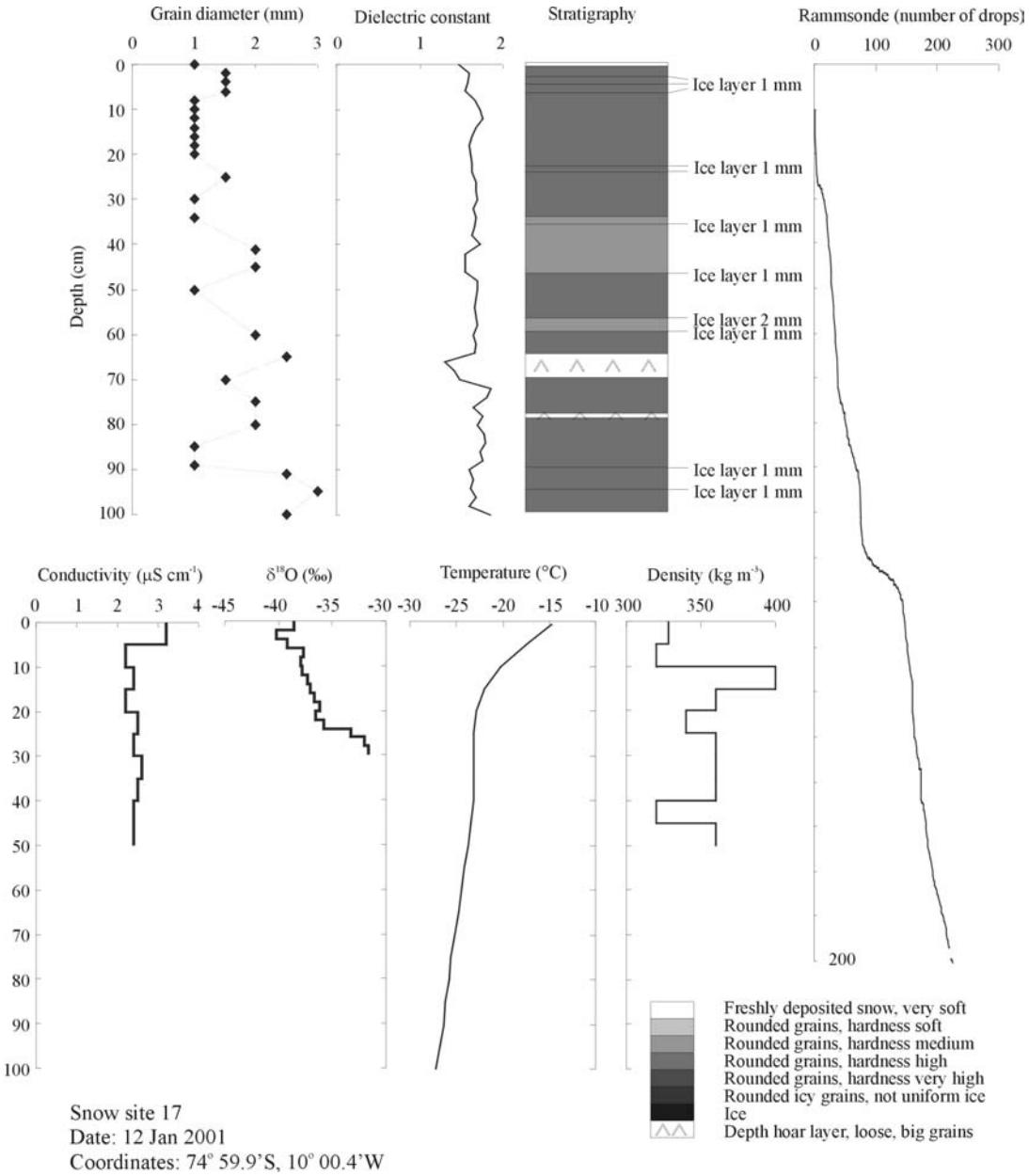

Snow site 17
Date: 12 Jan 2001
Coordinates: 74° 59.9'S, 10° 00.4'W

REPORT SERIES IN GEOPHYSICS

1. Noponen, I., 1974: Comparison of crust and upper mantle structure between shield and arc areas.
2. Palosuo, E. 1975: Pintaveden lämpötila- ja suolaisuuskartasto Pohjanlahdella, I. Kesäkausi. Atlas of surface water temperatures and salinities on the Gulf of Bothnia, I. Summerperiod.
3. Hiltunen, T., Huttula, T., 1976: Vanajaselän virtausoloista talvella. (Current measurements in the ice covered water of Vanajanselkä).
4. Hiltunen, T., 1976: Vesimassojen liikkuminen Vanajanselällä kesällä 1975. Käsiluotaushavainnot. (The movement of water in Lake Vanajanselkä in summer 1975. Part I).
5. Uusitalo, S., 1976: Mean surface velocities on southern Bothnian Bay determined by an indirect method.
6. Palosuo, E., Hiltunen, T., Jokinen, J., Teinonen, M., 1977: Lumen kitkan vaikutus suksen luistoon. The effect of friction between snow and skis.
7. Virta, J., 1978: A rainfall-runoff model for catchment areas with an abundance of lakes.
8. Tyrväinen, M., 1978: Lämpötilaolot Suomenlahdella sekä mallisovellutuksia. Temperature conditions and simulation in the Gulf of Finland.
9. Mäki-Lopez, M.-L., 1978: Geomagnetic variation study in Hidalgo and Grant counties, southwestern New Mexico, USA.
10. Keinonen, J., Palosuo, E., Korhonen, P., Suominen, H., 1978: Lumen ja suksenpohjanmuovien välisen kitkan mittauksia. Measurements of friction between snow and sliding materials of ski.
11. Palosuo, E., 1978: Hiihtokauden ajoittumisesta Suomessa. The length of the skiing season in Finland.
12. Pellinen, R., 1979: Induction model and observations of onset of magnetospheric substorms.
13. Palosuo, E., Keinonen, J., Suominen, H., Jokitalo, R., 1979: Lumen ja suksenpohjamuovien välisen kitkan mittauksia. Osa 2. Measurements of friction between snow and ski running surfaces. Part 2.
14. Nevanlinna, H., 1980: Geomagnetic secular variation described by dipole models.
15. Kahma, K. K., 1981: On the growth of wind waves in fetch-limited conditions.
16. Palosuo, E., 1982: Jään vahvistaminen Finlandia-82 hiihdon lähtöpaikalla. Strengthening of the ice at start of the Finlandia-82 ski event.
17. Pihkala, P., Spring, E., 1982: A simple dilatometer for determination of the free water of the snow.
18. Leino, M. A. H., Spring, E., Suominen, H., 1983: Coefficients of kinetic friction of skis on snow determined from sliding length and velocity of the skier.
19. Leino, M. A. H., Spring, E., 1984: Determination of the coefficient of kinetic friction between ski and snow from the gliding velocity of a skier.
20. Pihkala, P., Spring, E., 1985: A practical method for photographing snow samples.
21. Erkkilä, J., Hämäläinen, T., Pihkala, P., Savolainen, S., and Spring, E., 1985: A cinematographic method for determination of the kinetic friction of skis on snow.
22. Pihkala. P., Spring, E., 1986: Determination of the contact area between ski and snow using a simple thermal conductivity meter.
23. (Distribution limited)
24. Pulkkinen, K., 1989: Calibration and basic manipulation of SC-ADCP data.
25. Pulkkinen, K., 1991: Water sample -based calibration of VARIOSENS turbidity meter with some comparisons with other soundings.
26. Simojoki, H., 1992: Geofysiikan tulo oppiaineeksi Helsingin yliopistossa (2nd ed.).
27. Leppäranta, M., Haapala, J. (eds.), 1993: Proceedings of the first workshop on the Baltic sea ice climate, Tvärminne, Finland, 22-26 August 1993.
28. Vihma, T. (ed.), 1994: Evening sessions of the summer school on physics of ice-covered seas, Savonlinna, Finland, 6-17 June 1994.
29. Pulkkinen, K., 1995: STD-12 mini-CTD:n käyttö ja datan kalibrointi (English summary: The use of STD-12 mini-CTD and calibration of data).
30. Pulkkinen, K., (ed.), 1995: Underwater optical measurements made during the first concentrated field effort (CFE 1) of NOPEX - A data report.
31. Multala, J., Hautaniemi, H., Oksama, M., Leppäranta, M., Haapala, J., Herlevi, A., Riska, K., and Lensu, M., 1995: Airborne electromagnetic surveying of Baltic sea ice.
32. Pulkkinen, K., (ed.), 1995: Proceedings of the 2nd Finnish-Estonian seminar on underwater optics with applications, Helsinki, 10-12 April 1995.
33. Launiainen, J., and Cheng, B., 1995: A simple non-iterative algorithm for calculating turbulent bulk fluxes in diabatic conditions over water, snow/ice and ground surface.
34. Stipa, T., 1996: Water renewal and vertical circulation of Pohja Bay.
35. Haapala, J., Alenius, P., Dubra, J., Klyachkin, S. V., Kõuts, T., Leppäranta, M., Omstedt, A., Pakstys, L., Schmelzer, N., Schrum, C., Seinä, A., Strübing, K., Sztobryn, M., and Zaharchenko, E., 1996: IDA. Ice data bank for Baltic Sea climate studies.
36. Leppäranta, M., (ed.), 1996: AISA lake experiment 1993-94. Final Report.
37. Haapala, J., Leppäranta, M. (eds.), 1997: ZIP-97 data report.
38. Pulkkinen, K., (ed.), 1998: Proceedings of the 4th Finnish-Estonian seminar on underwater optics with applications, Lammi, 22-24 April 1997.
39. Saloranta, T. M., 1998: Snow and snow ice in sea ice thermodynamic modelling.
40. Leppäranta, M., (ed.), 1998: Downscaling in sea ice geophysics.
41. Herlevi, A., (ed.), 1999: The optics ground truth of the Finnish SALMON experiment.
42. Haapala, J., 2000: Modelling of the seasonal ice cover of the Baltic sea.
43. Zhang, Z., 2000: On modelling ice dynamics of semi-enclosed seasonally ice-covered seas.
44. Jevrejeva S., V.V. Drabkin, J. Kostjukov, A. A. Lebedev, M. Leppäranta, Ye. U. Mironov, N. Schmelzer and M. Sztobryn, 2002: Ice time series of the Baltic Sea.
45. Herlevi, A. 2002, Inherent and apparent optical properties in relation to water quality in Nordic waters.
46. Leppäranta, M. (ed.), 2003, Proceedings of the seminar “Sea Ice Climate and Marine Environments in the Okhotsk and Baltic Seas – The Present Status and Prospects”.

ISBN 952-10-0953-5
ISSN 0355-8630

Helsinki 2003
Yliopistopaino